Final Report
Project Title: Recovery Act: Advanced Direct Methanol Fuel Cell for Mobile Computing
Project Period: January 1, 2010 to December 31, 2011
Reporting Period: January 1, 2010 to December 31, 2011
Date of Report: March 30, 2012

Recipient: University of North Florida

Award Number: DE-EE0000476

Working Partners: University of Florida

Cost-Sharing Partners: University of Florida

Contact: Dr. James Fletcher, Principal Investigator; jfletche@unf.edu; 904-620-1844

DOE Managers: DOE HQ Technology Manager-Dr. Ned Stetson, DOE Field Manager-Dr. Katie L. Randolph

A.   PROJECT OBJECTIVE

The objective of the project is to advance portable fuel cell system technology towards the commercial targets as laid out in DOE's R&D roadmap by developing an advanced direct methanol fuel cell power supply that meets the initial commercial entry requirements for power density, energy density and lifetime. It will enable mobile computers to operate non-stop, unplugged from the wall power outlet, by using the high energy density of methanol fuel from a fuel cartridge. Specifically this project will focus on balance of plant component integration and miniaturization, as well as extensive component, subassembly and integrated system durability and validation testing, resulting in a pre-production power supply design that meet the rigorous demands of consumer electronic applications. It is expected that at the end of this project an integrated direct methanol fuel cell power supply for mobile computing, that has the functionality and durability to meet initial product introduction requirements, will have been developed and demonstrated.

B. PROJECT SCOPE

Background:

This project will develop a direct methanol fuel cell power supply for mobile computing. This new technology power source will use methanol fuel cartridges as the source of energy and provide power to operate a laptop computer non-stop without wall power. It will use the novel passive water recycling MEA technology acquired by the University of North Florida (UNF) from PolyFuel, Inc. which enables significant simplification and miniaturization of fuel cell systems. The goal of this project will be to accelerate commercialization by focusing on product durability and lifetime and durability of the core technology. Volume reduction benefits gained by balance of plant and packaging advances (through component miniaturization and integration) will be, in part, be used to provide lifetime margin for the overall integrated device.

C. TASKS

The proposed work plan is designed to meet the project objectives, which correspond directly with the objectives outlined in Topic 5B of the Funding Opportunity Announcement: to engineer the fuel cell balance of plant and packaging to meet the needs of consumer electronic systems, specifically at power levels required for mobile computing. UNF will leverage off existing balance of plant component technologies developed under its current US Army CERDEC project as well as a previous DOE project

completed by PolyFuel and further refine them to both miniaturize and integrate their functionality to increase the system power density and energy density. Benefits of UNF's novel passive water recycling MEA and the simplified system architecture it enables form the foundation of the design approach. The package design will be hardened to address orientation independence, shock, vibration, and environmental requirements. Fuel cartridge and fuel subsystems will be revised to ensure effective fuel containment.

The Appendix gives a list of all tasks and subtasks defined for the project.

Overview

The University of North Florida (UNF), with project partner the University of Florida, recently completed the Department of Energy (DOE) project entitled "*Advanced Direct Methanol Fuel Cell for Mobile Computing*". The primary objective of the project was to advance portable fuel cell system technology towards the commercial targets as laid out in the DOE R&D roadmap by developing a 20-watt, direct methanol fuel cell (DMFC) portable power supply based on the UNF innovative "passive water recovery" MEA. Extensive component, sub-system, and system development and testing was undertaken to meet the rigorous demands of the consumer electronic application. Numerous brassboard (unpackaged) systems were developed to optimize the integration process and facilitating control algorithm development. The culmination of the development effort is shown in Figure 1 which shows a photo of the fully-integrated, DMFC power supply.
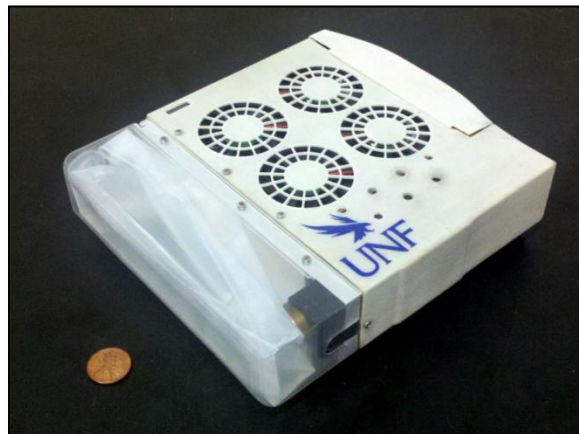

Figure 1 Fully integrated, DMFC power supply.

Table 1 shows the critical performance characteristics of the DP4 power supply. Initially, the system performed more robustly with the methanol concentration sensor because the methanol cross-over was minimized by close concentration control. Due to MEA improvements, brassboard testing showed the system performed as efficiently and robustly without the methanol concentration sensor. Therefore, two configurations of the system are listed, one including the ISSYS methanol concentration sensor and one without.

Table 1 DP4 25 W power supply specifications

Characteristic	DP4 with ISSYS Methanol Sensor	DP4 without ISSYS Methanol Sensor
Beginning of Life Net Power (W)	28	28
Weight (kg)	0.784	0.675
Volume (L)	0.577	0.506

Table 2 shows the specific power (W/kg), power density (W/l), and energy density (W-hr/l) project goals and system performance. It should be noted that the specific power and power

density were for the power section only, not including the hybrid battery. The energy density is based on three 200 ml fuel cartridges, also not including the hybrid battery. The results show that the DP4 system configured without the methanol concentration sensor exceeds all performance goals. With the sensor, the system exceeds the energy density and approaches the goals for specific power and power density.

Table 2 Project goals versus system performance.

Characteristic	Project Goals	DP4 with ISSYS Methanol Sensor	DP4 without ISSYS Methanol Sensor
Specific Power (W/kg)	40	35.7	41.5
Power Density (W/L)	55	48.5	55.3
Energy Density (Whr/L)	575	585	623

During the project, the DOE revised their technical targets, and the definition of many of these targets, for the portable power application. Specific power, power density, specific energy (W-hr/kg), and energy density are based on the total system including fuel tank, fuel, and hybridization battery. Fuel capacity is not defined, but the same value is required for all calculations. Table 3 and Table 4, respectively, detail the DOE 2011 status and the DOE 2013 targets as well as the current performance of the DP4 power supply based on the same definitions. The data shows that the DP4 exceeds the 2011 current status and approaches the 2013 targets.

Table 3 DOE 2011 Technical Status for Portable Fuel Cell Systems (10-50 Watts) versus DP4.

Characteristic	DOE 2011 Status	DP4 with ISSYS Methanol Sensor	DP4 without ISSYS Methanol Sensor
Operation Duration (hrs)		10	10
Specific Power (W/kg)	15	28.7	32.3
Specific Energy (Whr/kg)	150	287	323
Power Density (W/L)	20	34.1	37.3
Energy Density (Whr/L)	200	341	373

Table 4 DOE 2013 Technical Target for Portable Fuel Cell Systems (10-50 Watts) versus DP4.

Characteristic	DOE 2013 Targets	DP4 with ISSYS Methanol Sensor	DP4 without ISSYS Methanol Sensor
Operation Duration (hrs)	14.3	14.3	14.3
Specific Power (W/kg)	30	26.4	29.4
Specific Energy (Whr/kg)	430	378	421
Power Density (W/L)	35	30.2	32.8
Energy Density (Whr/L)	500	432	468

UNF has successfully met the project goals. A fully-operational, 20-watt DMFC power supply was developed based on the UNF passive water recovery MEA. The power supply meets the project performance goals and advances portable power technology towards the commercialization targets set by the DOE.

Task 1: Component Engineering

Component Design Requirements & Component Design Failure Mode Effects Analysis

Modeling and analysis of the design requirements using passive water recovery MEA technology guided the development of component, subassembly, and system component design requirements (CDRs). Preliminary modeling of a 20W system using the current state of knowledge of the system components guided development of the CDRs.

Based upon a 20 Watt system capable of meeting this power at End-of-Life, a set of CDRs were released for all components, subsystems, and the overall system. These were based upon the system modeling and the preliminary concept design with integrated subsystems with new components, or in some cases, newly designed components. The CDRs were revised as data were collected from newly designed subsystems and further compromises in the overall system design dictated.

A component design failure mode effects analysis (DFMEAs) was completed for each component and/or subsystem within the DP4. Information gained from the prior DP3 design significantly influenced the design and selection of future components.

Balance of Plant Engineering

After completing the CDRs (component design requirements), the balance of plant components were separated into the following two categories: those commercially available, such as the cathode blower; and, those with unique requirements, such as the recirculation tank sub-assembly portion of the integrated fluid reservoir subsystem, that require in-house prototype design. For the commercially available components, extensive testing identified appropriate candidates that meet the CDRs. For the other components, design and manufacture of prototypes were completed and performance and durability testing were completed. Based on the performance and volume constraints of the elected components, a preliminary design of a packaged system, based upon prototype system components, with arbitrary allocation of volume for to-be-designed control board(s) and hybrid battery was completed. A concept design review was held in January 2011. Concept design of the 3-D layout of all known components, the package shell, fuel cartridge, and hybrid battery were reviewed.

Integrated Fluid Reservoir Subsystem

The DP4 system is comprised of three key subsystems: the fuel cell stack, the air supply subsystem, and the integrated fluid reservoir subsystem. One key feature in the integrated fluid reservoir subsystem is the pressure–activated valve system which isolates liquid in the tank when the system is in the OFF state. Pressure from the fuel recirculation pump is used to activate all three valves and enable fluid flow only when the pump is active. This aspect of the system is key to water management; its design was revised during Q4/2010 to improve the valve sealing and to

incorporate an extra expansion tank for brassboard testing. The fluid interface for the fuel cell stack was modified to adapt to an integrated gas-liquid separator which would be mounted directly onto the fluid reservoir.

A modification to the liquid retention valve system, based on experimental observations from brassboard operation, was performed to limit the valve close travel during periods of increased fluid flow. As shown in Figure 2, the integrated design is a complex shape to enable incorporation of the fuel feed pump, the fuel isolation valve, the liquid recirculation pump, methanol sensor and the liquid level measurement board, into a form which fits the integrated package design.
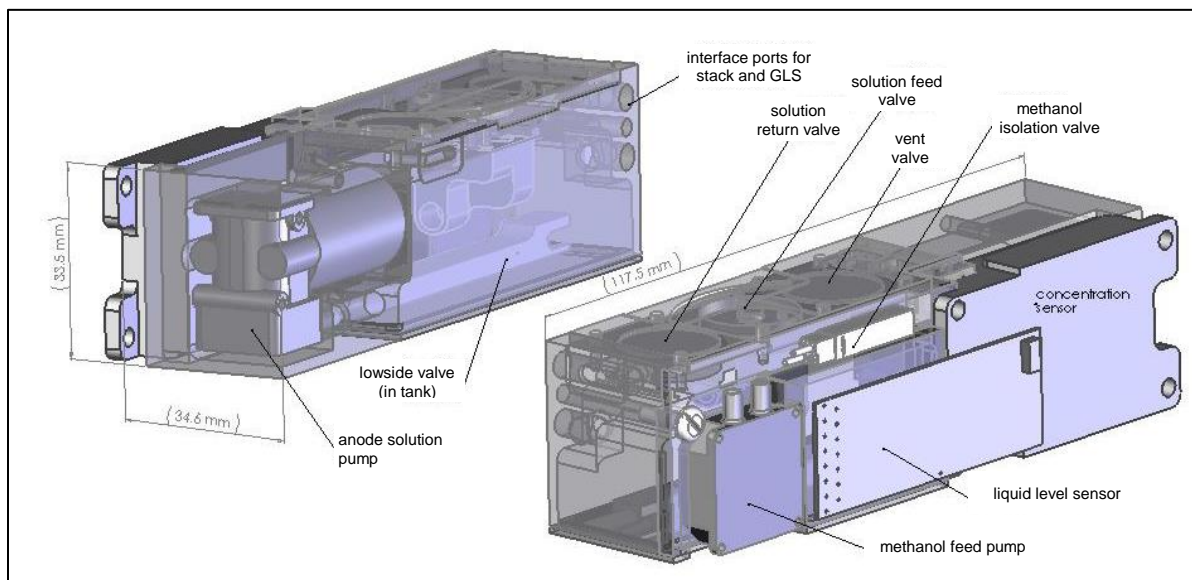

Figure 2 Integrated fluid recirculation tank sub-assembly

Fuel Cartridge

The fuel cartridge design follows a similar path to what is done in the DMFC industry – a 'bag in box' approach. The fuel cartridge detailed design was conducted, including interface & latch design. Positive shut-off fitting by CPC are used on each side of the fuel cartridge and power section to ensure liquid fuel does not drip from this interface when a fuel cartridge is removed or replaced.

Gas Liquid Separator

The stack fuel exhaust stream gas-liquid separator was further engineered and changes were made to improve its design principles. New materials were reviewed, new designs were tested, and durability was evaluated. This component utilizes the material properties of EPFE and appeared to suffer from 'wet-out' of the pore structure after extended use. Various designs

showed durability was sensitive to some design principles which is discussed in detail in the Gas Liquid Separator (GLS) section in the paragraphs that follow.

Electrical Subsystem

Initially, electrical subsystem development focused on the adaptation of DP3 system control boards and liquid level sensors to be tested on the DP4 brassboard system. A total of five control boxes were built using repaired, old-stock DP3, control boards. An external battery box was used, which provides both the SMBus communication signal back to the DP4 control box, but also enables testing of the brassboard using an external load bank (as compared to a laptop itself). Due to the improved reliability and repeatability of UNF-made MEAs, the DP4 system did not incorporate cell-voltage-monitoring (CVM), but this useful tool was desired for brassboard testing, so a lab-version CVM was designed and fabricated for this use.

The control boards that were adapted for the DP4 brassboard control board incorporated minor design changes in order meet the power requirements for new system components, such as the fuel feed pump, liquid recirculation pump, cathode fans, and input power isolation during shut-down.

The addition of a low power microcontroller and ideal diode were implemented into the new DP4 design in order to reduce parasitic loads during operation and sleep modes. The control and power boards replaced the single board used in the DP3 due to the integrated package volume constraints. These two boards mount on the opposite end of the fuel cell stack from the fluid recirculation tank assembly, and a flexible interface board is used to connect to the various components on the tank assembly.

The system has an internal hybrid battery to enable operation as a stand-alone power source without any need for external power. For this design, this is viewed as a key function; but, in the future, the internal battery may be in eliminated once the technology is integrated into a target device which has its own battery. Analysis of various startup algorithms was conducted and an appropriate, if not conservative, battery was specified. It contains approximately 20 W-hr of energy, and could accommodate the longest possible startup protocol including a scenario of a 'failed start' due to empty fuel cartridge (e.g., from a prior run), followed by a second start. In the first phase of operation, while the fuel cell is coming up to normal operating conditions, the net power of the fuel cell may be less than the target output power; hence the internal battery will drain, but thereafter will re-charge back to a healthy state-of-charge.

Task 2: Component Testing

Cathode Subsystem Development

Fan Testing

In order to choose the proper sized fan or blower, with the proper pressure and flow characteristics to support the DP-designs, a cathode subsystem development test cell was designed, constructed, and calibrated. The test cell is shown in Figure 3 and Figure 4.
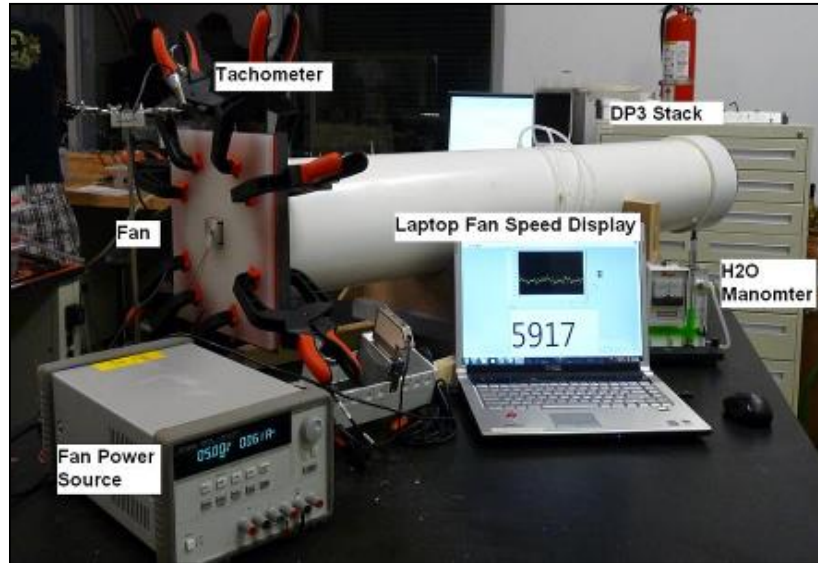

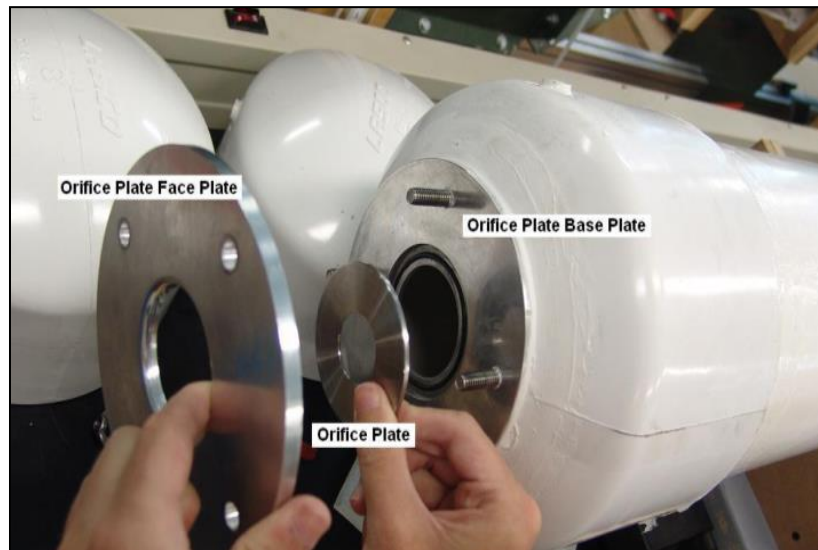**Figure 3** Cathode Fan Test Cell

Figure 4 Orifice plate mounting flange for cathode fan test cell.

The test cell was designed to allow testing of fans and blowers over a flow range of 0 to 400 standard liters per minute (slpm) against normalized pressure differences (normalized to atmospheric pressure) of 0 to 0.001 (or 0 to 100Pa). The flow and pressure calibration curves, shown for example in Figure 5, were produced by measuring the pressure drop across calibrated, sharp-edged, orifices produced by a carefully measured flow. Then, by running candidate fans and blowers at specific values of blade rotational speeds and measuring the associated pressure rise through the fan or blower against the load provided by the various orifices, a fan or blower characteristic map could be easily produced.
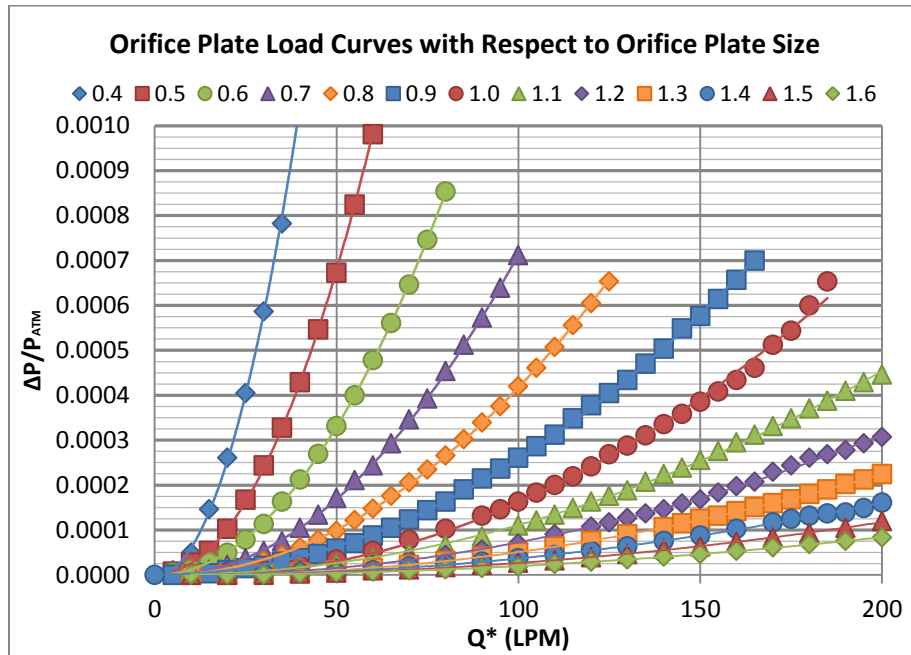

Figure 5 Orifice plate load curves with various orifice plate sizes in inches.

A typical characteristic map of a fan is shown in Figure 6. Also shown in the figure is the stack loading curve for the DP4 stack, i.e., the characteristic loading curve for that particular fan as applied by the flow passages in the DP4 stack.
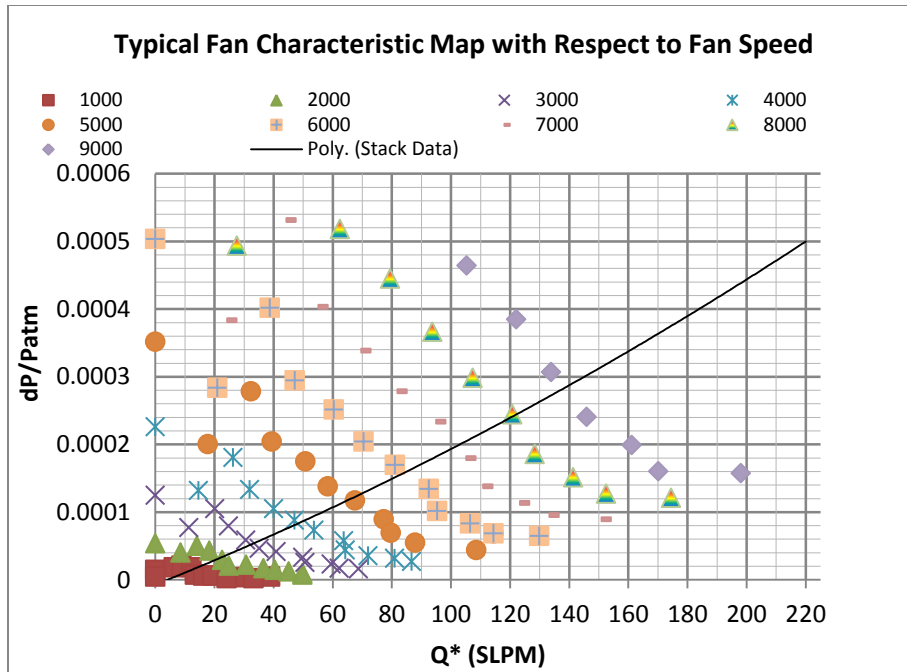
Figure 6 Typical fan characteristic map with stack load curve at various fan speeds.

In the design and analyses for the DP3 and DP4 devices (and the DP4 brassboard), over 50 different fans and blowers were tested in detail. These fans and blowers spanned types as diverse as crossover blowers, axial fans, axial-centrifugal fans, and centrifugal blowers. Being sought was a fan or blower that could supply the required pressure drop through the cathode flow system of the stack over the full flowrate requirement and at acceptable levels of parasitic electrical loads on the stack output. A four-ganged configuration of the Adda fans was found to meet these requirements and is shown in Figure 7.
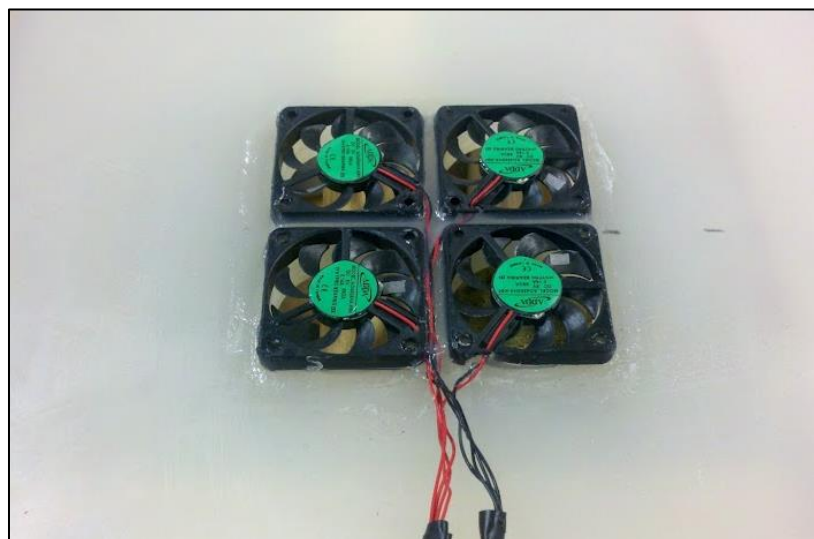

Figure 7 Four ganged configuration of ADDA fans for testing on cathode fan test cell.

The general application for fans of this type is to supply cooling air flow to electronic components. It was necessary to assure that the fans could operate in a relatively high temperature and high humidity environment, as much as 60°C and 100% relative humidity. Toward that end, the Adda AD4505HX-K90 axial fans were subjected to a 3000 hour accelerated lifetime test at 50°C to determine lifetime degradation. Eighteen of the fans were employed in three different configurations. Six fans were operated continuously against a near dead-head hydraulic load, six fans were operated in a start/stop (10 sec on/10 sec off) configuration, and six fans were operated against a load that matched the anticipated system load. Six fans were also operated at varied on/off times with the anticipated system load level. Two were operated 1 hour on/6 hours off; two were operated 3.5 hours on/3.5 hours off; and, two were operated for 6 hours on/1 hour off. The start/stop and continuously operated fans were mounted to shrouds for the degradation testing, which were not removed for performance testing. For comparison, a new fan was mounted to a shroud and tested to obtain new fan data. This performance testing difference shows up in the graphs below if comparing the six fans operated against the system load versus the twelve fans operated at elevated temperature.

The first three figures show the hydraulic power for the three sets of fans that were tested. Figure 8 displays data for fans operated against the anticipated system load at various intervals. All of the results showed an improvement over fan data from tests when the fans were new. It is highly unlikely that the fans improved in performance, so this is considered a negligible change. It is of interest to note that the fans operated at 1 hour on/6 hours off did show better performance than the fans operating at 6 hours on/1 hour off. The difference is small, but it should be noted. Original equipment manufacturer (OEM) performance can be expected from fans operated over these intervals for a 2000 hour lifetime with high confidence.
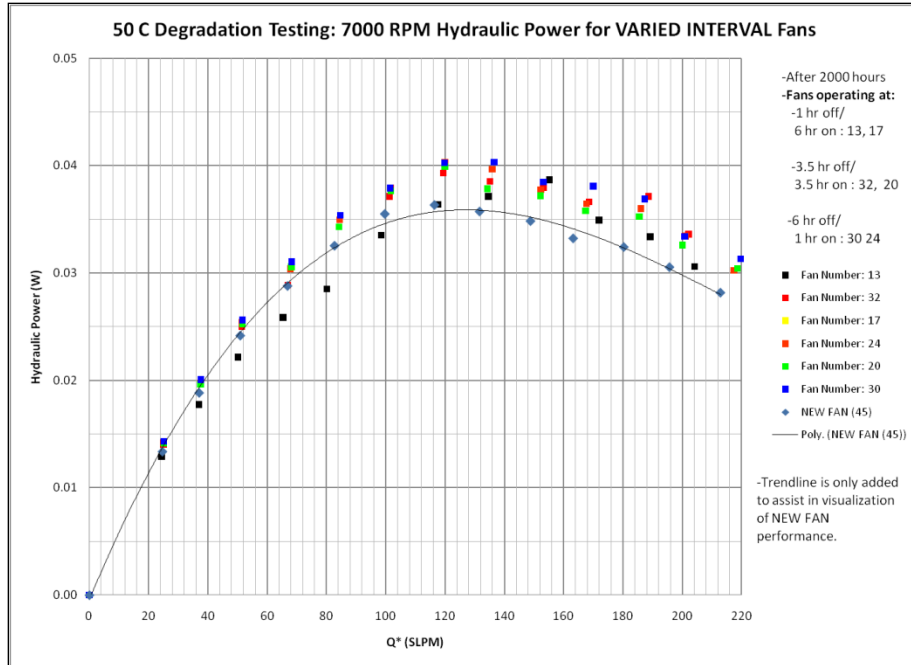
Figure 8 Fan hydraulic power for varied interval testing

Figure 9 shows the hydraulic power for fans that operated continuously for 2000 hours at 50°C. The results show that the performance is very close to the data from a new fan. Again, these data gave high confidence in the use of this Adda fan in the system.
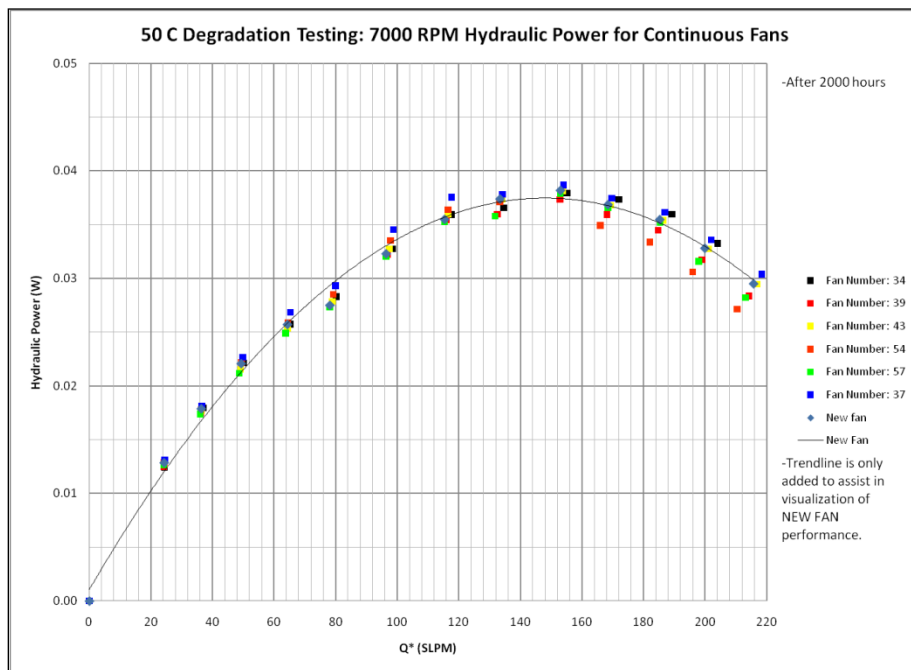

Figure 9 Fan hydraulic power for continuous operation

Figure 10 shows the hydraulic power for the fans subjected to the interval of 10 seconds on/10 seconds off. The performance of these fans does show some increased scatter relative to the data in the previous figure, but the change in performance is still acceptable. Even in the worst case (Fan 35), the fan can still meet the design requirements without requiring excessive electric power and decreasing the efficiency of the system.
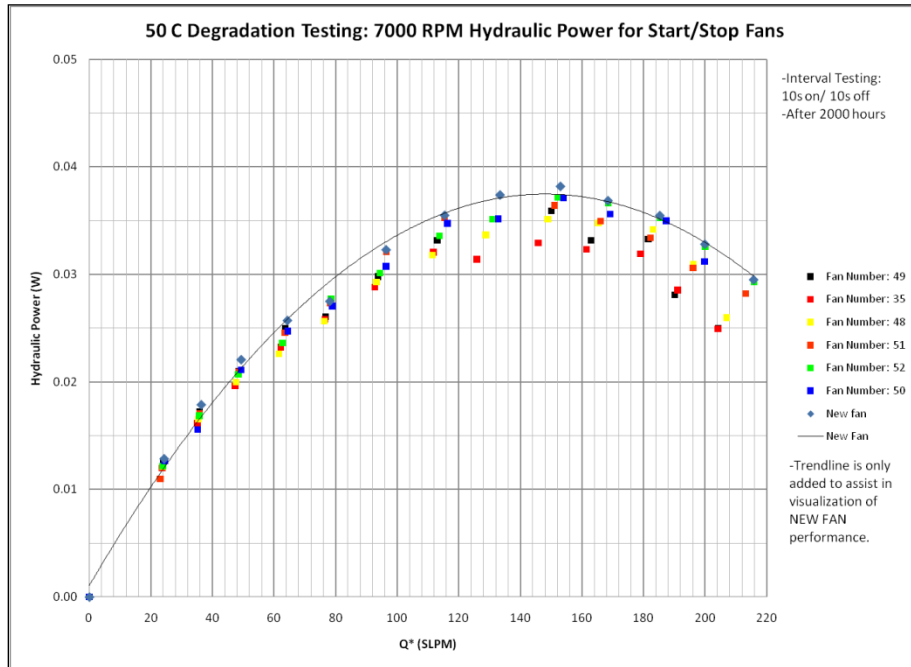

Figure 10 Fan hydraulic power for start/stop operation

The next three figures show the electric power requirements for the fans subjected to degradation testing. Figure 11 shows the electric power for the varied interval fans. Five out of the six fans follow the new fan data with negligible errors, with one slightly deviating (and that one at reduced power requirement levels).
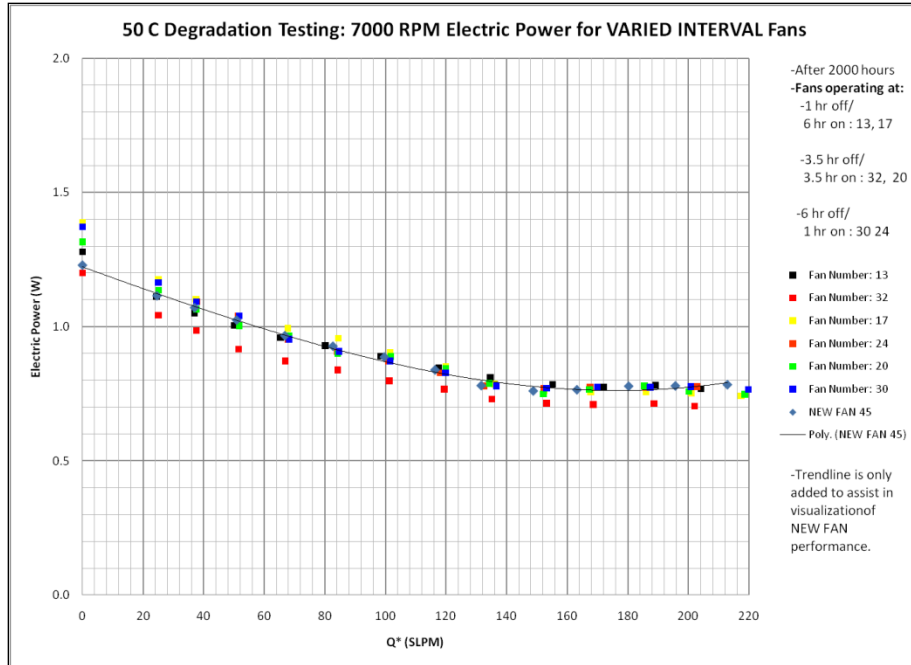
Figure 11 Fan electric power for varied interval operation

Figure 12 shows the electric power for the fans operating continuously for 2000 hours. The degradation data matches the new fan data very well.

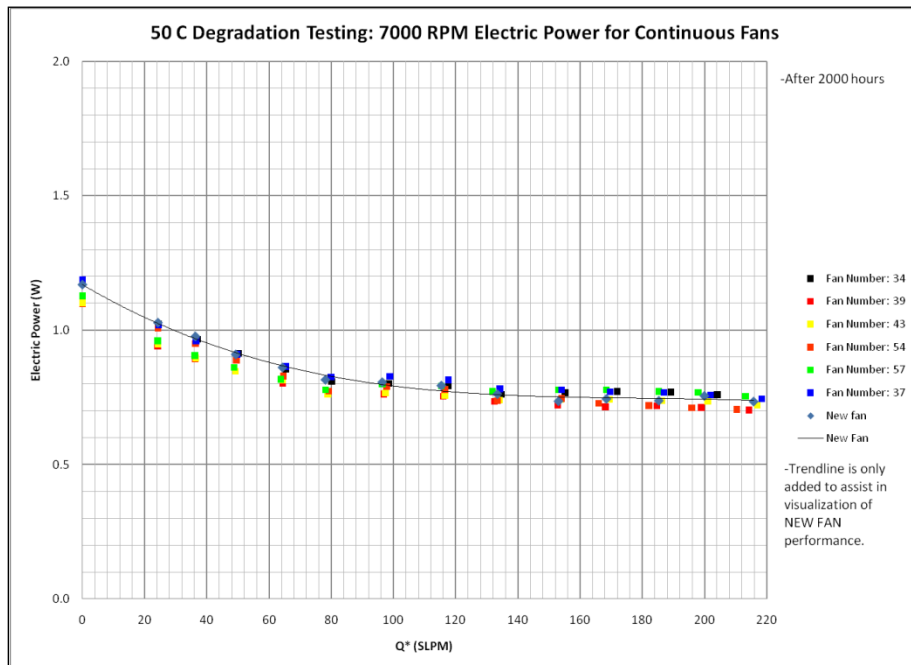
Figure 12 Fan electric power for continuous operation

Figure 13 shows the electric power for the start/stop testing. Fan 52 is the only fan that performed significantly differently than the other fans. The rest of the degradation data showed

that the rest of the fans match the new fan data with no substantial increases in electric power requirements. For this reason, the electrical power data associated with fan 52 is considered an outlier, and the data are not considered for these results.
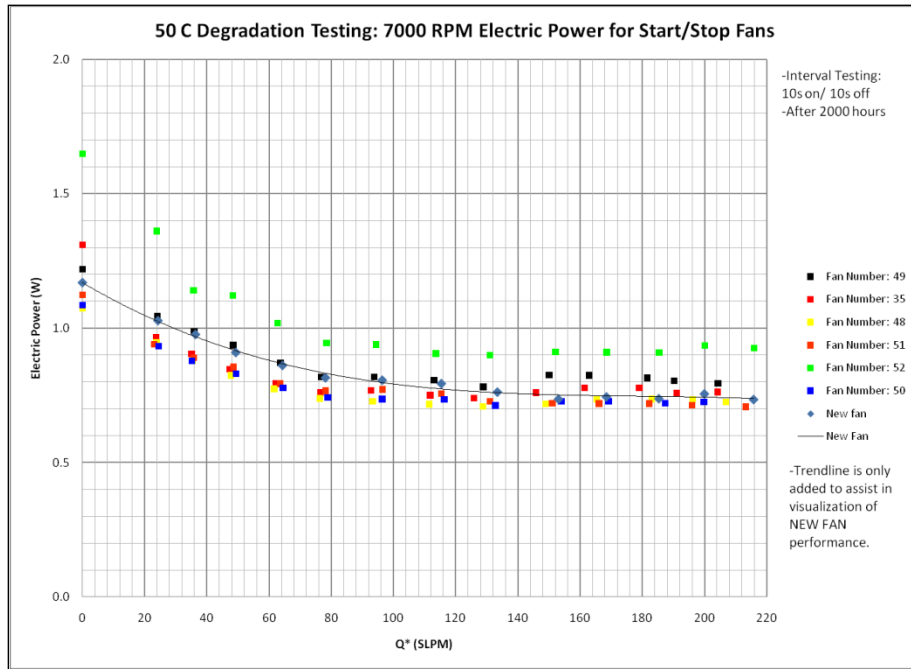
Figure 13 Fan electric power for start/stop fans

The last 3 figures represent the pressure rise vs. standard volumetric flow rate 7000 RPM performance curves for each of the degradation tests. Figure 14 shows the performance curve for the varied time intervals. The performance for each of the fans matches the new fan performance very well.

Figure 14 7000 RPM speed curve for varied interval operation

Figure 15 shows the performance curve for the continuously operated fans. The performance of the fans after 2000 hours of operation has not degraded significantly, if at all.

Figure 15 7000 RPM speed curve for continuous operation

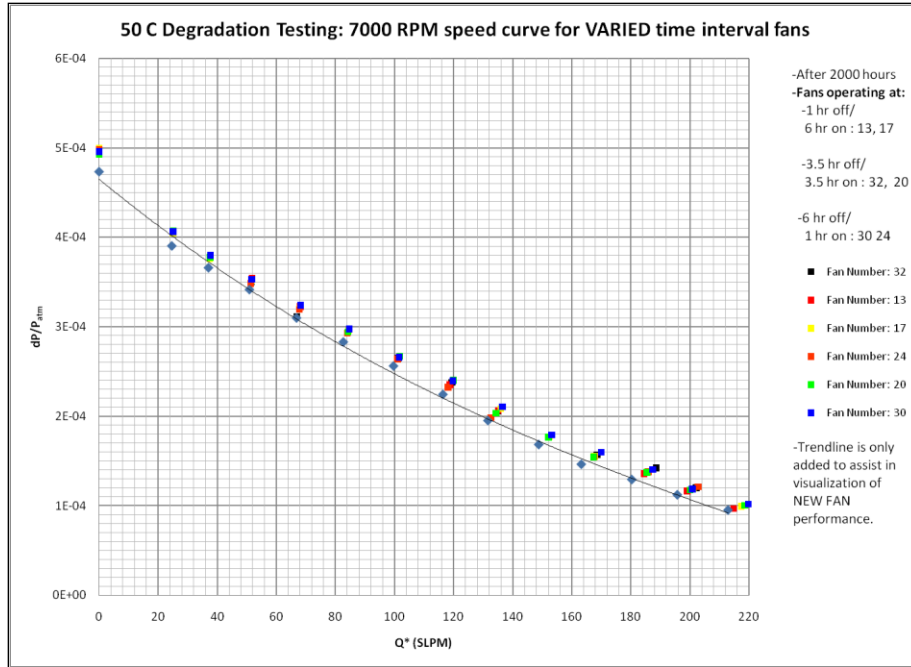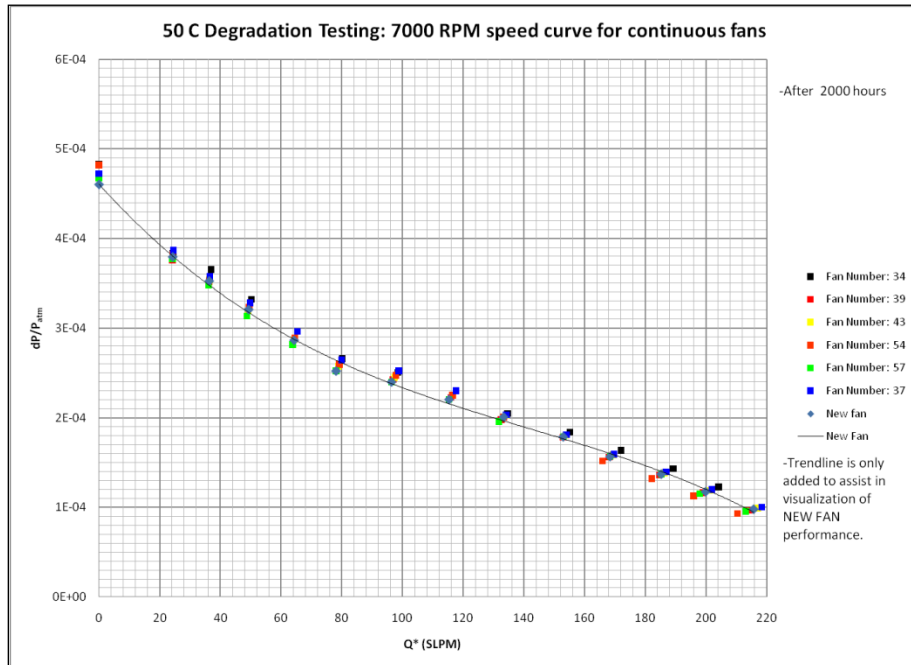Figure 16 shows the performance at 7000 RPM of the fans subjected to start/stop cycles. The performance of these does show a slight decrease. The change in performance is minimal though, and these fans can still meet the design requirements without requiring excessive electric power.
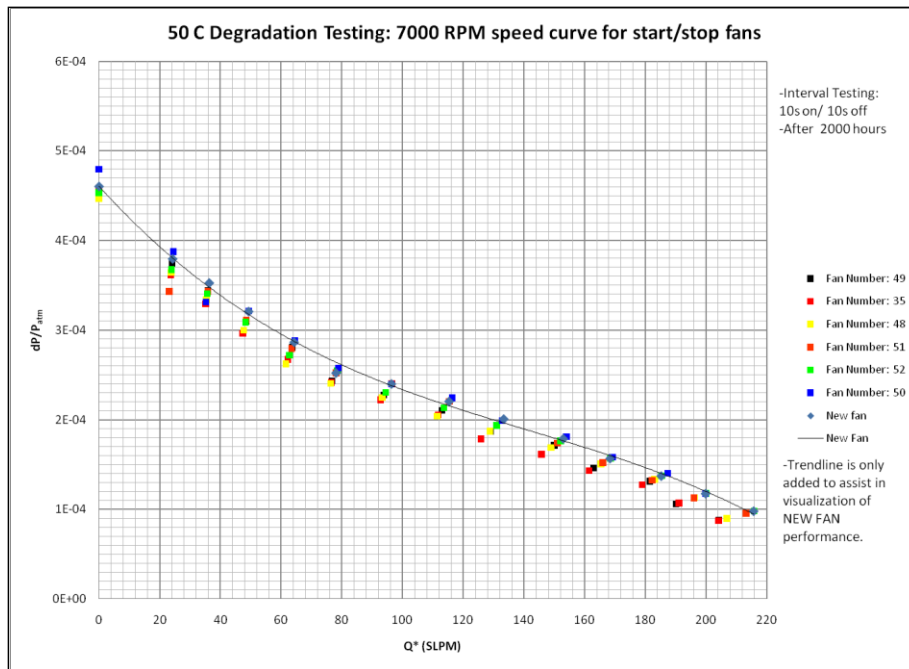

Figure 16 7000 RPM speed curve for start/stop operation

All of the fans were operating satisfactorily after the 2000 hours at 50 °C. Zero fans failed, giving the project team high confidence in these fans meeting and exceeding the system requirements throughout the life of the system.

Little to no variation in performance, relative to a new fan, was measured in any of the 18 fans tested after 3000 hours; therefore, they are not shown herein. It is important to note that two of the fans did seem to be experiencing a slight degradation in the hub bearing performance as they showed some resistance to initial start-up but almost immediately spun up to operating speed with no other problems for the duration of the tests. A statistical analysis of the expected fan lifetime based on the test results was initiated. It is beneficial to understand how well the manufacturer lifetime data matches the data collected by the project team (henceforth referred to as UNF lifetime data) in the case that a variation of the current fan was required (a similar model fan with a speed output wire was considered). In that case, over 3000 hours (per fan) worth of performance test data along with valuable resources could be saved by having confidence in the OEM-supplied lifetime data.

The literature review was initiated in search of typical analyses for lifetime experiments. Ideally an industrial standard for lifetime testing would have been found to which to compare the UNF data. However, no industry standards were found regarding fan lifetime analyses. A paper

published by IBM discussed the need for standardized life evaluation procedures back in 1994. The paper also covered typical acceleration factors for temperature for lifetime tests, which tended to vary between manufacturers. There were no acceleration factors presented for the type of an operation (continuous vs. start/stop), voltage above rated, and ambient environment, which would have helped for the results here at UNF. The paper also discussed that the use of the Weibull distribution provided the most accurate results for lifetime analyses due to the fact that it can account for wear-out, unlike an exponential distribution. However, for the Weibull distribution to be used, failures must have taken place around which the distribution could be formulated. A major factor discussed is the great dependence of fan operation on the bearings, and the grease within the bearings. Equations are presented for estimation of the grease life with parameters of the grease known. It would be ideal if Adda would have offered the information covering the particular parameters of interest for the grease used in their bearings. However, Adda uses a patented hypro-bearing and did not want to release information on it. It was assumed that this information would not be available and the project team was stuck with the results for the fan as a whole.

Y.S. Tech and Sunon both offer lifetime analysis examples for their fans. Y.S. Tech actually has produced a document detailing how to determine fan lifetimes from an accelerated test, shown in Figure 17.

Yen Sun Technology Corporation

MTTF calculating philosophy

Step.1 Evaluation how many testing time, t, we need.

The L_{10} Expectancy @ 40°C for YW09225012BSS-12 and YW08020012BS-6=<u>65000</u> (This value is what we expect our fan life according to product characteristics)

MTTF ≒ 7 × L_{10} =7 X 65000=<u>455,000</u> Hours

Y.S. TECH rely on a zero failure Weibull test strategy and accelerated testing technique, to determine the total test time (t):

$$t = 1.036 \times MTTF \times [(B_{r,c}) \div n]^{0.91} \div AF \text{ , and } AF = 2^{(Ts-Tu)/10} \text{ --------equation (A)}$$

Where

t: total testing time.(hours)

MTTF: mean time to failure.

AF: Accelerating factor contributed by temperature stress.

$B_{r,c}$: Poisson probability distribution factory with CI(confidence interval) defined.(Here we set CI equals 90% as a constant.) The suffix r means failure number and c means CI. This factor we could easily obtain from GEM table.

n: quantities of testing devices.(generally the quantities are 50 pieces for life testing)

Ts: Stress temperature what we set 80°C as a constant for life testing.

Tu: Un-stress temperature what we set 40°C

As MTTF is 455,000 hrs, $AF=2^{(80-40)/10}=16$, $B_{0,c}=2.303$ and n=50, we could calculate from equation (A) about how many total testing time we need for fan life evaluation. Here t is <u>1790</u> hours with zero defects found. (This means our actual testing time should be over 1790 hours with zero defects)

Step.2 Actual testing time we performed.

Take YW09225012BSS-12 for example, the actual testing time, T, could be obtained from test period column, 2007/02/27 to 2007/05/13.T is 1807 hours.

Note: We must confirm T is over t.

Step.3 Verified MTTF be calculated.

From equation (A), now we have T=1807,and AF=16, $B_{r,c}$ =2.303 and n=50 are as same as we apply in setp.1, finally we could derive from equation(A) that **Verified MTTF= T ÷(1.036×[($B_{r,c}$)÷ n]$^{0.91}$÷AF)**.Here the verified MTTF is <u>459,297</u> hours.(Verified MTTF is also over MTTF we assumed at first)

Step.4 Verified L_{10} be calculated from verified MTTF.

Since MTTF ≒ 7 × L_{10}, we could get the verified L_{10} as we already get the verified MTTF.

Finally, the verified L_{10}≒MTTF ÷ 7=459,297÷ 7=<u>65,614 hours @ 40°C</u>.

Figure 17 First page of Y.S. Tech fan lifetime testing description

However, the method according to Y.S. Tech uses a GEM table, or a generalized exponential model. The IBM paper showed that the exponential model was not as accurate as the Weibull distribution; however, it is unclear whether or not the GEM table is based on the exponential model. The lifetime data supplied by Adda does also refer to this GEM table, so this should be acceptable. Regardless of the results presented by the IBM paper, it was at least a good start to approach the lifetime data with the Y.S. Tech philosophy. This test method involves four steps:

1. Evaluation of test time

2. Actual test time

3. Verification of mean time to failure (MTTF)

4. Verification of time for 10% of the fans to fail (L10).

This method assumes that a lifetime test is being designed for a particular fan. The UNF testing was already complete; however, the procedure from Y.S. Tech was modified to work. Using the Y.S. Tech philosophy and the UNF lifetime results, three separate cases were investigated. For all cases, the rated temperature was assumed to be 30°C, at which Adda rates their fan lifetimes. In the first case (case 1), no acceleration factors were considered. As 18 fans were tested for 3000 hours apiece, the total test time was 54,000 hours. With a 90% confidence interval and zero failures, the MTTF for this case was 8023 hours. In other words, all of the fans tested would fail at 8023 hours, on average. The anticipated time for 10% of the fans to fail, the L10, was calculated to be 1146 hours. This result is not realistic, as none of the 18 fans tested failed within 3000 hours.

A second case (case 2) was considered where the acceleration factor for temperature was included. The acceleration factor for temperature assumes that fan life is halved for every 10 °C rise in operation temperature. Therefore, there would be an acceleration factor of four (4) relative to case 1. The resulting MTTF for this case would be 32,100 hours and the L10 would be 4590 hours. The results from case 2 seem much more reasonable than case 1. However, there is a voltage acceleration factor that was also found from a link on Y.S. Tech's webpage. The voltage acceleration factor simply takes the ratio of the test voltage over the rated voltage. For the test performed at UNF at 50 °C, the test voltage for the fans was 6.5 volts, resulting in an acceleration factor of 1.3. The third case considered included both the temperature acceleration factor as well as this voltage acceleration factor. The resulting MTTF in this case was 41,720 hours and the L10 was 5960 hours. Similar to case 2, these results are much more realistic than the results from case 1.

From these results it seems reasonable that the previously described acceleration factors should be included for accurate lifetime measurement. However, there should also be an acceleration factor for fan hydraulic loading during the test as well as the operation interval. Start/stop testing is more strenuous on the fans than continuous operation. The results presented from the 2000 hour lifetime testing on the Adda fans showed that fans operated continuously did show slightly better performance than the fans operated in start/stop intervals. There never was an acceleration factor found for either of those conditions.

Another lifetime test performed on the Adda fans consisted of fan operation at an elevated temperature of 50 °C in a near-condensing environment with raised levels of CO_2. These fans were powered using a type of pulse-with modulation (PWM) similar to that on the DP4 brassboard. This test was initiated after multiple sets of fans indicated potential start-up issues after operation in the brassboard for only weeks of time. As the fans are in the exhaust stream (they pull air through the stack), they are exposed to highly humid air with raised levels of CO_2. The fans in the brassboard are also powered by a type of PWM at times, which is not recommended for some of the brushless dc motor fans. One of these factors, either the ambient conditions, or the PWM power supply, was thought to be causing the potential starting problem.

A lifetime value for the test was not determined since fan degradation was expected within 1000 hours (based on the *ad hoc* brassboard data).

Thus, the Adda AD4505HX-K90 axial fans employed in the DP4 design prototype system were subjected to this accelerated lifetime test for more than 4000 hours (4368 hours). The results from this testing is described in two sections. The first section investigates the anticipated lifetime that should be expected from the fans. The second will determine if the performance of the individual fans after this extended duration of operation in the accelerated environment has changed.

The lifetime results have been analyzed and the performance of the fans over the 26 week duration of testing can be seen in Figure 18. Even after approximately four months in this CO_2-rich, high temperature and humidity, environment, with conditions thought to cause faster degradation, and being powered with a type of pulse width modulation, there was no evidence of degradation.
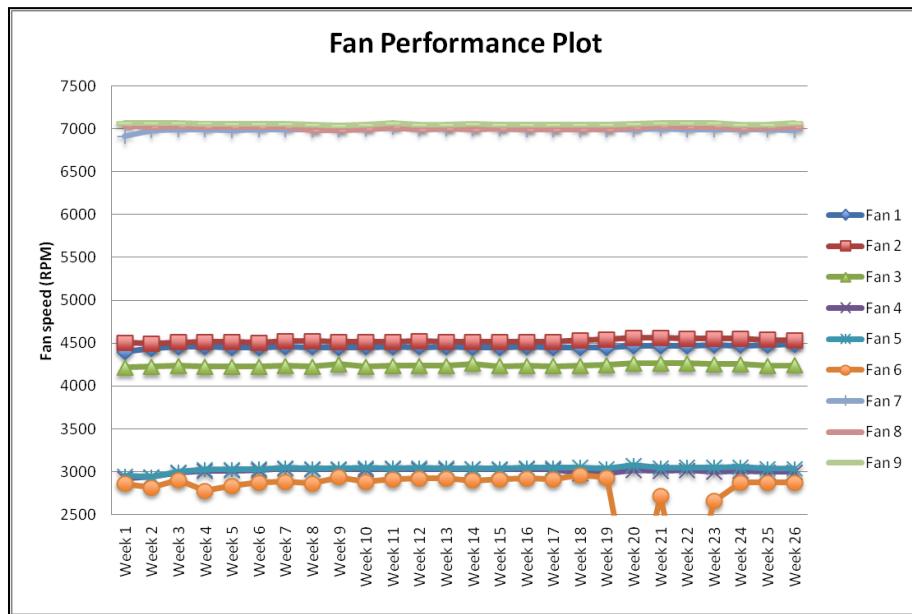
Figure 18 Fan performance vs. 26 week test duration

As previously mentioned, nine axial Adda fans were present for this test. Six of the nine were in the accelerated environment, where three of them were located outside of the environment to have a reference to help determine if the accelerated environment caused more degradation than just the extended fan operation. The lifetime results were analyzed using the method identical to that of the manufacturer, the Adda Corporation. This method includes the assumption that the fan failure rate follows an exponential distribution and such that a generalized exponential model (GEM) should be followed for a time-terminated test, as this lifetime test was. The MTTF is then a function of the total test time and failure quantity. In this test, eight fans operated for 4,368 hours, while one fan ran for 3,868 hours. There were no

failures for the test, and from the GEM table, a value of 2.3026 should be used. The MTTF is the total time divided by the failure rate value from the GEM table. The resulting MTTF is 16,855 hours. The expected time for ten percent of the fans to fail is the L10 value. The L10 value is the MTTF divided by 7. The L10 value for these fans is 2,407 hours. The anticipated system lifetime is 2,500 hours currently, which offers confidence when operating with four of these axial fans in the system that none of them will fail within the system lifetime.

The individual fan performance was also investigated to determine if any 'wear-out' had occurred. This would have shown up as altered fan performance as the test time increased. From reviews of manufacturers' data, it is very common that if 'wear-out' occurs, the fan speed will increase as the test time increases. However, when viewing individual fan performance against time, none of the fans exhibited this feature commonly associated with fan 'wear-out'. This signifies fan 'wear-out' did not occur for this lifetime test. Therefore, the project team is confident the fans can operate in the fuel cell stack exhaust stream without worrying about degradation due to the composition of the stack exhaust.

At first glance, it seems that this test is not truly investigating the cause of degradation in these axial Adda fans. However, it does seem that there have been no reported problems with the DP4 brassboard in the last few months. It may have been a separate problem causing only a few of these fans to show degradation after only a few weeks on the brassboard, but that is hard to determine. This issue has been closely monitored with no recurrence of the problem.

Stack Flow Distribution Testing

Another aspect of the cathode blower subsystem under investigation was the airflow distribution through the passages in the fuel cell stack. The primary concern of the cathode blower/fan is to supply the necessary airflow for sufficient oxygen to reach the cathode reaction sites as well as to maintain the thermal system balance. Therefore, uniform airflow distribution to the cell passages is important. A major factor that can impact this airflow distribution is the offset distance between the fuel cell stack exit and the fan inlets. Ideally, this dimension would be minimized to satisfy volumetric constraints, and the fans would be placed as close as possible to being flush with the stack. However, when placed in that configuration, there can be insufficient airflow through the corners of the stack (i.e., four round fans generating airflow through a rectangular stack), leading to potential air starvation and overheating, which can permanently damage the stack.

For this reason, once a candidate fan was selected, experiments were designed and performed to quantify the effect of varied offset distance. The experiment consisted of a 2-D scan of the entrance of the fuel cell stack using a hot film anemometer to determine the airflow's velocity as it enters the stack. An example of a flow diagram can be seen in Figure 19.
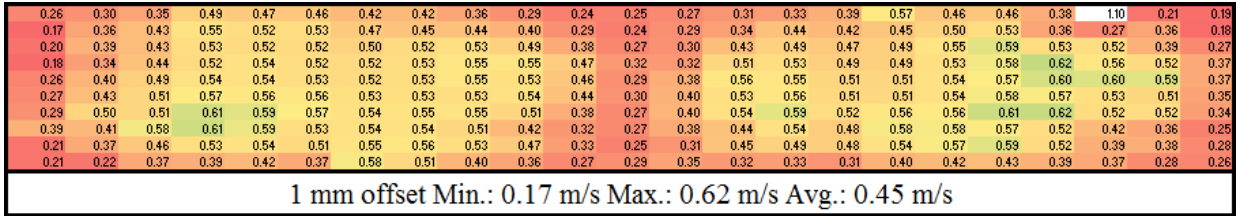
0.26	0.30	0.35	0.49	0.47	0.46	0.42	0.42	0.36	0.29	0.24	0.25	0.27	0.31	0.33	0.39	0.57	0.46	0.46	0.38	1.10	0.21	0.19
0.17	0.36	0.43	0.55	0.52	0.53	0.47	0.45	0.44	0.40	0.29	0.24	0.29	0.34	0.44	0.42	0.45	0.50	0.53	0.36	0.27	0.36	0.18
0.20	0.39	0.43	0.53	0.52	0.52	0.50	0.52	0.53	0.49	0.38	0.27	0.30	0.43	0.49	0.47	0.49	0.55	0.59	0.53	0.52	0.39	0.27
0.18	0.34	0.44	0.52	0.54	0.52	0.52	0.53	0.55	0.55	0.47	0.32	0.32	0.51	0.53	0.49	0.49	0.53	0.58	0.62	0.56	0.52	0.37
0.26	0.40	0.49	0.54	0.54	0.53	0.52	0.53	0.55	0.53	0.46	0.29	0.38	0.56	0.55	0.51	0.51	0.54	0.57	0.60	0.60	0.59	0.37
0.27	0.43	0.51	0.57	0.56	0.56	0.53	0.53	0.53	0.54	0.44	0.30	0.40	0.53	0.56	0.51	0.51	0.54	0.58	0.57	0.53	0.51	0.35
0.29	0.50	0.51	0.61	0.59	0.57	0.54	0.55	0.55	0.51	0.38	0.27	0.40	0.54	0.59	0.52	0.56	0.56	0.61	0.62	0.52	0.52	0.34
0.39	0.41	0.58	0.61	0.59	0.53	0.54	0.54	0.51	0.42	0.32	0.27	0.38	0.44	0.54	0.48	0.58	0.58	0.57	0.52	0.42	0.36	0.25
0.21	0.37	0.46	0.53	0.54	0.51	0.55	0.56	0.53	0.47	0.33	0.25	0.31	0.45	0.49	0.48	0.54	0.57	0.59	0.52	0.39	0.38	0.28
0.21	0.22	0.37	0.39	0.42	0.37	0.58	0.51	0.40	0.36	0.27	0.29	0.35	0.32	0.33	0.31	0.40	0.42	0.43	0.39	0.37	0.28	0.26

1 mm offset Min.: 0.17 m/s Max.: 0.62 m/s Avg.: 0.45 m/s

Figure 19 Stack Uniformity at 1mm standoff distance

Figure 19 depicts the airflow through the stack with the fans flush against the stack. Lightly colored areas correspond to high flow areas. It is important to note that peak airflow occurs in stack channels directly adjacent to the fan blades. Channels that are not adjacent to the fan blades' swept area have drastically reduced airflow. Figure 20 shows a similar image but with an increased offset distance.
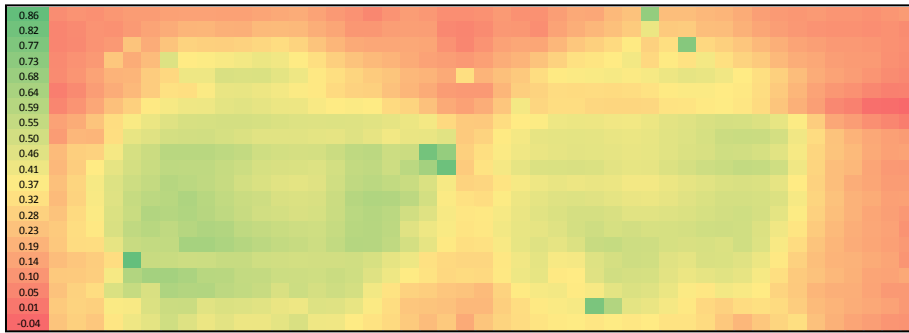

Figure 20 Sample data revealing areas of varying flow

To fully quantify the relationship between airflow distribution uniformity and offset distance, this experiment was repeated for the following offset distances (mm): 0, 5, 10, 20, 54, and 100. Sample results are displayed in Figure 21.
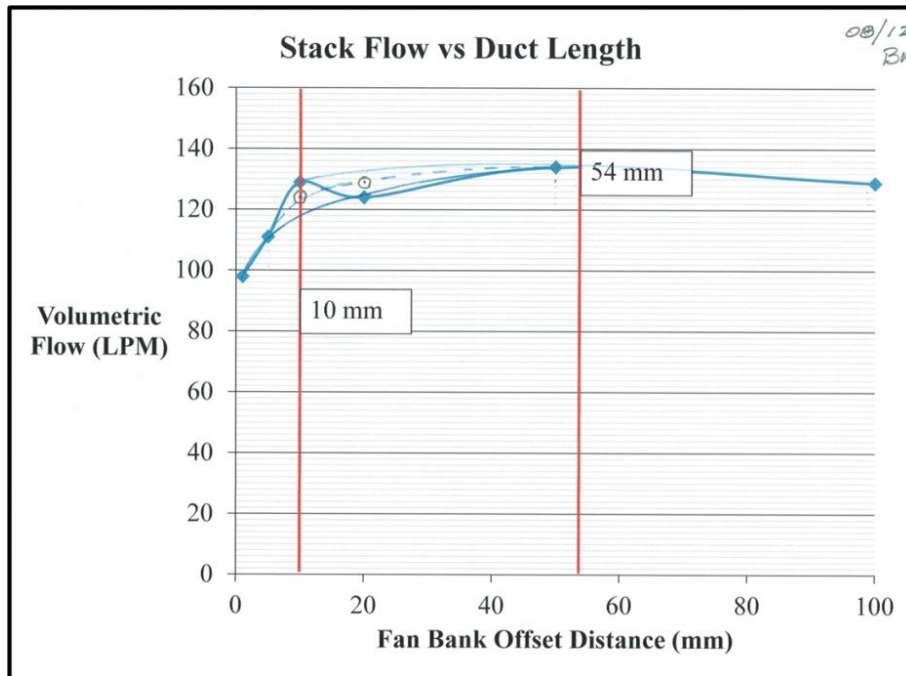
Figure 21 Overall flow rate as a function of duct length

Figure 21 shows the relationship between stack offset distance and total volumetric flow rate through the fuel cell stack. The reduced performance at lower offset distances signifies that the length of the duct between the fan inlet faceplane and the stack exit plane changes the airflow distribution across the inlet side. As the fans are positioned closer, the fan volutes and sharp angles through which the air must flow impedes the inlet velocity, reducing flow uniformity and therefore overall flow rate. For the DP4 experiments performed, flow drops off significantly at 10 mm. Continuing testing resulted in prescribing offset distances of between 5 and 10mm were acceptable.

Methanol Sensing

Because knowledge of the methanol concentration is essential for efficient operation of any DMFC system, a test bench was developed for testing methanol concentration sensors that might be suitable for the DP4 device. The test bench enables the measurement of sensor accuracy, transient response, pressure loss, and sensor drift with respect to temperature and flow rate.

Several methanol sensing technologies that measure physical properties of methanol solutions have been investigated by the project team. These properties include surface acoustic wave propagation, heat capacitance, density, viscosity, refractive index and electrochemical techniques.

ISSYS Density Based Methanol Sensor

The previous sensor used in the DP3 system, the ISSYS FC6 shown in Figure 22 below, has proven to be problematic in the areas of robustness and long-term accuracy. The ISSYS sensor is shown in the figure alongside a Siargo TSC-2000 sensor, which proved to be unsuitable due to shock sensitivity as discussed in the section on the Siargo Thermal Conductivity Based Methanol Sensor

The ISSYS device, while not shock sensitive, was found to have problems with drift and zero offset, but otherwise to be satisfactory.

Figure 22 The ISSYS FC6 sensor shown at right with the Siargo TSC-2000
sensor at the lower left.

UNF has worked closely with the manufacturer of the ISSYS sensor used in the DP3 system, the ISSYS FC-6, to upgrade the sensor with several improvements in the key areas of robustness and long term accuracy. The new sensor from ISSYS was denoted as the FC-10. Like the FC-6, the FC-10 employs microelectromechanical systems (MEMS) technology and operates principally as a density meter. Several of these devices were tested for accuracy and repeatability as seen in the results shown below in Figure 23.
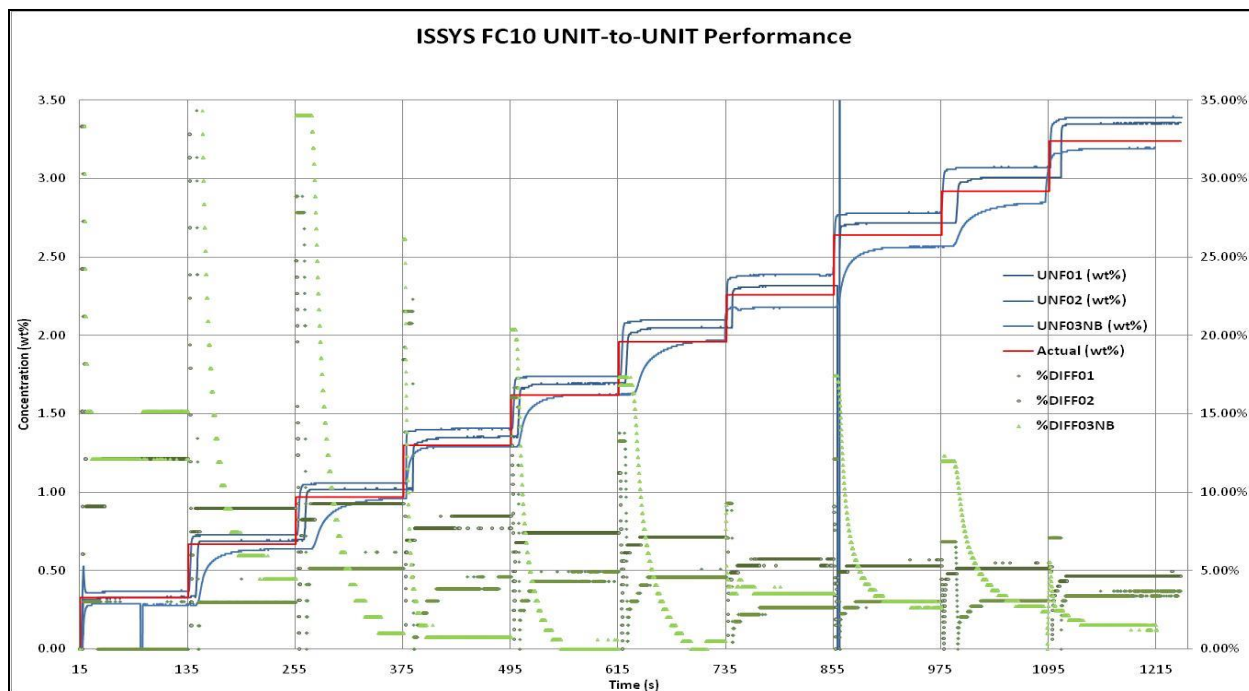
Figure 23 Results above were taken from testing three different FC-10 devices for solutions ranging from 0.1 – 1.0 M with a step change of 0.1M. Error results are also shown at the lower portion of the graph.

After a rigorous series of testing, the FC-10 was selected as the primary methanol sensor candidate. The results of this testing revealed much improvement over the first generation sensor used in the DP3 system, the FC-6. Improvement was observed specifically in repeatability, as the FC-10 did not exhibit the same drift in measurement over time at room temperature (i.e. 20 ^{0}C) as the earlier model. The FC-10 was able to meet the majority of the requirements outlined in the CDR; however the primary deficiency is its relatively high weight and volume.

Furthermore, testing revealed a temperature sensitivity with respect to the measured methanol concentration over the range of operating temperatures for the system (5 – 65 ^{0}C). The sensors were exposed to solutions of known concentrations at incremented temperatures along this range, allowing the sensor to reach a steady state temperature for each test. This experiment demonstrated that the sensor has a temperature sensitive response, and the results are shown in Figure 24.

The key point in understanding the data in Figure 24 is that the concentration of the solution is not changing, but the concentration output of the FC-10 is since the density of the solution, which is being reported by the sensor as concentrations, changes. That is, as temperature increased during each test at fixed concentration, the reported concentration increased.
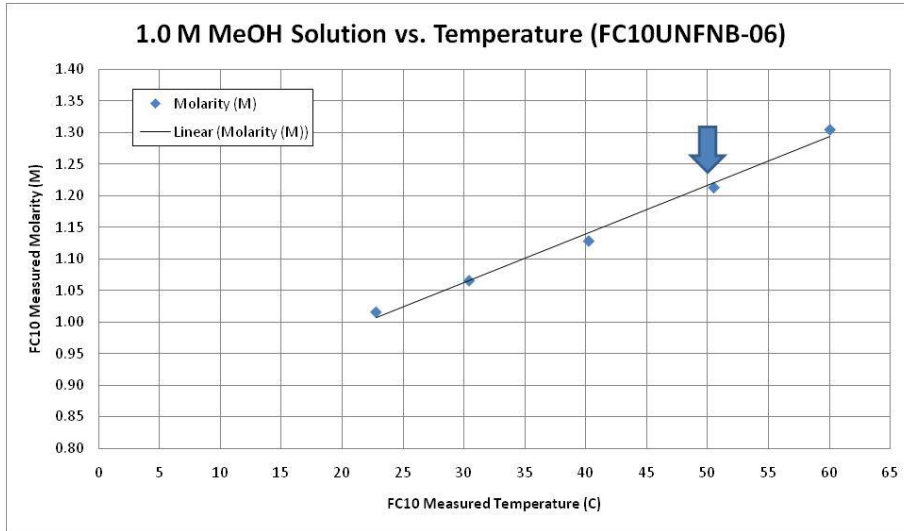
Figure 24 Concentration and temperature measurements taken from an FC10 sensor for a fixed 1.0 M methanol solution heated to various temperatures.

At the nominal system operating temperature of 50 ^{0}C, an error of approximately 20% was observed in the sensor concentration reading. At lower molarities (e.g. 0.7 M), this type of behavior would put the fuel cell stack at risk of fuel starvation, and potentially shorten the life of the stack. To further characterize this sensitivity, the effect of concentration under these conditions was examined in the range of normal operation (0.6 − 1.6 M). Linear curve fits of these data for the tested molarities were critical in formulating a system temperature compensation equation shown below. The actual value of molarity, then, is used in setting the operating point of the device.

$$M_{Actual} = M_{Measured} - 0.0075 * T_{Sensor} - 20$$

Shock testing was conducted for the FC-10 sensor through a series of 1-m drop tests. The first series of preliminary drop tests revealed challenges in maintaining a clear and repeatable drop. The preliminary drop test series consisted of five individual drop tests. The sensor was first characterized before subjection to drop testing and then following each subsequent drop test. A sample of results from this testing are shown below in Figure 25.
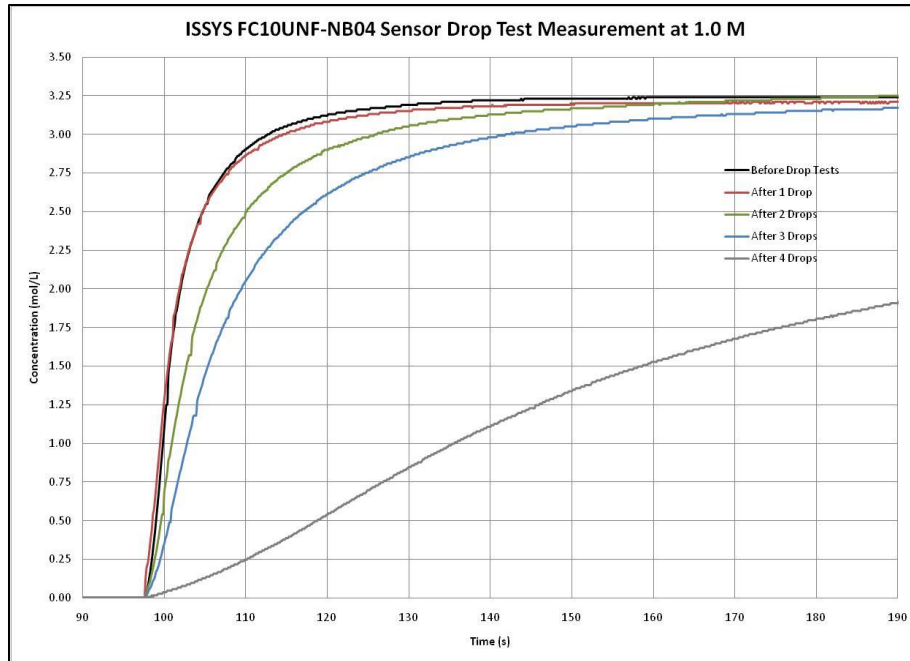
Figure 25 Data taken from ISSYS FC10UNF-NB04 methanol concentration sensor during preliminary drop testing.

The data from Figure 25 suggest that a single shock equivalent to a 1 m drop on concrete will not compromise the integrity of the sensor's concentration measurement. The data also show that subsequent drops have some effect on the time response of the sensor. It was noteworthy however that only the fourth drop affected the sensor's accuracy. A suggested hypothesis for this phenomenon was that particulate from the walls of the internal flow path of the sensor has become dislodged from the impact and is now blocking part of the flow path. This was confirmed in part because the test flow rate through the sensor decreased by more than 50%. In addition, the blockage must be occurring somewhere in the flow path other than the micro measurement u-tube due to the fact that added mass in the tube would have a significant impact on the accuracy of the concentration measurement. Discussions with ISSYS have resulted in a consideration by them relative to increased inspections of the devices but these tests have not been rerun with newly inspected sensors.

During the temperature sensitivity characterization of the ISSYS methanol concentration sensor, endurance tests at the system operating conditions of 0.8 M methanol solution at 50 °C revealed several sensor failures, all of which had the observed sensor reading of the error data form XX.XX for temperature and concentration. Due to the increasing number of these failures, a meeting was arranged at the ISSYS facility in Ypsilanti, MI, with the micro-fluidic division personnel to discuss possible failure mechanisms and solutions.

During the visit to their facility, it was discovered that other ISSYS customers and internal testing had both revealed similar failures as UNF, of which three primary failure modes were

identified. In this analysis, it was determined that the failure mode for all UNF sensors was due to water or solution ingress from epoxy failures between the MEMS chip and internal sensor header. In all cases for UNF sensors, the chip had completely separated from the header or was essentially leaking water into the sensor's internal cavity. Accelerated testing of the epoxy bond, as seen in **Figure 26** below, was conducted by ISSYS to determine the conditions of this failure.
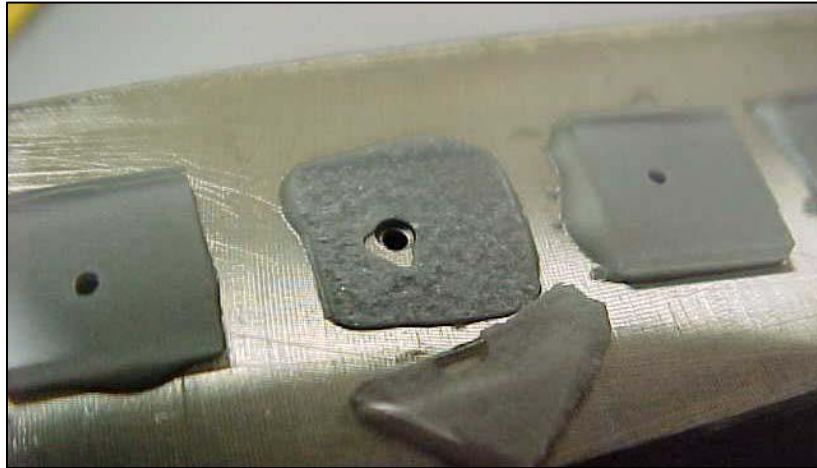

Figure 26 Accelerated epoxy testing apparatus showing the stainless steel header with several test sites of which one has experienced a failure.

Figure 26 above shows the stainless steel header constructed to allow for 10 MEMS chips to be applied using the current epoxy. The headers with MEMS attached were then soaked long term in various fluids (pure methanol, pure ethanol, DI water, etc.) at 60 °C. After hot soaking the headers in fluid, they were placed in a separate oven at 80 °C under high pressure cyclic loading (900 – 1000 psi). Of the fluids used in the hot soak, DI water and aqueous solutions were found to cause the greatest number of failures. This finding was consistent with the failures seen in UNF laboratories and systems (i.e. pure water, 1.0M solutions). A process was initiated by ISSYS personnel to select and test new chemically resistant epoxies, and from this testing an epoxy was selected that outperformed the former by a factor of 3 at minimum and a factor of 8 at the maximum.

A resolution to the UNF sensor failures was identified, and relations between the project team and the micro fluidic division were greatly improved. Discussion was also initiated concerning the possibility of a custom ISSYS build for use in the UNF fuel cell system. To date, no new epoxy FC-10 methanol sensors have failed.

Japan Radio Corporation Surface Acoustic Wave Based Methanol Sensor

Another methanol sensor that was investigated measures the surface acoustic wave (SAW) within the methanol solution. The prototype sensor, shown in from Japan Radio Co. (JRC), has two parallel piezo-elements over which surface waves are propagated. One element surface is in complete contact with the methanol solution and the other is electrostatically shielded, but still in

mechanical contact. The difference in coupling to the methanol solution changes the relative impedance of the two elements, and the difference is measured in the phase shift of the two signals (waves) as they arrive at the opposite end of the sensor. The device has the advantages of less volume required than the ISSYS sensor, Figure 27.
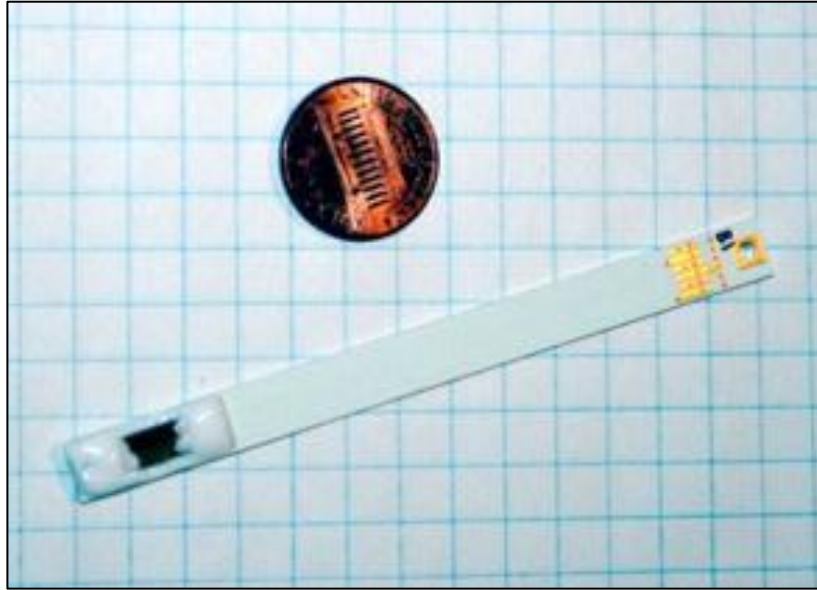

Figure 27 SAW device sensing elements at the lower end of the substrate in view.

The initial prototype JRC sensor was tested, and the results shown below in Figure 28 and Figure 29 were both promising and concerning.
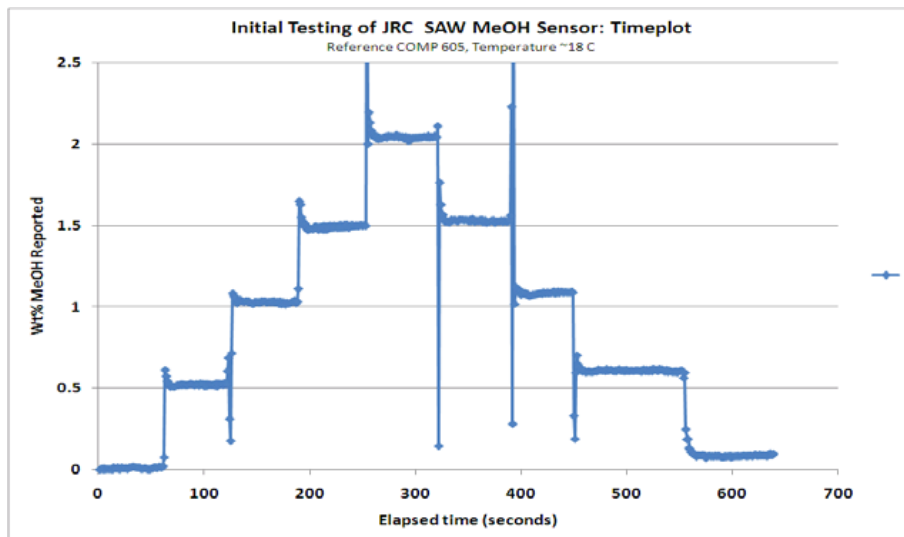

Figure 28 Data taken from a JRC prototype surface acoustic wave sensor over a range of methanol concentrations (0.0 - 2.0 M).

The initial test data from Figure 28 shows that the device is very fast in detecting changes in solution strength. To achieve the data shown in Figure 28, the sensor was moved from beaker to beaker of different solution strength methanol.
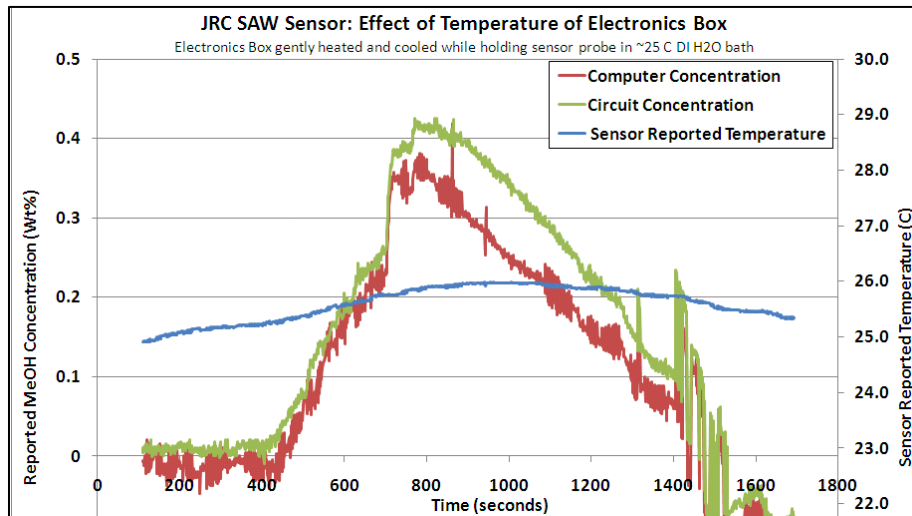

Figure 29 Temperature and concentration data taken from experiments that were conducted to analyze heat effects on the electronic circuit controlling the JRC sensor.

Further testing indicated a drift in the concentration reading over time. Through additional testing, it was discovered that the drift was largely, and perhaps entirely, related to the temperature of the support electronics and not the sensor device itself. In Figure 29, the electronics box was heated with a hot air gun for a total time of 800 seconds. The box was then allowed to cool for an equivalent time. Throughout this heating and cooling experiment, the sensor and the solution were kept at a constant temperature. Due to the nature of prototype devices and the lack of support with the SAW sensor, it was determined that the SAW sensor could not be developed in time to be implemented in the DP4 system.

Siargo Thermal Conductivity Based Methanol Sensor

An alternative technology that was investigated is the thermal conductivity sensor from Siargo Inc., also seen in Figure 22. The sensor's operating principle is based on a comparison of the thermal conductivity of the sensor's substrate and the test fluid in the region of the sensor's heaters. The first generation of these sensors proved even more fragile than the ISSYS sensor, as seen from Figure 30 (a) and (b) below.
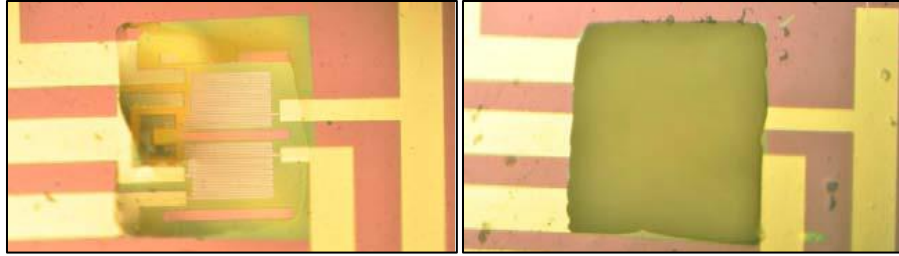
Figure 30 (a) This 10X image of a TSC-2000 sensor shows significant membrane cracking along with (b) that shows the entire portion chipped away from the sensor.

A second generation of the thermal conductivity sensor was produced by Siargo with a thicker membrane and was tested at the UNF laboratory. Testing revealed that the technology is still immature for methanol sensing in a DMFC power supply.

Nomadics/TI Spreeta Refractive Index Based Methanol Sensor

The project team identified another potential candidate methanol sensor that measures the refractive index of the solution to determine methanol concentration. This sensor is a developmental device that was first introduced by Texas Instruments for use in the methanol sensing market. It is now being used in the biomedical industry for identification of proteins by Nomadics, Inc. The sensor operates by utilizing a phenomenon known as surface plasmon resonance (SPR). Figure 31 below shows a sketch of the Spreeta sensor and the light path (shown in yellow) used in the SPR sensing method.
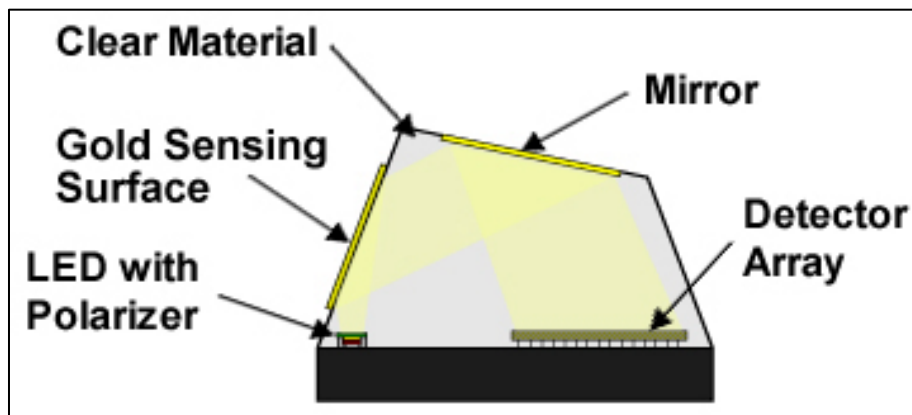

Figure 31 Sketch of the Spreeta sensor showing the light emitted and reflected internally onto the detector.

Polarized, near-infrared light is emitted by an LED onto a gold sensing surface that is near or in contact with the liquid being examined. The light is then reflected back via a mirror onto a photodiode detector array consisting of 128 pixels. The pixels are used to detect a minimum in the reflected light intensity; the point at which the SPR phenomena occurs. Essentially, surface plasmons (quantized electromagnetic waves moving parallel with and tangent to the gold sensing surface) interact with the light from the LED and produce a minimum on the output curve at the

point when total internal reflection would otherwise cease to occur. Using this principle, a curve representing light intensity per pixel in the detector array can be generated. This is shown below in Figure 32. Light intensity is subsequently converted to an index of refraction for the liquid which in turn correlates to methanol concentration of the fluid.
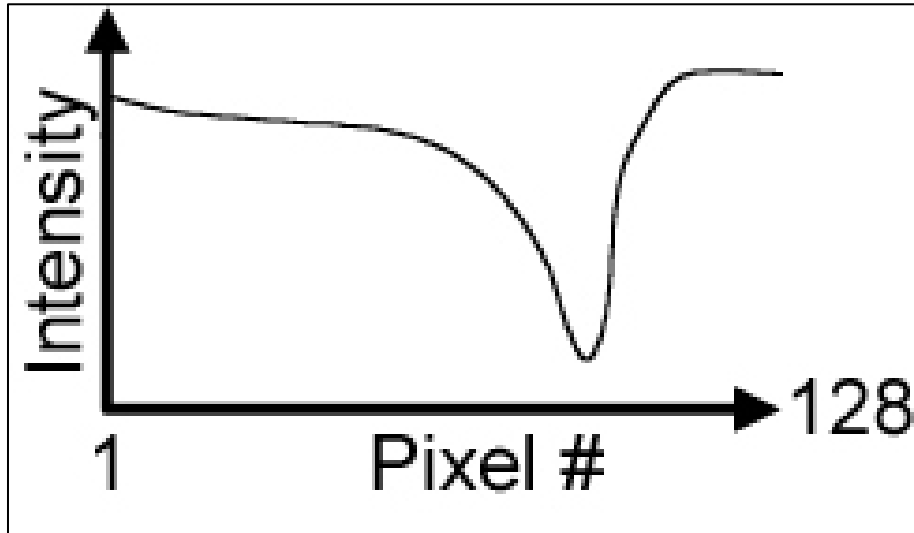

Figure 32 SPR curve generated by a Spreeta sensor.

Initial testing with the Spreeta devices at UNF laboratories was conducted with sensors without the gold sensing surface. The metallic surface was predominately a development for the biomedical application. Without a gold layer, surface plasmon resonance is not possible and the curve from Figure 32 would have no discernible minimum point. It would simply decrease until the intensity tapered off completely. Ordinarily, the gold surface and its associated SPR would prevent the light from completely exiting the sensor at the point where total internal reflection ceased. In this configuration, the slope of the decline in the curve would be the measure of change in light intensity. Preliminary test results from a 0.8M methanol solution are shown in Figure 33.
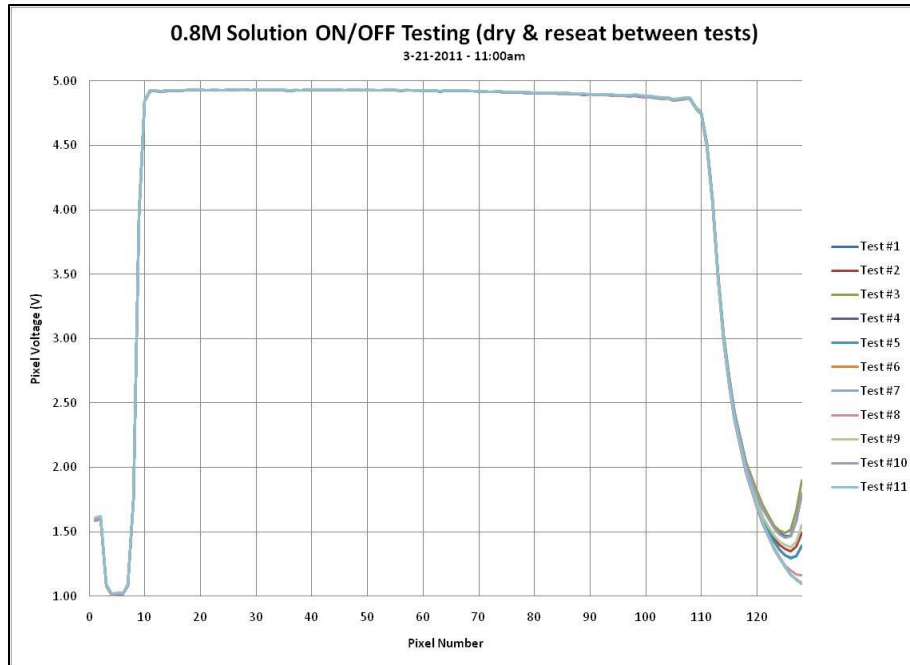
Figure 33 Data taken from tests in 0.8M methanol solution with Spreeta sensor (without gold surface).

The results from Figure 33 show initially that the sensor performs well in repeatability of measurement. Several solutions were mixed in the range of operation for the fuel cell system (0.6 – 1.8 M). A few of the solutions were passed through the Spreeta sensor, but the resulting resolution between slopes of different solutions was not acceptable for reasonably accurate measurement. Due to the limited availability of prototype sensors, the Spreeta sensor was also reserved for future development.

Nanocrystalline Indium Tin Oxide (ITO) Gas Sensors

Nanocrystalline Indium Tin Oxide (ITO) gas sensors and photo-electric chemical sensors (PECS) were investigated at the UNF laboratories. ITO sensor arrays are assembled with Poreflon tubing with a porosity that allows for the diffusion and deposition of methanol vapor on the sensor surface resulting in a change in electrical resistance. The PECS sensors operate by illuminating metal electrodes with TiO_2 coated surfaces with LEDs. The subsequent degree of methanol oxidation is sensed in the solution. Testing with these sensors revealed a response to methanol concentration; however no strong correlations were able to be established using these measurement techniques.

Methanol Concentration Estimator

The team has pursued the development of a soft-sensor for detecting methanol, namely an algorithm that can predict the methanol concentration in the reservoir tank without using methanol-concentration sensor hardware. Experiments were carried out at University of Florida,

to measure voltage across fuel cell and methanol crossover at various operating conditions. Physical models based on fundamental principles are developed to describe methanol crossover phenomenon and polarization curve and least-squares analysis has been performed to fit these models to the experimental data.

Figure 34 shows the estimated and experimentally measured values of crossover current density as a function of cell current density at various bulk methanol concentrations in the feed and cell temperatures. The blue lines in plots correspond to the experimental data collected at different operating hours of the stack as mentioned in the labels. The red lines are the estimates from the physical model for the crossover phenomenon.
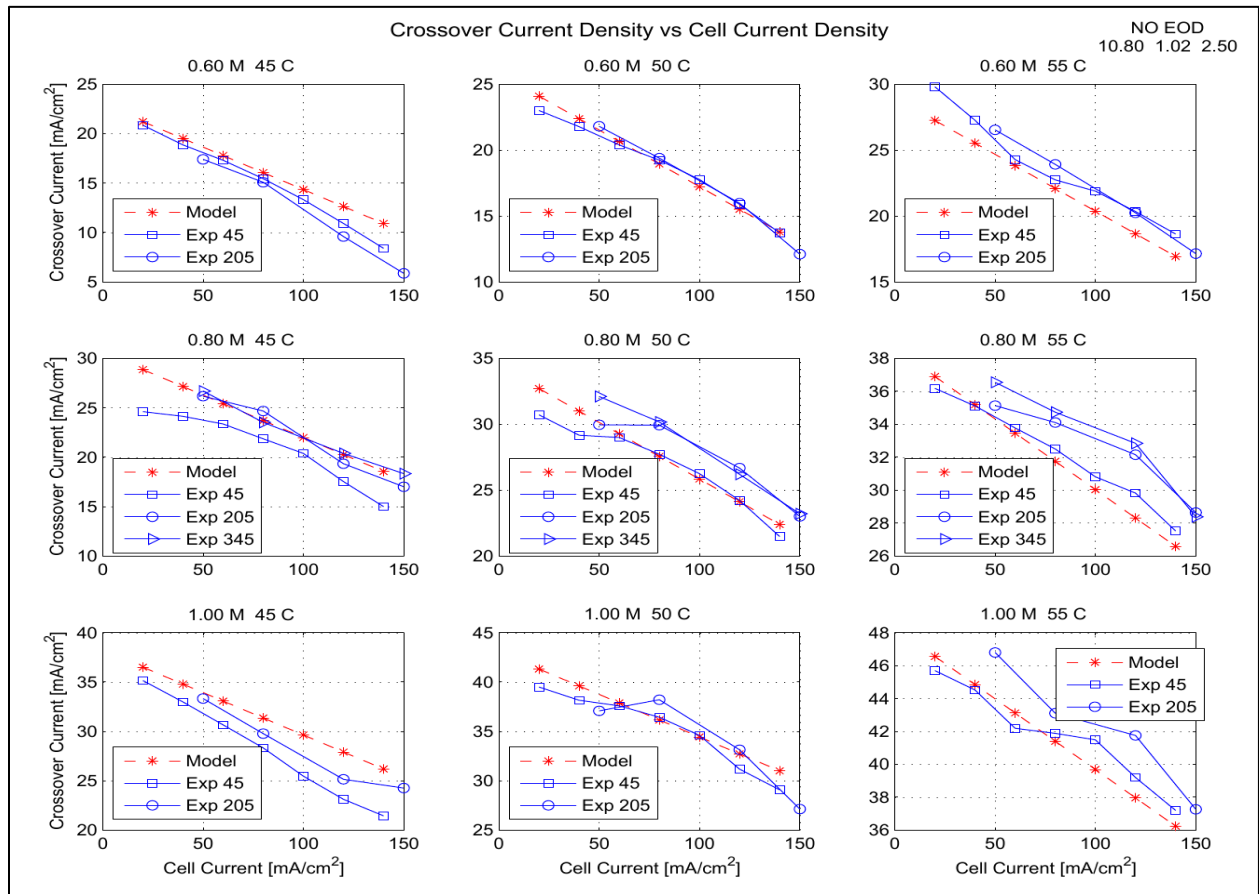
Figure 34 Crossover current density vs. cell current density at various methanol concentrations and cell temperatures

Figure 35 and Figure 36 show the estimated and experimentally measured polarization curves at various bulk methanol concentrations in the feed and cell temperatures. The solid lines with circle markers in the plots correspond to the experimental data and the dotted lines with star markers are the estimates from the physical model for the polarization curve.

Figure 35 Polarization Curves at various methanol concentrations and cell temperatures

Figure 36 Polarization Curves at various methanol concentrations and cell temperatures
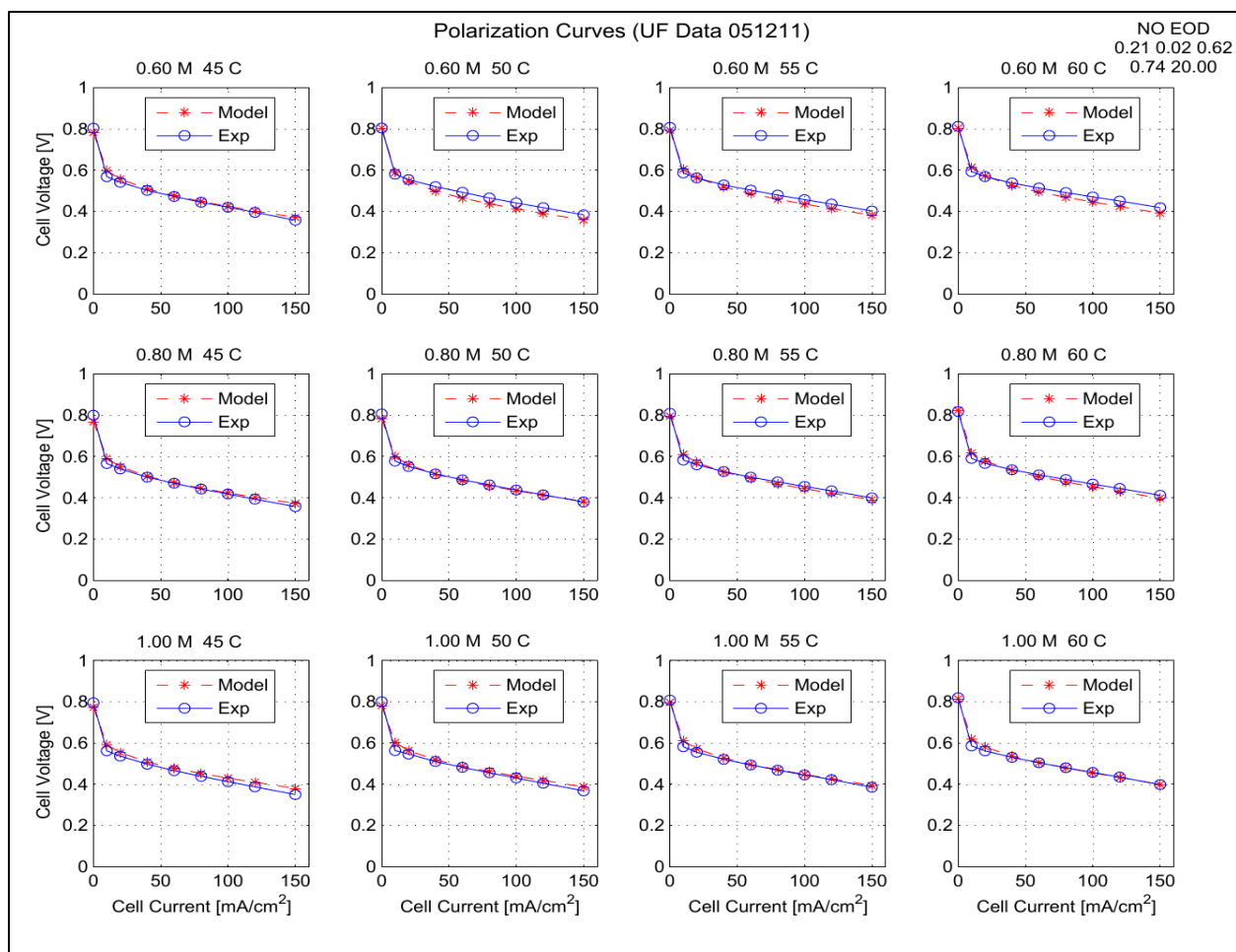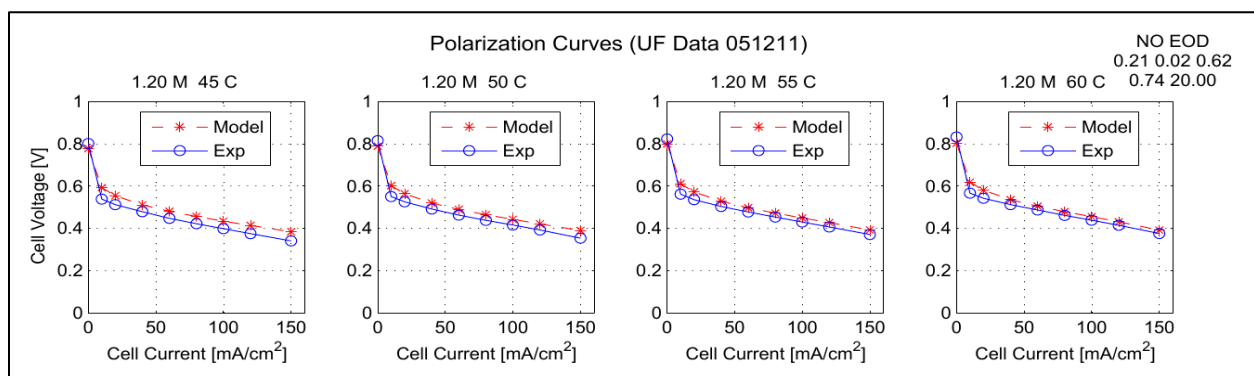
Experimental data for 0.6 M, 0.8 M and 1 M have been used to fit the parameters in the model using least square method and the model is tested on 1.2 M data. As shown in the figures, the model performs well in predicting the experimental observations.

A nonlinear model based on fundamental principles was developed to describe the fuel cell system which includes the fuel cell stack, gas liquid separator, reservoir tank, pumps and other components. A linear model is derived from the nonlinear model at an operating condition for the fuel cell system. Using these physical models, two algorithms, namely a full-state observer and reduced-state observer, were developed which can predict the concentration of methanol in the reservoir tank and there by the use of methanol concentration sensor can be avoided. Both estimators show good performance when simulated using the models. Furthermore, the simulation studies indicate that the reduced state observer is significantly faster and exhibits better performance than the full state observer.

The methanol concentration estimator has yet to be interfaced with the DP4 brassboard or packaged system. However test station data suggests this method of methanol concentration determination is a viable means of methanol concentration determination.

Fuel Feed Pump

Pump design

The pump selected for use in the fuel feed subsystem is a piezoelectric diaphragm pump manufactured by the Microbase Technology Corporation (model MBP2115BD). This pump is a miniature pseudo-positive displacement pump that uses internal electronics to drive a piezoelectric diaphragm that performs work on the fluid. It is specifically rated for use with methanol. The advantages of using this particular pump are as follows:

- It is specifically rated for use with pure methanol and all concentrations of methanol and DI water.

- Its stated specifications satisfy the pressure and flow requirements of the system.

- It has on-board electronics to drive the piezoelectric element, meaning that the fuel cell control system need only provide 3-5V DC, rather than a high-voltage AC signal.

Pump requirements

The requirements for the fuel feed pump and their planned validation methods are listed in Table 5.

Table 5 Fuel feed pump requirements and validation methods

#	Description	Criteria	Validation method
1	Max back pressure	5 kPa gage	Generate pump curve @ 40°C & ambient T
2	Min flow rate	4.0 mL/min	Generate pump curve @ 40°C & ambient T
3	Max absolute pressure	36 kPa gage	No leak/failure when pressurized
4	Performance degradation in pure methanol	<5% after 1 month @ 60°C	Generate pump curve after 1 month soak in pure methanol
5	Orientation independence	All angles	Generate pump curve in 4 orientations (bottom, side, top, 45°)
6	Self priming	1 minute with no damage	Start siphon with long tube
7	Self priming	50mm head of gas	Start siphon with 50mm height tube
8	Max noise level	30dB at 1m	Ambient noise meter
9	Power consumption	50mW	Record V & I during pump curve tests

Self-priming testing

There are two requirements on the fuel feed pump with respect to its self-priming characteristics:

- Able to draw fuel when the line is initially filled with gas to a suction head of at least 50 mm

- Able to maintain suction for at least 60 seconds with the presence of vapor bubbles in the liquid fuel stream

To test these criteria, the inlet and outlet of each pump were attached to a 70 mm length of dry tubing and suspended 50 mm above a reservoir of water. The ends of the tubes were then submerged in the water and the pump was started with a power supply of 5V DC. If the pump was able to draw the water up the inlet tube and produce a liquid stream, it was marked as "Pass" in Table 6.

Table 6 50 mm self-priming test results

Serial #	50mm siphon test	60 sec siphon test
10317-18SPP	Pass	Pass
10329-18SPP	Fail	Fail
10332-18SPP	Pass	Pass
10339-18SPP	Pass	Pass
10341-18SPP	Pass	Pass
10344-18SPP	Pass	Pass
10346-18SPP	Pass	Pass
10347-18SPP	Pass	Pass
10348-18SPP	Pass	Pass
10349-18SPP	Fail	Fail
10350-18SPP	Pass	Pass
10351-18SPP	Pass	Pass

All pumps passing the 50 mm siphon test were also able to continue pumping despite the presence of vapor bubbles in the lines for over 60 seconds, and therefore met the second requirement stated above (see Table 6). Two of the twelve pumps were unable to produce 50 mm of suction, leading to an out-of-the-box (nascent) failure rate of 17%.

Test rig design

Figure 37 shows a schematic of the test system setup, the design of which is similar to the setup detailed for the recirculation pump testing.
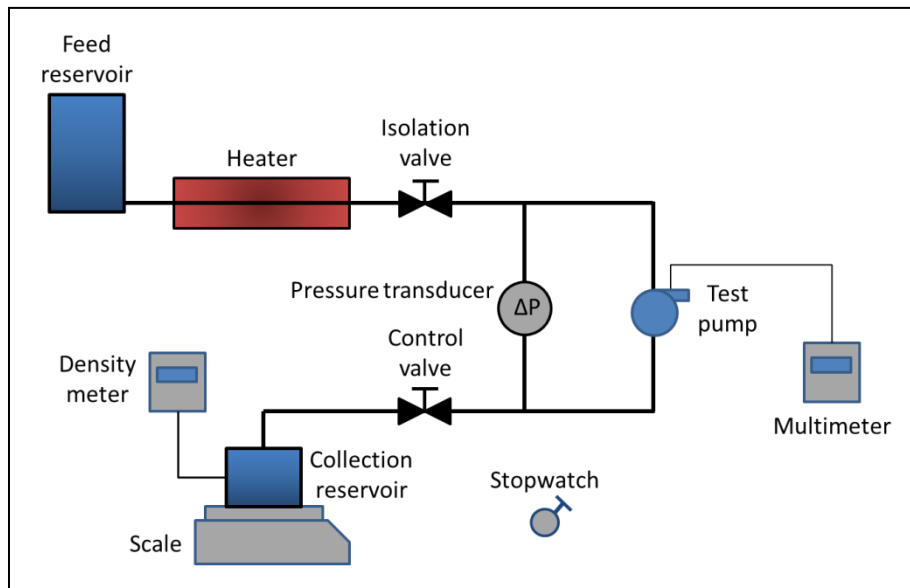

Figure 37 Schematic of fuel feed pump evaluation rig (not to scale)

Fluid is provided at constant pressure to the test system from a constant-height reservoir. (During testing, the working fluid is either deionized water or pure methanol; however, in the fuel cell system, the fluid will be pure methanol.) This constant-height reservoir is capable of selectively having gas introduced into the fluid stream in order to test the self-priming performance of the pump. The fluid first passes through an electric heater, which is controlled to a desired temperature (system requirements call for testing both at ambient temperature and 40°C). The fluid then passes through a length of tubing at least 10 times the inner diameter of the tubing and enters the pump, which can be placed in a variety of orientations. A pressure transducer (range 0-200 W.C.) measures the pressure increase due to the pump's work. A control valve placed a length of tubing greater than 10 times the inner diameter of the tubing downstream of the pump allows for the back pressure, and hence the pressure differential across the pump, to be varied. Finally, the fluid collects in a collection reservoir, where the mass and density of the fluid are measured. This mass and density, along with the time taken to fill the collection reservoir, is used to calculate the volumetric flow rate. For determining the electric

power consumed by the pump, the voltage and current used are recorded from a multimeter in the pump-power circuit.

Test Results

Using the data generated using the test rig, characteristic ΔP versus flow rate pump curves were generated and calculations for pump efficiency were performed.

To judge the performance of the Microbase pumps, a selection of those labeled "passing" in Table 6 were characterized using the test setup described above. For comparison, a group of pumps that had been soaked in methanol were also characterized. The test results are presented in Figure 38, where the shaded area represents anticipated operating conditions.
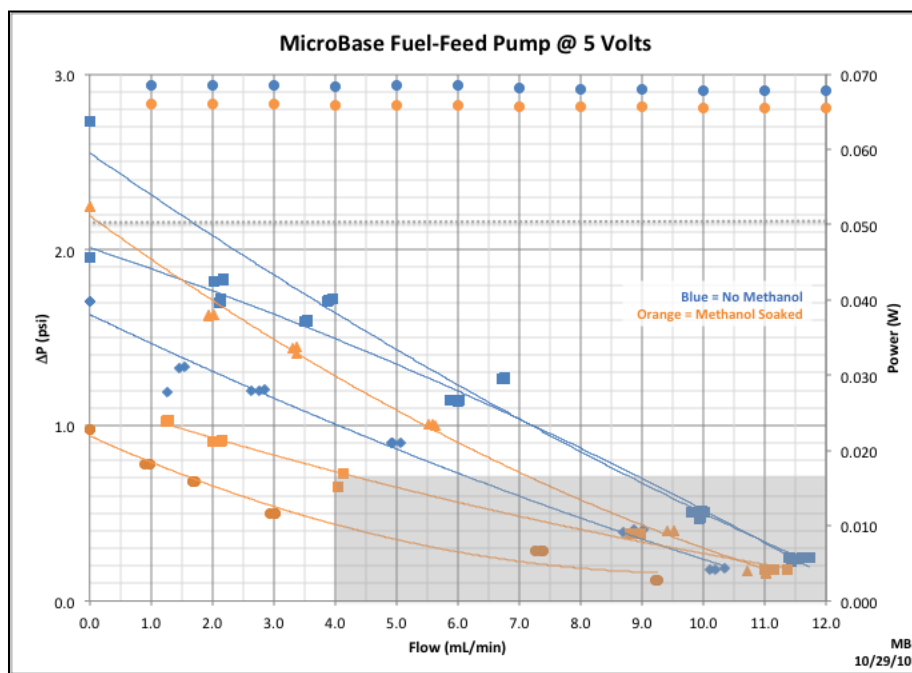

Figure 38 Fuel feed pump hydraulic performance and power consumption

While nearly all of the pumps meet the flow rate requirements, it should be observed that the hydraulic performance of the methanol soaked pumps was lower than that of the pumps that were not exposed to methanol. Although the pump manufacturer states that the MBP2115BD is methanol compatible, it is possible that the polymers and glues inside of the pumps absorbed some methanol, as there was no liquid methanol remaining in the pumps after the soak. It should also be noted that all of the pumps exceeded the power usage requirement of 50 mW.

To address the reliability concerns of the MicroBase pump an endurance test was conducted over 2250 hours. During this time the pump was run continuously at maximum voltage at a dead-head condition with methanol as the pumped fluid. The results of the test are shown in Figure 39.
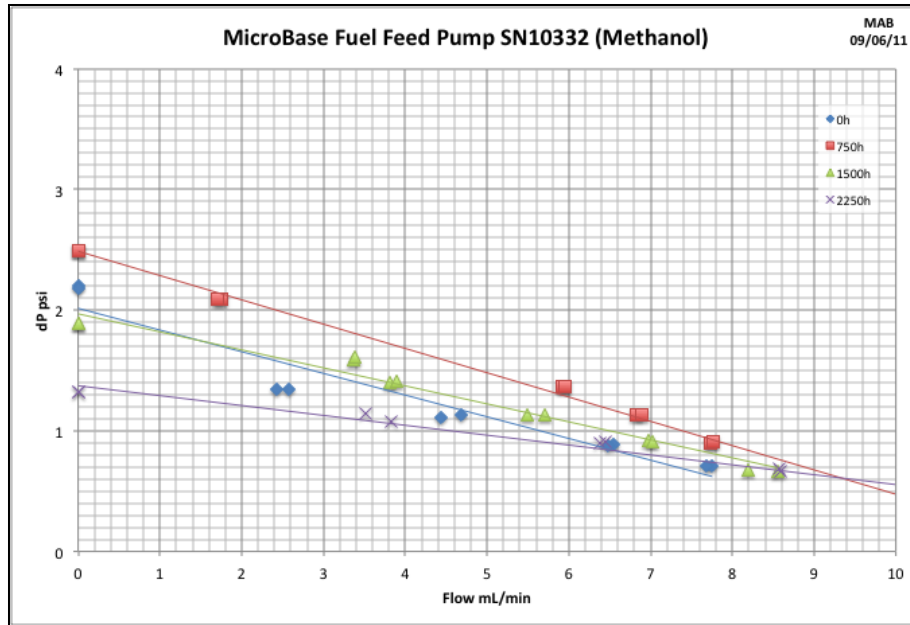
Figure 39 Microbase pump methanol endurance test results

As can be seen from the figure, the performance of the pump degraded very little during the test period in test conditions that are far more severe than will be encountered in the system.

Although the MicroBase pump is not the ideal solution to fuel dosing (more accurate dosing is desirable), it is generally reliable and well suited for use in the system due to its small size and relatively low power consumption.

Anode Solution Recirculation Pump

Selection and Characterization

Six candidate pumps were characterized for potential use in the anode fuel stream recirculation subsystem: the KNF5 RPDC-L (KNF Neuberger), the Xavitech P1500-LIQ (Xavitech Intelligent Pumps), the TCS M200S (TCS Micropumps), the Schwarzer SP200, the Parker-Hargraves 1F17N2, and the UNF DP4 prototype. The latter two pumps would not run reliably, and were therefore not viable candidates for use in the system. The Parker-Hargraves pump was unable to operate steadily due to the viscosity of the test solution (the pump was designed to primarily handle gases), and the UNF DP4 prototype experienced issues with seizing, especially on startup.

A summary of the results of the characterization of the remaining candidate pumps is shown in Figure 40 and Figure 41.
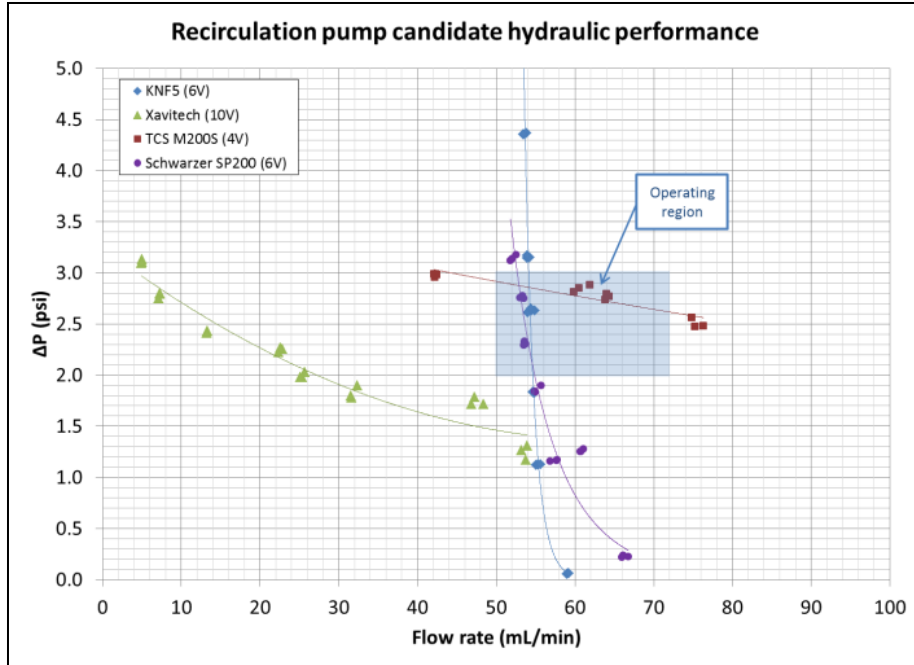
Figure 40 Summary of recirculation pump candidate hydraulic performance
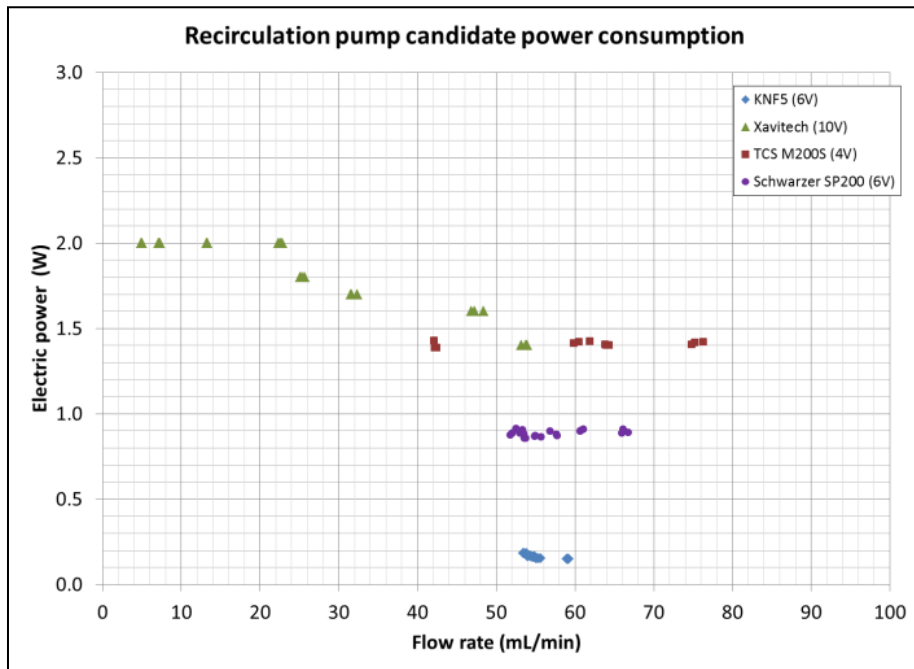
Figure 41 Summary of recirculation pump candidate power consumption

Currently, the best recirculation pump is the KNF5, manufactured by KNF Neuberger. As can be seen in Figure 41, this pump consumes the least amount of electrical power (approximately 0.2 W). Because it is a valved positive displacement pump, the KNF5 produces a nearly-constant flow rate for a given RPM, making control of the fluid stream's flow rate a matter of simply changing the input voltage. In addition, the pump is self-priming, a valuable

characteristic that it does not share with centrifugal pumps such as the TCS M200S. The primary drawback of the KNF5 is that it is physically larger than the design requirements specify: the CDR requires that the recirculation pump occupy no more than 6 cm3, while the KNF5 occupies a space approximately 16.4 cm3 (4.1 cm x 2.5 cm x 1.6 cm).

Endurance Testing

For endurance testing the KNF5 recirculation pump, a test loop was built (see Figure 42 below) that allowed the pumps to safely run continuously. The loop consists of a heater and a reservoir. Three KNF 5 pumps connected in parallel continually pump fluid around the loop. The liquid is 0.8 molar methanol solution and the system is maintained at 50ºC.

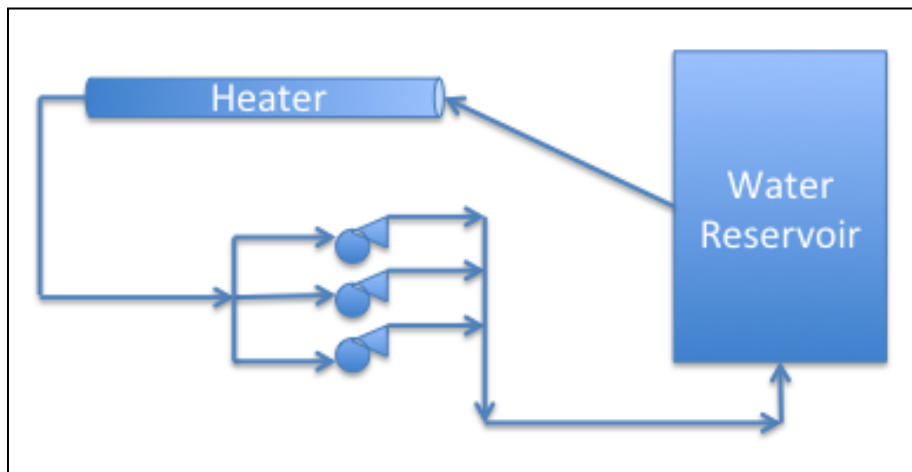**Figure 42** Endurance test loop for KNF recirculation pumps.

Before the test was begun each of the pumps were characterized. The pumps were characterized again every 750 hours until the test was completed after 3000 hours. The test results are displayed in Figure 43, Figure 44, and Figure 45 below.
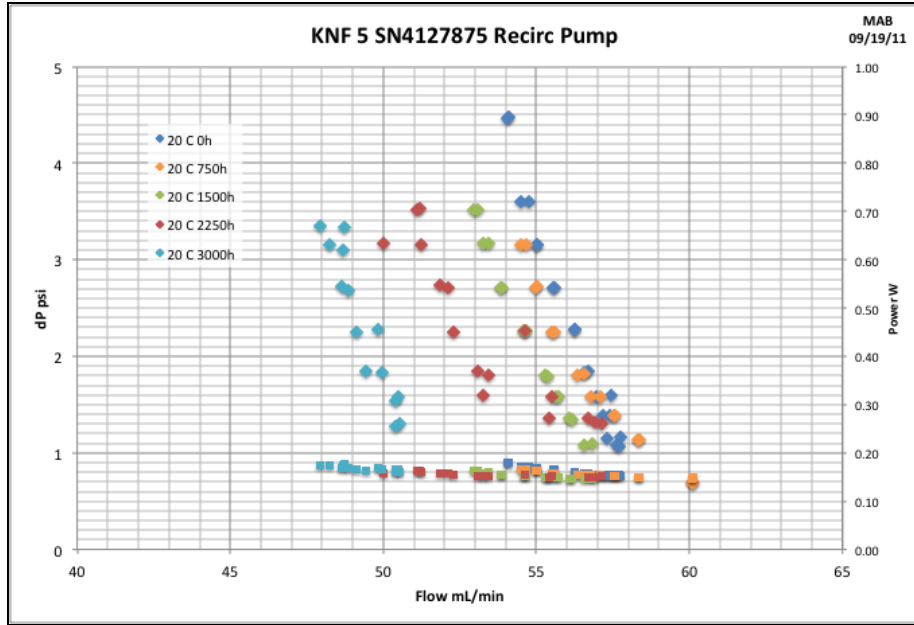
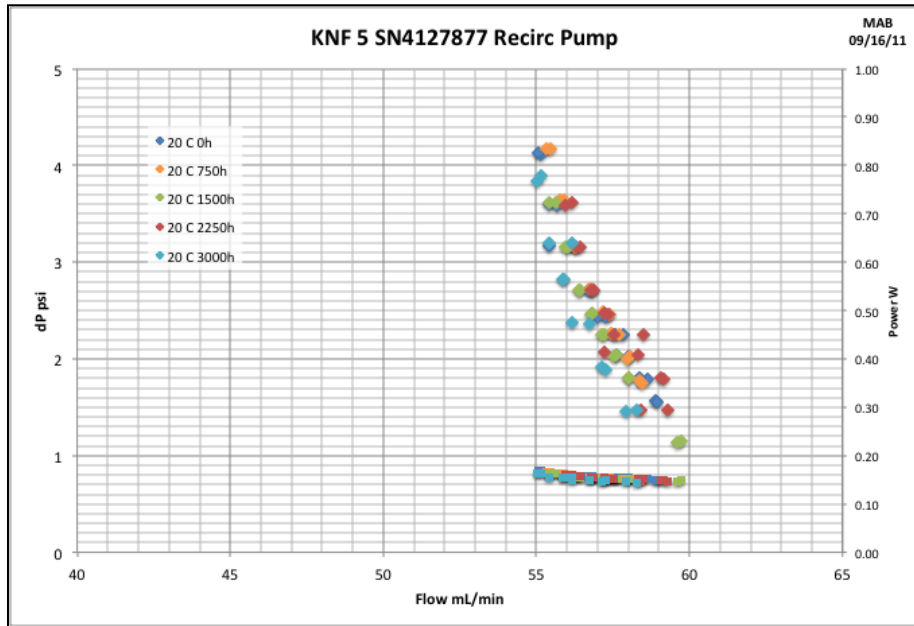**Figure 43** KNF SN4127875 endurance test results

Figure 44 KNF SN4127877 endurance test results
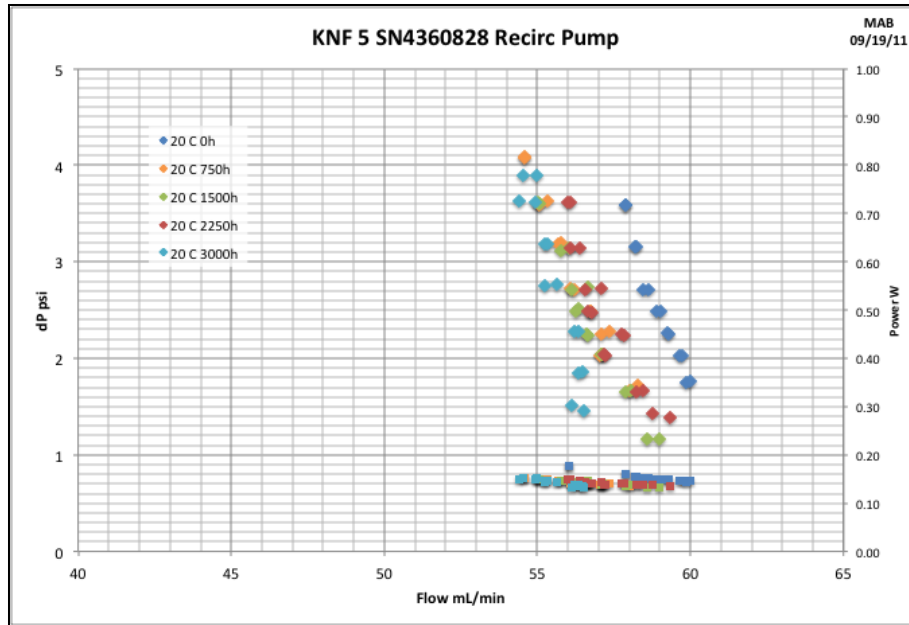
Figure 45 KNF SN4360828 endurance test results

When pump SN4127875 was removed at 3,000 hours, a rattle in the pump head was observed the valve had become unseated and was to blame for the loss of performance. After the valve was reseated the flow rate returned to normal.

With the exception of pump SN4127875, the pumps demonstrated acceptable performance with flow rates of approximately 55 mL/min at 4 psi backpressure. These results indicate that recirculation pump performance should remain nearly constant over the pump's lifetime, in excess of 3,000 hours. Based on its performance, reliability and power consumption, the KNF5 has proven to be the best choice for the anode recirculation pump despite being slightly larger in size than the original design specifications.

Gas Liquid Separator

The gas-liquid separator (GLS) is a component which allows venting of the CO_2 waste product from the recirculating anode fuel-water stream during fuel cell operation under electrical loads. Because it was one of the larger components in the balance of plant, the objectives were focused on decreasing its volume in order to meet DOE goals. However, in order to ensure that DOE operability goals were also met, the device had to meet other performance specifications such as minimization of water/methanol loss and orientation independent performance. Various GLS designs involving hydrophobic porous membrane technology were the primary approach for meeting these requirements; due to their potential for venting CO_2 at any orientation, while simultaneously retaining liquid. The first design that was investigated was referred to as the 'single-sided' design as seen Figure 46.

Figure 46 'One-sided' GLS prototypes

The 'single-sided' prototypes were tested on an ex-situ test jig at typical system conditions (i.e. 1.0 Molar methanol-water solution, 50C, Vliq = 55mL/min, VCO_2 = 250 mL/min). It was found that the bubbles vented reasonably well for short periods of time, but failed to vent all incoming CO_2 gas bubbles after only a few hours of operation. This result was attributed to condensation within the pores, which was believed to have been induced by the relatively large temperature gradient across the membrane (i.e., from approximately 50°C to approximately 20°C). Prior to the venting failure, the excess H_2O vent (EHV) parameter was found to be 60.2%, where the EHV parameter is used to relate the amount of additional water lost through the GLS test cell compared to the unavoidable water loss associated with the flow of saturated CO_2; both were measured over a 24 hour period. This large amount of excess water loss was attributed to the evaporation of the high temperature liquid phase.

In an effort to prolong the operation of the GLS and reduce the amount of water loss from the system, a new prototype, referred to as the 'isothermal' design, was designed such that the temperature gradient across the porous membrane might be minimized. This design was essentially composed of two 'one-sided' prototypes sandwiched together as seen in Figure 47.

Figure 47 'Isothermal' GLS prototype design

With an EHV of 10.2%, the 'isothermal' design appeared to be superior to the 'one-sided' design, however, the venting performance remained inadequate for extended test runs (i.e. < ~24 hours). These results motivated a series of parametric tests involving the current 'isothermal' design, as well as other commercially available GLS devices with the primary objective of determining the root cause of the venting failures. From these tests it was concluded that the venting failures were influenced by a combination of high temperature, elevated methanol concentration, and lack of a positive pressure gradient from the interior of the GLS to the pressure in the vent space (i.e., the atmosphere). This pressure gradient is produced by raising the "back pressure" of the fluid leaving the GLS, i.e., essentially raising the internal pressure within the GLS), and was found to be the primary cause of failure.

Specifically, it was found that when the 'isothermal' design was tested at standard DMFC conditions at a back pressure of approximately zero psi the device failed to vent within 24 hours; however, when a back pressure of approximately one psi was applied for the same conditions, the GLS vented continuously in excess of two weeks. During the two week test period, the methanol concentration and temperature was increased from 1.0 to 4.0 molar and from 50 to 65°C, respectively, for a duration of ~24-36 hours without causing a significant decrease in CO_2 venting performance. Based on these discoveries, a GLS device incorporating the 'isothermal' design and applied back pressure was developed for integration into the packaged DMFC system, as see in Figure 48.
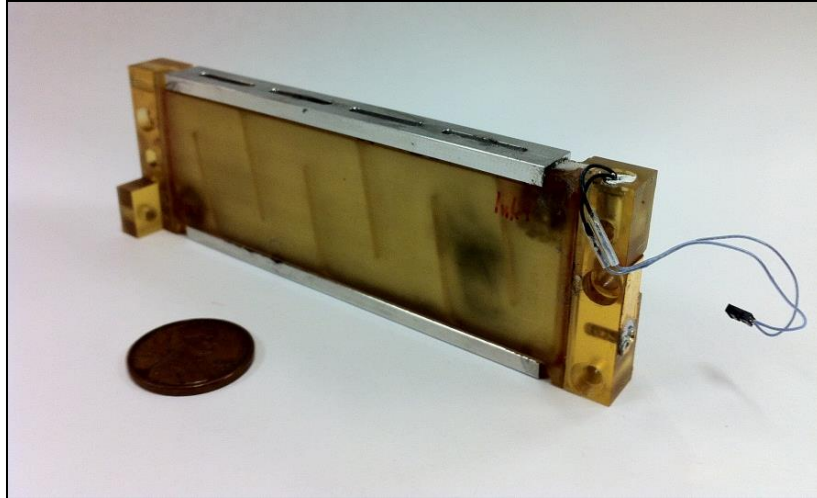
Figure 48 Packaged GLS device with 'Isothermal' design

The packaged GLS device was essentially the same as the 'isothermal' prototype used in performance testing. However, in order to make the device interface well with the rest of the system some of the hardware used to seal the device was modified. As a result, it became much more difficult to prevent liquid leaks from occurring around the perimeter of the device. While this appeared to be a serious issue, recent developments in our MEA's ability to retain water proved that the water loss associated with the GLS was no longer a major concern. In addition, the recirculation tank has been re-designed to actively vent gas at any orientation. As result of these two recent developments, the GLS will most likely be removed from the BOM for the next generation of DMFCs.

Fluid Reservoir Subsystem

Recirculation Tank Validation Testing

Early observations indicated that operating the system at certain orientations would cause the recirculation tank to lose prime on the suction side of the recirculation pump, resulting in insufficient fuel delivery to the stack. Ex-situ testing of the recirculation tank revealed that the pump provided a diminished flow rate when the tank was appreciably rotated about its y-axis (see Figure 49 for tank coordinate system) due to the unporting of the pump inlet supply.
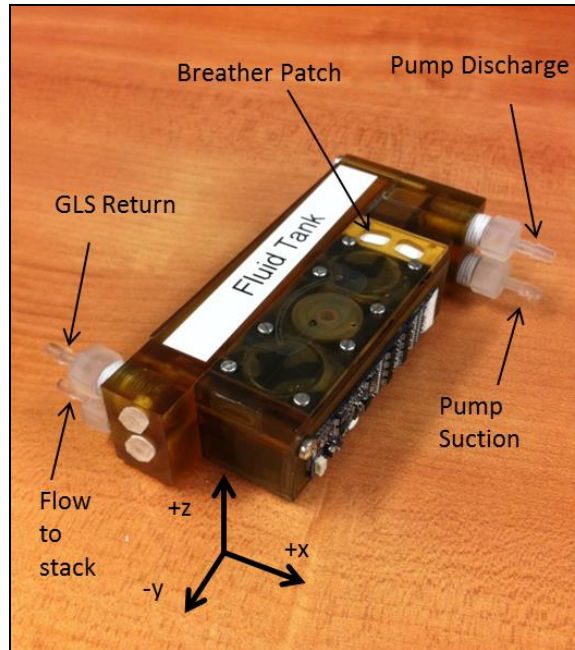
Figure 49 Tank with coordinate system defined

A picture of the ex-situ test setup is shown in Figure 50. As can be seen, the flow rate delivered by the recirculation pump was measured using a digital flow meter. Valving and pressure transducers were used to ensure that the tank remained at operating pressure.
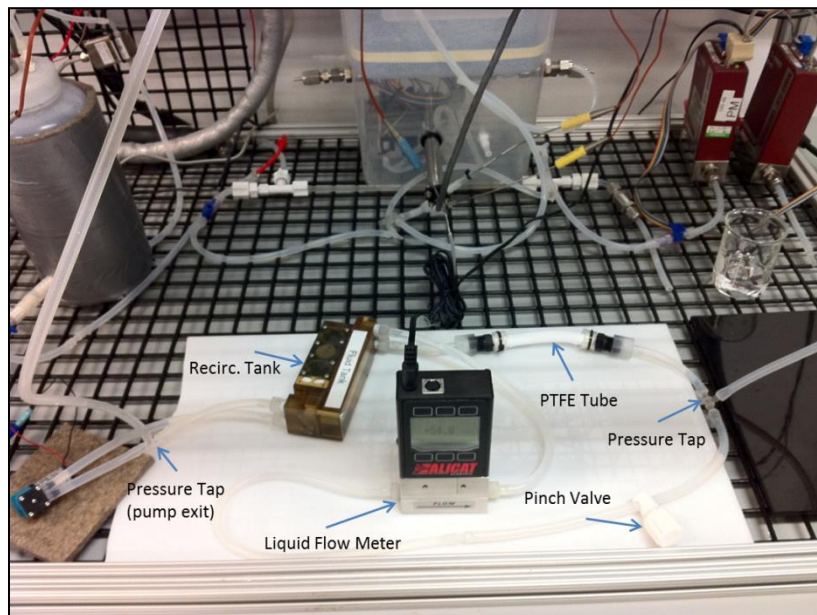
Figure 50 Tank orientation experimental set-up

As previously mentioned, there were three orientations at which the recirculation tank failed to keep the pump primed. Each orientation was also tested at four different tank liquid levels (¼, ½, ¾, and full) to determine if the loss-of-prime issue was affected by the amount of liquid in the

tank. Rotation about the x-axis was determined to be satisfactory for ±90°. This is to be expected, as the gravity valve in the tank was designed expressly for dealing with rotation in this axis. The experimental results for rotation about the y-axis are summarized in Table 7 below.

Table 7 Tank orientation test results

Tank Orientation	Conditions (liquid only)	Measured Liquid Flow Rate At Various Liquid Levels			
		25% Full	50% Full	75% Full	Full
45° CCW about negative y-axis	20°C, 1.5 psig back pressure, DI water	~14-30mL/min	~20-30mL/min	~20-30mL/min	~20-30 mL/min
90° CCW about negative y-axis	20°C, 1.5 psig back pressure, DI water	Fail (flow not measurable)	Fail (flow not measurable)	Fail (flow not measurable)	Fail (flow not measurable)
180° about y-axis	20°C, 1.5 psig back pressure, DI water	Fail (flow not measurable)	Fail (flow not measurable)	Fail (flow not measurable)	Fail (flow not measurable)

As shown in Table 7, when the tank is oriented beyond 45° counter-clockwise about the negative y-axis, the pump suction port is no longer fully submerged in liquid, resulting in insufficient liquid flow to the stack (the same is true for 45° clockwise rotation about the negative y-axis). This issue does not appear to be mitigated when the tank level is increased beyond 25% full. Therefore, there is a ±45° tolerance for movement about the y-axis without running the risk of reduced fuel flow to the stack.

In its current implementation, the tank is 100% orientation independent when the unit is not operating. During operation, it is capable of operating in ±90° about the x-axis and in any rotation around the z-axis. However, rotation about the y-axis is limited to less than ±45° before the stack flow rate is diminished. This has been recognized as a limitation, and a redesign effort is currently underway to improve the tank's orientation independence.

Tank Level Sensing Using Piezoresistive Pressure Transducers

In the previous design prototype, the amount of fluid in the tank was measured by using an array of conductive pins which were placed at different locations throughout the tank. By sensing how many pins were in contact with liquid, the fluid level in the tank could be measured. While generally satisfactory, this technique required a relatively large and expensive circuit board to be attached to the side of the tank. Measurement issues were also encountered when pins would sometimes be "bridged" when a drop of fluid connected two pins, despite being above the fluid level and therefore giving a false reading. In order to address this issue as well as the significant cost associated with the pin sensor, the concept of measuring fluid level with a pressure transducer at the bottom of the tank was examined. However, after testing, it was determined that using pressure transducers in this fashion was not feasible for this application, as the best

available sensors were not compatible with methanol and the sensor output characteristics were not repeatable from sensor to sensor.

Due to the small volume of water that is to be stored for use in the system, the sensors that are ultimately selected for this application need to measure extremely low pressures (P < ~1 kPa). While many sensors can be found within that range, none could be found that meet the main requirement of being methanol compatible. Therefore, two liquid-compatible sensors were selected for evaluation that were rated at much higher pressures than those that will be seen in the system.

The two sensors selected for evaluation are both produced by Freescale Semiconductor. The MPXC2011DT1 is rated for a maximum pressure of 10 kPa and the MPVZ5004G7U is rated up to 3.92 kPa. Both sensors feature a fluorosilicone gel that isolates the die surface and wire bonds from the methanol environment, as can be seen in Figure 51. It should be noted that the MPXC2011 does not have the stainless steel cap above the fluorosilicone gel.
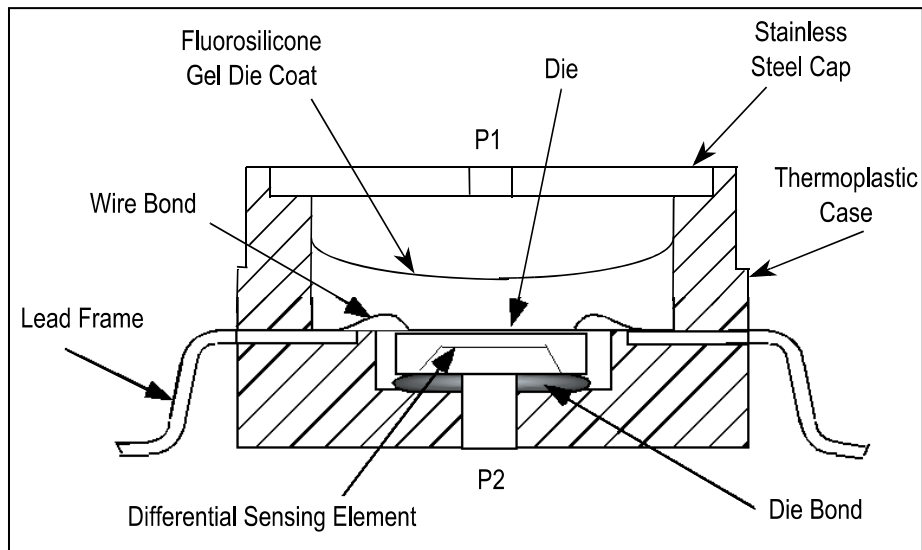
Figure 51 Cross-sectional diagram of MPVZ5004 series pressure sensor

The two sensors also vary in size, with the MPVZ5004 being nearly twice as large as the MPXC2011. This is partly due to the fact that the MPVZ5004 includes output signal amplifying circuitry within the casing.

Because both sensors' maximum rated pressure greatly exceeds the maximum pressure in the system, the first test was conducted to determine if the sensors' output voltage is predictably linear within the 0 − 1 kPa range. Using the test setup in Figure 52, the pressure applied to the sensor was varied (by raising or lowering the flask) in increments of 1 mm of water. This pressure was measured using a column of water.
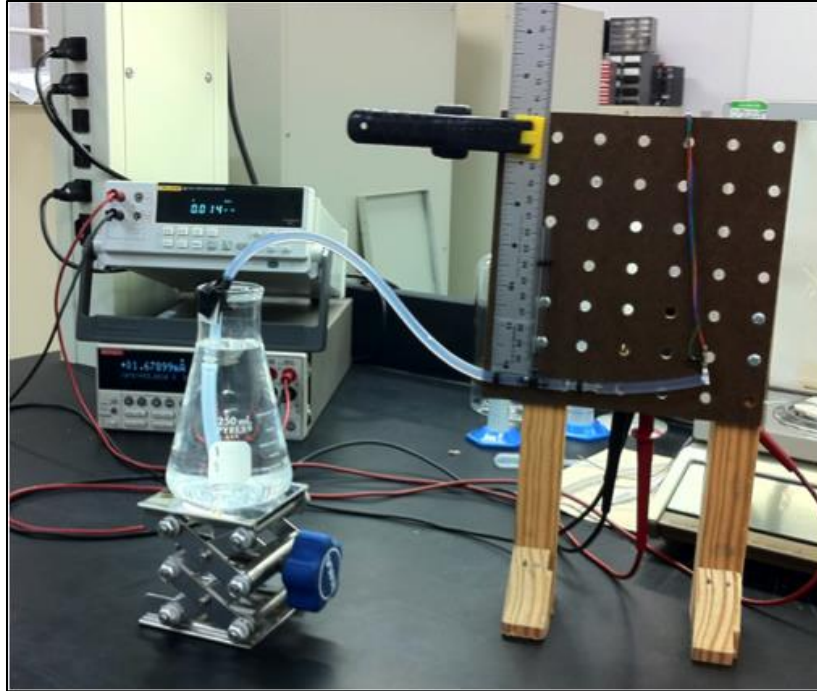
Figure 52 Test setup for measuring output voltage versus pressure for pressure transducers

Each (MPX series) sensor was tested six times and the results (minus the upper and lower bounds) were averaged. The results of the test for three different sensors are presented in Figure 53.
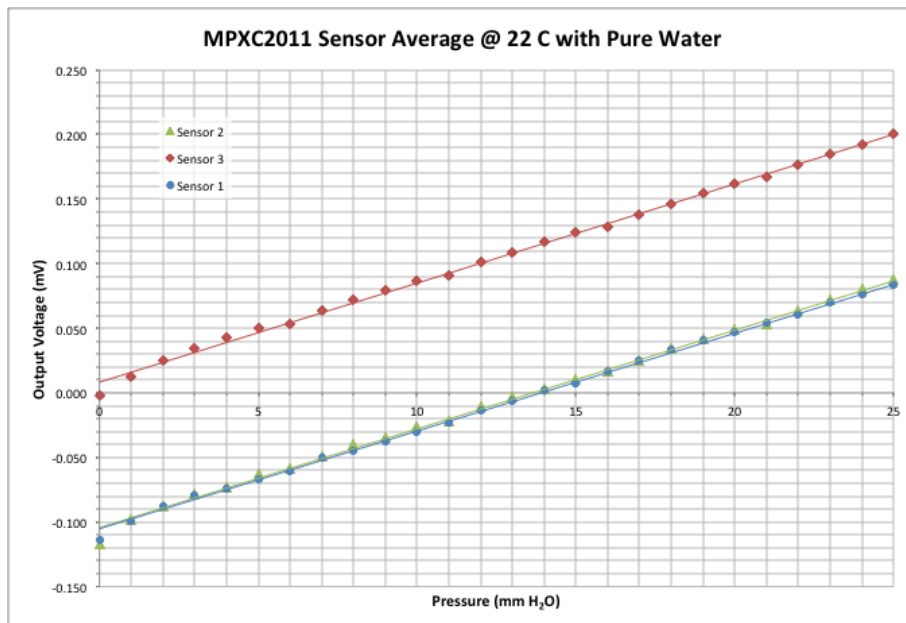
Figure 53 Average sensor test results at 1 mm of water

From the figure it can be seen that all of the sensors operate linearly over the pressure range of interest. Each of the sensors also exhibit the same rate of change of voltage with respect to pressure and each give consistent results when tested multiple times. The only difference between sensors is the zero offset voltage. This is the voltage that the sensor transmits at zero pressure and is a characteristic of the individual sensor. While some sensors do have the same zero offset voltage, it cannot be assumed that is the same for all sensors manufactured. This would become problematic in large-scale production, as each sensor would have to be characterized prior to installation in a unit and the sensor's zero offset voltage programmed in to each specific unit's control system.

The same test was then conducted with pure methanol. The results of the methanol test showed that the fluorosilicone gel swells when exposed to methanol. Because the gel is in direct contact with the sensing element, the swelling leads to increased and erroneous pressure readings. As the MPX series was the best available sensor found for this application and exhibited serious issues both in terms of methanol compatibility and zero offset voltage, it was determined that pressure measurement to determine liquid level was not feasible. Therefore, the current method of using an array of conductive pins was chosen as the level sensing technique going forward.

Methanol Injection Diffuser

During operation of the DP4, a relatively long time lag was observed from when the methanol injection pump was energized to when a response in the methanol concentration sensor was detected. A shorter time delay for the methanol sensor to respond is preferred in order to achieve tighter control of methanol concentration. Based on the flow paths that were designed into the DP4, the system was expected to have a faster response. An investigation was initiated in order to determine the root cause of the delay in methanol response. The pressure drops across all of the wetted paths (tank, interconnects, methanol sensor, etc.) were measured in order to rule out the flow path as a source of methanol response delay. All of the wetted paths were determined to have no observable detrimental effect on the methanol concentration response. Another hypothesis for reduced methanol concentration response time is the possibility of poor mixing in the reservoir tank between the pure methanol and methanol-water solution. A qualitative test was performed to test this hypothesis. The ex-situ test revealed that when dye is added to methanol and the colored methanol is injected into a beaker of water, a considerable amount of time is required for the methanol to fully disperse. It is believed that the disparity in densities is the root cause of poor mixing. In future iterations of the DP4 tank, a diffuser will be implemented in the solution tank in order to mitigate poor mixing.

Task 3: System Engineering

Concept Design

The concept design of the new system shown in Figure 54 incorporating new subsystems was completed and reviewed in the first quarter of year two. All of the parts were sent out for fabrication and the final package shown in Figure 55 was complete in the second quarter of year two.
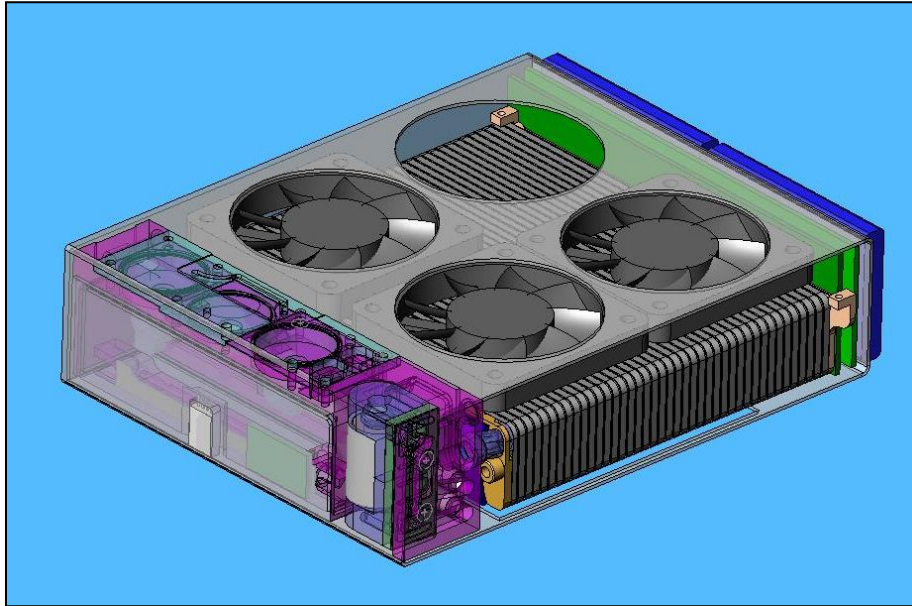

Figure 54 Concept design of integrated power section.
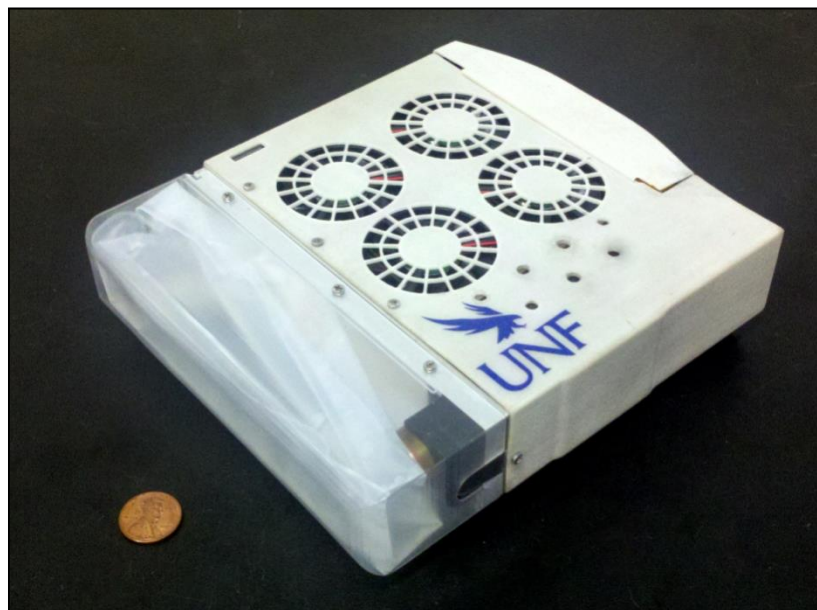
Figure 55 DP4 20 W DMFC power supply.

Brassboard Fabrication & Operation

Construction of the first brassboard system using design intent components was performed in the third quarter of year one, Figure 56. This used all prototype system components but used the previous version control board (DP3). After initial testing, a decision was made to use the commercial off-the-shelf (COTS) diaphragm pump instead of the in-house design recirculation pump, as a more conservative path for system operation. This had a minor impact upon system size (the COTS pump is about twice the volume) but this is offset by the lower parasitic load of the COTs pump (0.25W versus a target budget of 1.25W, and 2.0 W for the un-optimized prototype reciprocating piston pump). Modifications to the PCB control board were required to address various minor electrical changes, including the higher voltage resulting from the increased cell count in the stack.

A significant amount of effort was applied to the design, fabrication and commissioning of three DP4 brassboard systems. These represented the design intent components, the fuel cell stack, and a control box with the target functionality, assembled on a two-layer 'board' (in this case made from acrylic instead of 'brass') which has all the functionality of the integrated system design. Each component was laid out independent of others (to the extent possible) such that it could be monitored directly during operation and any system integration issues identified.
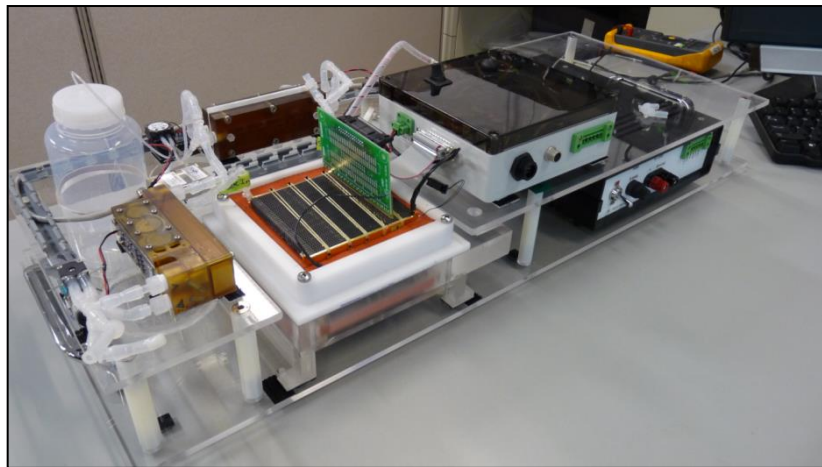
Figure 56 UNF DP4 brassboard with battery box.

Separate from the brassboard is a 'battery box' which represents the functionality of an external laptop in that it can provide output power to a load bank, has its own internal laptop battery with charge circuitry, communicates the battery SMBus signals back to the DP4 control box, and provides the power back to the DP4 during certain phases of operation, such as startup, shut-down, and rejuvenation cycles. This emulates an integrated DMFC power supply hybridized with a laptop. The DP4 design intent is to modify the battery box functionality to include within its own DP4 package a small hybrid battery for startup power, but communicate with the target

laptop to receive its SMBus signals (via a USB connection) and provide appropriate output power to the laptop to both charge and maintain the laptop battery at a healthy state of charge. This strategy provides the ability for the DP4 to be evaluated either as a stand-alone power supply (for some applications) or as a hybrid mobile computing power supply which could be integrated into a mobile computing device.

System Engineering

Efforts were made to improve the robustness of the firmware on the brassboard and to prepare for changes required by the new control boards designed for the integrated system.

Robustness improvements dealt primarily with responses to warning levels for various sensors and how to more effectively deal with these signals. Prior firmware dealt with these from a 'laboratory' perspective in that the approach was to provide protection from possible harm to the fuel cell by entering a 'fail state' if conditions were not perfect. While this approach was logical during the early stages of development, it led to brassboard system 'failures' more frequently than was truly necessary. Strategies to respond to warning signals through various mitigation strategies and to prevent unnecessary 'failures' were developed. Such strategies should be carried over to the next integrated system firmware.

The integrated system design required several key changes to the design of the control board. It was decided to minimize development risk and utilize the same microprocessor and as much of the existing schematic as possible, however the change of some of the system components, elimination of cell voltage monitoring, and incorporation of an internal hybrid battery, required a significant revision to the overall control schematic. Further, the package design required a complete new layout, with the power regulation and control functions split between two adjacent boards. Signals from the laptop battery SMBus will be read directly and USB will be used to communicate detailed information back to a LabVIEW monitor program.

When the new electronic boards were received, they were tested somewhat extensively. Function had been split into two sub-boards, one to deal with power regulation and the other to deal with control. Larger components associated with voltage regulation that required heat sinking were placed on the power board and intentionally placed in the air stream underneath the fuel cell stack to enable rejection of waste heat. Interfaces to the internal battery, the target laptop battery, the fuel cell stack, all system components, and to an external AC adapter power source were located on the power board. The microprocessor and the USB communication interface to the user were placed on the control board. The two boards had a direct, multi-pin connector to provide connections between the boards. Minor design issues were detected and 'patched'. A few minor board fabrication issues were also identified and fixed. All boards were sent out for conformal coating to ensure no issues develop due to the potential condensing environment anticipated during storage.

With the new boards, the firmware was tested and incremental changes made to the control code. One important issue was identified in that the target laptop selected (Panasonic Toughbook CF-C1) did not use the industry standard SMBus communication protocol. While an effort was spent to 'reverse engineer' the hexadecimal codes being transmitted by the laptop battery, a more flexible path was developed to allow the DP4 to run without having direct SMBus communication from the laptop. The technique employed is to suspend the power provided to the laptop for 75ms every 5 seconds and--during this brief--period to measure the laptop battery voltage. This enables the firmware to both estimate the laptop battery state of charge and to provide a suitable 'overcharge' voltage to the laptop battery, which is not too high--thereby avoiding any risk of overcharge, but also not too low—thereby enabling the DP4 to run the laptop. This algorithm appears to work as desired; however the laptop battery energy gauge (how much time is remaining in the battery), in some instances does not appear to deal correctly with the power supplied by the DP4 and, sometimes reports erroneous data to the user. As a side-note, the firmware can identify the absence of a laptop battery and can act as a continuous power source to a non-laptop device, such as a radio or a sensor. This feature is believed to be of value to potential customers who simply want a power source which can be used for a ~ 20 Watt load.

Methanol Injection Pump Adaptor Boot

During system validation testing, a system failure occurred due to high methanol concentration. The methanol concentration in the anode solution reservoir increased at a rate higher that what the methanol injection pump was capable of, causing the system methanol concentration to exceed 2.0 M. The increased methanol crossover, due to high methanol concentration, generated significant heat resulting in temperatures exceeding 70°C. The combination of high temperature and high methanol concentration can dissolve the ruthenium from the anode catalyst, which can migrate to the cathode catalyst causing permanent catalyst poisoning.

It was determined that the root cause of the high methanol concentration failure was a methanol injection pump adaptor boot. The adaptor boot provides an interface between the methanol injection pump, methanol isolation valve and the reservoir tank. The boot shown in Figure 57 suffered from a manufacturing defect which allowed for the methanol to bypass the isolation valve and flow directly into the anode reservoir tank. Because the adaptor boots are manufactured in-house, the manufacturing and quality control testing procedures have been updated to eliminate any future system failures due to adaptor boot manufacturing.

Figure 57 Methanol injection pump adaptor boot.

Liquid Level Sensor

After system shutdown, the anode solution that is left in the stack will evaporate over the course of a couple days. In order to maintain sufficient anode solution for future startups, it is imperative to keep a sufficient reservoir of anode solution. The liquid level sensor provides an essential measurement for determining the anode solution reservoir level. During extended system validation testing, erratic level sensing was observed which caused the system to also behave erratically. It was determined that due to the condensation of vented CO_2 from the gas liquid separator, corrosion started to occur on the bottom of the level sensor board where it would be in contact with condensate. Although all of the circuit boards on the DP4 are conformal coated to handle condensing environments, Figure 58 shows where corrosion was starting to form on the level sensing board.
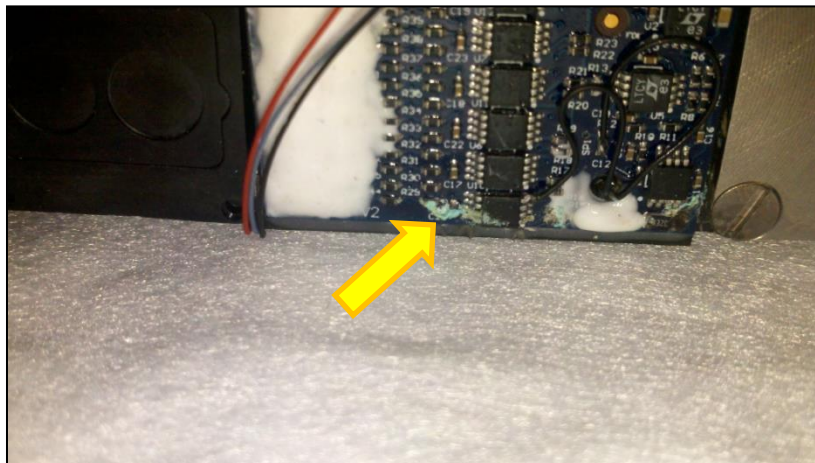
Figure 58 Corrosion build-up on level sensor circuitry (yellow arrow) due to gas liquid separator condensation.

In order to prevent corrosion build-up on the level sensor board, the level sensor is now entirely encapsulated in epoxy (Figure 59). No erratic level sensing has been observed since application of the epoxy coating.
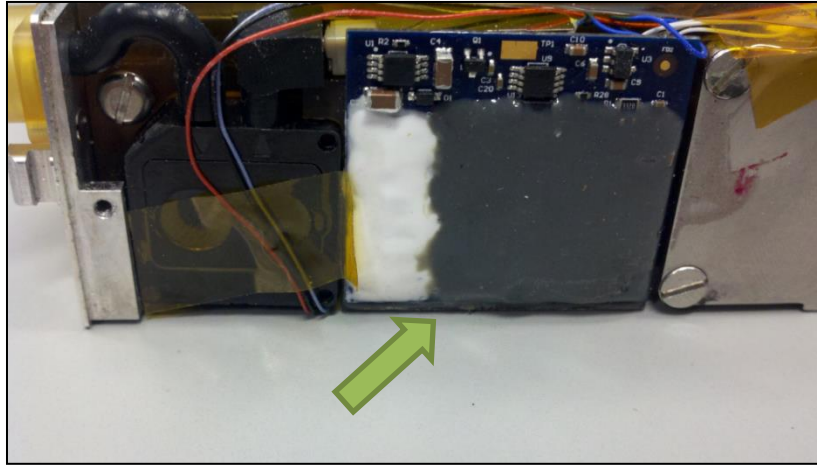
Figure 59 Epoxied coated level sensor circuit board (green arrow).

DP4 System Shell

During DP4 disassembly, a white crystallized deposit was observed in the gas liquid separator exhaust. The substance readily dissolved in water and analysis revealed that the majority of its composition was silica. After analyzing the fuel, water and DP4 shell material, it was determined that the formation of crystals was caused by the gas liquid separator exhaust coming in contact and dissolving the DP4 case material (Figure 60). The DP4 case (Figure 61) is now rigorously cleaned to remove any residual rapid prototyping material and conformal coated to resist further deterioration.
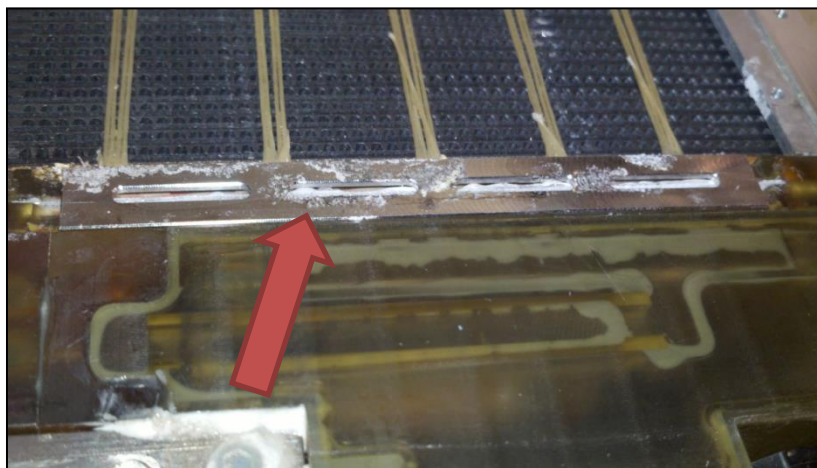
Figure 60 White silica crystals forming at gas liquid separator exhaust (red arrow).
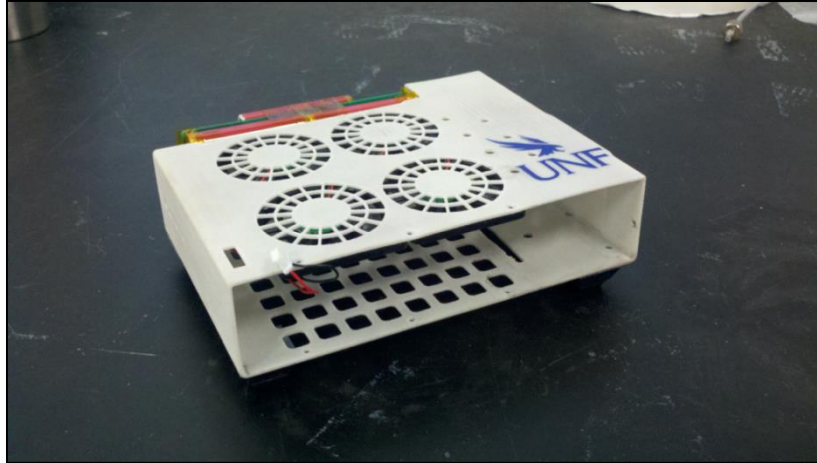
Figure 61 DP4 system shell.

Task 4: Control Strategy

Control Strategy

Overview

The DP4 DMFC power supply has its own microprocessor control board which dictates how the system will operate. It uses a system state approach with various algorithms particular to each state.

Controller Description

The electronic control of the UNF DP4 is carried out using the UNF designed DMFC fuel cell controller. The Atmel ATmega128 microprocessor system-on-a-chip, running at 16MHz, forms the heart of the controller and contains the firmware to read sensors and control actuators for the safe operation of the fuel cell system. The code is generally written in C, with the exception of a few subroutines written in assembly language. The software is compiled using IAR's Embedded Workbench and downloaded to the DP4 using a JTAG ICE II and Atmel's AVR Studio 4 software. The state diagram for the DP4 is shown in Figure 62.
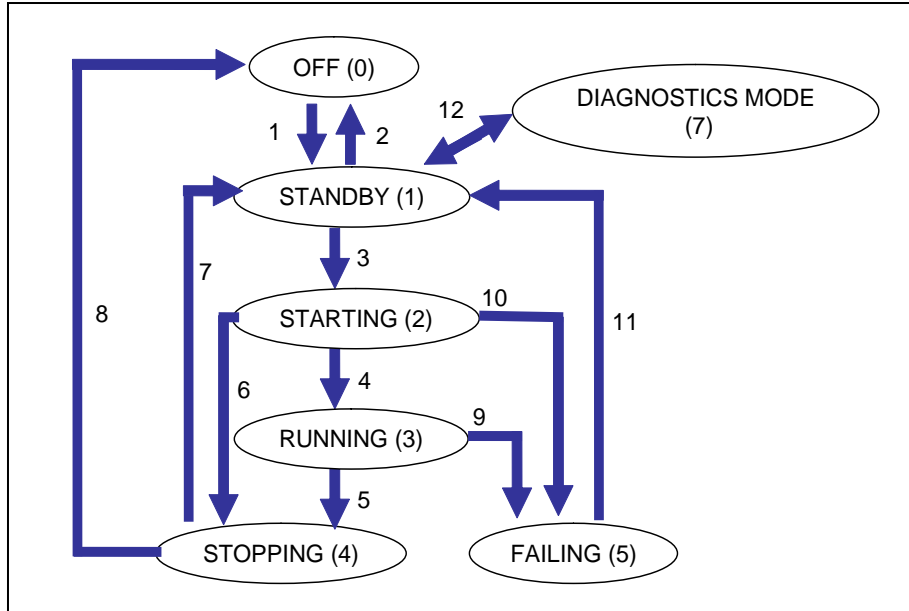
Figure 62 State Diagram of DP4

State Definitions

Off **(State 0)**	Controller has no power and is unable to execute instructions. If the User Interface button is pressed, it enables power to the microcontroller and allows the system to move to Standby State.
Standby **(State 1)**	Controller is awake and reads all sensors. Communications are established with the monitoring computer and a status message is sent periodically. The Amber LED will flash slowly in Standby State.
Starting **(State 2)**	The controller follows a prescribed sequence to start the fuel cell system. Reactants are applied to the fuel cell stack, its response is monitored and small onboard loads are applied. If several conditions are met at the end of startup, the controller will enter Running state. If these conditions are not met within the time limit, a failure is declared and the controller proceeds to Stopping State. Communications with the monitoring computer are active. The Pushbutton LED should be turned on solid during Starting.
Running **(State 3)**	Reactant systems are controlled to provide the fuel cell with proper conditions for operation. The fuel cell produces power for the external load as well as powering onboard loads. Communications with the monitoring computer are active. The Green LED is on solid during Running.

Stopping

(State 4)

The controller follows a prescribed shutdown sequence to safely stop the stack operation. Communications with the monitoring computer are active. The Red LED will be on solid during Stopping.

Failing

(State 5)

The controller follows a prescribed shutdown sequence to safely stop the stack operation. The reason for the failure and a selection of data will be recorded to EEPROM. Once the shutdown sequence is complete, the controller will remain in the Failing state until the user presses the Pushbutton button to acknowledge the failure occurred, or this will be reset in 60 seconds for a maximum of three successive failures. Communications with the monitoring computer are active. The Red LED should flash quickly in Failing.

Fault

(State 6)

Fault state can be entered from any state as a result of a program error. This state is never encountered during normal operation and is used exclusively during software development.

Diagnostics

(State 7)

Upon request from the monitoring computer, the controller can enter Diagnostics mode from Standby State. It is not possible to enter Starting state from Standby state while in Diagnostics mode. This is the only state in which EEPROM changes can be made.

In Diagnostics mode, the monitoring computer can send commands to control the DP4 control outputs. The Firefox Add-on "Diagnostics" utilizes these capabilities to allow the user to monitor inputs and control outputs. This is mostly useful when assembling, testing, and debugging a DP4 assembly.

System Tasks

Each second of system time is divided into 40 x 25 ms intervals during each of which a set of tasks or procedures is performed. The nature, number, and order of these tasks are interval-specific, but each task is performed at least once every second. A C-language function implements each of these tasks and the control program is executed as a fixed sequence of one to four such function calls in each 25 ms interval, depending on the length of time a task will typically take.

The behavior of most tasks depends on the current system state but all task functions are called in all states because most have at least some work to perform in every state.

Stack Voltage Control

It is desired to not let the stack voltage drop below a pre-determined minimum which would represent a desired maximum power point for the stack. To achieve this, the stack DCDC converter current limit is adjusted to draw the appropriate current from the fuel cell stack and keep the stack at or above this pre-determined voltage. The DCDC converter current limit is adjusted using PID control based on an EEPROM setting of the Target Stack Voltage. If the load drawn by the external device requires less power, the stack voltage will rise, stack current will fall, but the output voltage will remain constant at its set-point, a separate parameter defined in firmware.

If the stack voltage falls below a warning threshold, a remediation strategy is employed, where the DCDC converter current is set to a low value and checks for a period of time to see if the stack voltage comes up above this threshold. If it does not, then the system goes to Failing State, where the stack is disconnected from all of its loads and the unit shuts down safely.

Stack Temperature PID Control

The cooling fan speed is adjusted to hold the fuel cell at the target temperature using PID control to achieve the desired Target Stack Temperature, by modulating the fans used to supply the coolant and reactant air. This is independent from the strategy used to select the Target Stack Temperature, as defined in the liquid inventory control task.

There are a few nuances to the temperature control strategy. To ensure that fresh oxygen is always supplied to the fuel cell stack, a minimum air flow is supplied by operating the fans at a low voltage. In order to avoid issues with fan aging, studies conducted by UNF identified the minimum voltage required to start the fans spinning. A voltage significantly above this is used as the minimum fan voltage but this is applied in a 'pulsed' manner, such that the fans are provided this voltage for 500ms and then the voltage is turned off for another 500ms. The choice of the on versus off time and the minimum voltage were determined by experimentation and are firmware parameters. This 'fan pulsing' strategy is only in effect if the stack temperature is below a threshold and if the stack current is below a threshold, i.e., when the DP4 is loaded with a reduced load (<10 W).

If the temperature is above a high temperature warning level, regardless of the PID control action, the fans are turned on to 100% for a pre-set amount of time, and if the temperature has not come down to a safe level after this time, the unit will go into Failing state.

Liquid Inventory Control

Perhaps the most critical and difficult to comprehend aspect of the Passive Water Recover MEA technology used in the DP4 system is the control and maintenance of the amount of liquid in the system. It is desired to maintain the liquid inventory in a ± %5 range (~ 70% is typical).

The Target Temperature the key control parameter which dictates if the system is in a liquid generation or loss mode, depending upon the operating point of the stack, the composition of the source fuel (i.e., how much water is mixed into the methanol, if any), and the design of the MEA (i.e., the strength of the K value of the cathode barrier, and the cross-over characteristics of the membrane used). Based on measured operating conditions and values of design parameters set in EEPROM, the micro-controller calculates the 'liquid balance' temperature, then depending upon the amount of liquid in the system, both in the stack and in the recirculation tank, the Target Temperature is adjusted either above or below the ideal liquid balance temperature, to either reject or accumulate liquid, until a target inventory level zone is reached.

If the liquid inventory is below the target level by a significant amount (set in EEPROM), two levels of remediation strategy are employed. If the inventory is below level 1 (set in EEPROM, but typically 50%), then a first level remediation is set where the methanol concentration target is increased to 1.5M, thereby increasing the amount of water produced directly by cross-over. If the inventory is below level 2, then a 'maximum liquid generation mode' is entered whereby the methanol concentration target is at 1.5M and the stack target temperature is set of 40°C, both parameters determined by analysis to have the highest liquid accumulation rate.

Fuel Concentration Control

The fuel injection pump flow rate is adjusted to hold the methanol concentration at the target level (set in EEPROM) using PID control plus a feed-forward term, to account for consumption and cross-over. The fuel valve is normally closed during operation and only opens when the fuel pump is running. Methanol concentration is through a flow-through sensor (ISSYS FC10) which is plumbed in parallel with the fuel cell stack, immediately after the recirculation pump. As there is a time delay between the injection of fresh fuel into the system and when a concentration change is measured, the PID parameters have been tuned extensively, and two additional strategies have been employed to provide additional robustness. The first of these strategies is the set the initial target higher than desired (the EEPROM setting), then let this target drift down slowly towards the desired target, letting the PID loop stabilize and avoiding undershoot of the concentration. The second strategy is to employ a warning / remediation strategy to both change the target concentration, and also to set the fuel feed pump to a high level for a pre-set amount of time. A very realistic operating scenario is to have the fuel cartridge run empty and have the user replace it during operation. This is dealt with by first alerting the user that there is a low methanol concentration warning level (LEDs and through the USB serial message), then the remediation strategy allows the user to switch cartridges 'on-the-fly' without incurring a low fuel concentration failure.

Check for alarm parameter warning and failure levels

The system checks all key parameters for their levels, and if warning levels are reached, specific remediation strategies are employed. If failure conditions are reached, the system will move from Running State into Failing State. Note that during some particular periods of operation, such as during rest, some specific alarm conditions will not cause remediation or failure actions.

Respond to user interface button press

The state of the User Interface button is monitored to determine when a user presses the button. When a button press is detected, the appropriate action is taken; when in Running State is to go into Stopping, then to Standby state. The User Interface button is also used to acknowledge failures in Failing state, which would then enable the system to go into Standby state, or to go from the OFF state to Standby.

Internal Battery Charging

The internal hybrid battery is charged by the fuel cell when its state of charge is below a threshold level (70%, set in EEPROM) and this charging is disabled if the SOC is above another level (80%, set in EEPROM). The charge current is set in firmware itself and varies depending on if the battery is charging or discharging.

External load control

The DP4 has been designed to provide a power to an external load when in Running State under three scenarios: a) if the external load is the charging of a battery which can communicate via SMBus protocols, b) if the external load is a battery which is does not communicate via SMBus, and c) a non-battery load. Integrated DP4 units have been tested with scenarios b and c, but not under scenario a, however brassboard versions of this system were tested under scenario a, using a Lenovo laptop battery. In the case of scenario b, a novel protocol was developed to interrupt the supply of power to the external battery, detect its voltage, and use this to set the DCDC output voltage of the DP4, such that the battery could be charged at a nominal rate. Appropriate limits on the output voltage and charge current were set. While this algorithm worked, it is much less preferred than to communicate directly with the external battery via a standard SMBus protocol, and required an interrupt of supply power, which would only be suitable in the case of an external battery. When the DP4 is used as a stand-alone power supply, the output power and voltage is constant.

Send serial message to monitoring computer and keep track of lifetime data

The DP4 communicates with an external computer to enable a user to monitor all parameters in the DP4, and track the unit performance over time. This is useful in today's development stage, but is not essential to the operation of the system.

Compute methanol consumption

The amount of methanol consumed during operation is estimated whenever the Stack Enable line is on. The formula takes into account three elements: the methanol consumed electrochemically in the fuel cell, the methanol lost in the CO_2 exhaust, and the amount lost due to crossover to the cathode.

General Algorithm

The DP4 system was designed to be a laptop power supply. When the system is connected to an AC/DC adapter, the system remains in a standby state. When the AC/DC power is removed from the system, the laptop must be powered by the hybridized battery pack from the fuel cell system. In parallel, the fuel cell should begin the startup sequence so that the electronic load can be sustained.

If the conditions for transitioning from Standby to Starting state are met, the unit will transition states and begin the starting algorithm. In this state the unit will first check to see if a fuel cartridge with fuel is present. It enables fuel to be pumped from a cartridge into the system and then waits an appropriate amount of time, checking to see if the concentration of fuel shows an increase.

The second potential step is a 'methanol hot-soak' algorithm which may or may not be execute, depending on if a user-selectable option in EEPROM has been enabled. If enabled, the DP4 will feed fresh fuel solution from the fuel cartridge for a period of time until it reaches 80% of the target hot-soak concentration, at which point the fuel feed pump is turned down somewhat until the target hot-soak concentration is reached. During this time the fans are off. This is to reduce the amount of possible over-shoot of concentration, with the aforementioned parameters set in firmware. After the target concentration is reached, the recirculation pump is turned off, and pulse on for 5 sec, off for 30 sec, until either a timer expires or the temperature reaches a target temperature (i.e., 70C). The system is allowed to stay in this condition, with the recirculation pump pulsing on & off, until the methanol concentration falls to a pre-set level or another timer expires, at which point the fans are turned on to 50% with the recirculation pump on, until the stack temperature falls below a threshold.

The next steps of the starting algorithm are a pre-connect delay, then a primary condition check, which examines the stack voltage and fuel solution molarity, after which the stack is

allowed to power hotel loads alone, followed by a post-connect delay, after which the external load is enabled.

During Running State the fuel cell is periodically interrupted to allow for cathode catalyst rejuvenation. Upon entering Running State the system first executes a programmable number of "fast" rest periods (defined in EEPROM), followed subsequently for a longer period between such rests. The rest procedure is generally as follows:

1. Put the stack into an 'open circuit' state, where the stack voltage rises significantly and no load is drawn from the stack. The length of this period is set in firmware.

2. Put the stack into an 'air starve' state, where load is drawn from the stack, but the fans are turned off. Power is available from the stack during this phase, but is typically less than 50% of what it was during normal Running State. Length of this phase is set in firmware.

3. Put the stack back into an 'open circuit state, similar to the first step, but for a different amount of time, again set in firmware

4. Wait for a brief period to ensure all stack parameters are above a healthy level

5. Resume normal operation.

This rest procedure reflects knowledge gained by stack experimentation by UNF, especially how low of a stack voltage should be achieved during the air starve portion of the rest. Various alarm parameter actions are disabled during the rest phases.

If the AC Adapter is plugged into the DP4 or if the user interface button is pressed, the unit will transition from Running state to Stopping state. In stopping, the first phase is a liquid recovery phase in which an algorithm is used to recover as much liquid from the stack into the recirculation tank as possible. It is presumed that some liquid will remain in the stack after shutdown and this liquid will, over time, evaporate to the ambient environment. Thus it is desired to recover as much as practical from the stack into the recirculation tank, which itself has valves which prevent liquid loss in the Standby or Off states. The liquid recover algorithm involves first running the system with significant current being drawn from the stack. After a short period of time, the recirculation pump is turned off, with the external load still turned on, and the evolved gas from the electrochemical reaction forces liquid out from the stack. After the liquid recovery algorithm is complete, the stack is disconnected electrically, and the system transitions into Standby state.

DMFC Modeling

A model was developed to predict cell performance, water balance and mass transport for the UNF passive water recovery MEA based on operation parameters and MEA construction materials. The model has undergone significant improvements over the course of the project by adapting the test station data with the model output.

The fundamental electrochemistry part of the model was developed and modified based on a published model in the literature [1]. The modeling domain originally included only three layers: anode diffusion layer, anode catalyst layer, and the membrane. The project team extended the original model to cover the cathodic catalyst, liquid barrier layer (LBL), and diffusion layers to closely represent the reaction and mass transport mechanisms of the novel design of the MEA. The transport of the species at the anode diffusion layer was described by Fick's law, a transport mechanism governed by the concentration gradient of the species. The electrochemical reaction at the anode catalyst layer was simulated with a non-Tafel reaction proposed by Meyers and Newman [2]. Beyond the anode catalyst layer, the transport of the species, the rate of crossover of methanol at the membrane, was expressed by the combination effects of the diffusion and the electro-osmotic drag. The fundamental anodic and cathodic transfer coefficients and ionic conductivity of the membrane were determined by running anode polarization and impedance experiments. The electrochemical reaction at the cathode side was described by Tafel equation. The oxygen concentration distribution at the cathode side was modeled using the Stefan-Maxwell equation, a multi-component mass transport equation, due to the counter diffusion of oxygen, CO_2, and water vapor. The mass transport of the species at the cathode diffusion and LBL layer were modeled separately because of their different length scales. The pore sizes of the LBL resulted in Knudsen diffusion dominant transport as compared to Fick's diffusion in the diffusion layer.

The water generation term inside the DMFC stack comes from the electrochemical reaction at the cathode side, including useful electrochemical reaction and net reaction of the crossover methanol. The water loss terms include the electrochemical reaction at the anode side and the water vapor loss at the cathode side because of the open-cathode design. The key parameter in the water balance model is the K_{H_2O} value, a lumped water vapor mass transport parameter of the effective diffusivity coefficient of water vapor and the length of the layers. The K_{H_2O} value of each new manufactured membrane electrode assembly is determined experimentally in an ex-situ test rig. However, the K_{H_2O} value in the model can be modeled by changing the pore size, porosity, and tortuosity of the layers.

[1] Garcia, B. L., Sethuraman, V. A., Weidner, J. W., White, R. E., and Dougal, R., 2004, "Mathematical model of a direct methanol fuel cell," J. Fuel Cell Sci. and Tech. 1, pp. 43-48.

[2] Meyers, J. P., and Newman, J., 2002, "Simulation of the Direct Methanol Fuel Cell-II. Modeling and Data Analysis of Transport and Kinetic Phenomena," J. Electrochem. Soc. 149(6), pp. A718-A728.

Figure 63 shows the experimental and modeling results of polarization curves for stack temperatures from 45 to 80 °C. As previously mentioned, the DMFC has greater cell performance at higher stack temperatures when operating at current densities less than 80 mA/cm^2. Typically at a given current density, the cell voltage is higher when the stack temperature is higher due to improved electrochemistry kinetics. However, the cell voltage experiences a sharp drop at higher current densities when the stack temperature is higher. The polarization curve of the stack temperature at 80 °C crosses the other polarization curves at a current density of 100 mA/cm^2. The same concentration overpotential phenomenon happens at stack temperatures of 60 and 70 °C. The modeling results reveal the same trend. When the stack is at a higher stack temperature, the amount of water vapor is much higher because the saturation water pressure increases nonlinearly. This increase of water vapor creates a mass transport limitation on the oxygen, resulting in lower oxygen concentration at the interface of the LBL and cathode catalyst layer (CCL). The lower oxygen concentration at the LBL and CCL interface results in higher overpotential because of the oxygen concentration limitation.
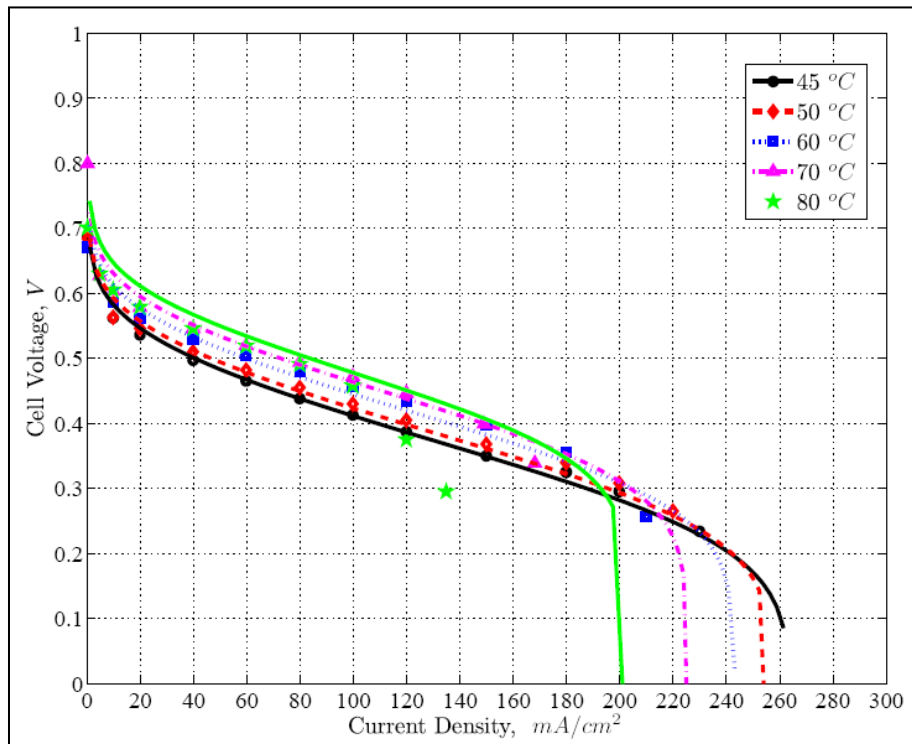
Figure 63 Experimental and modeling results of polarization curves for stack temperatures from 45 to 80 °C

DP4 Battery Charging Optimization

A 22 Watt-hour battery pack has been hybridized into the DP4 system in order to account for conditions where the system is unable to generate sufficient power (startup, rest cycles, shutdown) for the load. Typically, the state of charge in the battery pack is maintained between 70-80%. Due to the limitations in the control board circuitry, the system is unable to match the

load exactly which requires the system to switch back and forth from a charge mode to a discharge mode. Previously, the charge mode was very aggressive, where the stack would be loaded to a high power condition until the batteries were charged to 80%. When in discharge mode, the stack would sustain a light load in order to allow the batteries to discharge back down to 70%.

Not only is it inefficient to store and remove energy from the battery pack, it is also challenging to maintain stable control of the system due to the various effects of loading and unloading the stack. During charge mode, the stack produces more current and therefore more water. In order to maintain water neutrality, the system operates at a higher temperature. In discharge mode, the system produces less current and less water; consequently, it operates at a lower temperature to maintain the same water level.

In order to overcome this undesirable effect, the charge and discharge current for the battery pack were limited so that only a certain amount of energy could go into or out of the batteries. The current limits enabled the stack to better match the load resulting in significantly less swings in current and operating temperature while improving overall system efficiency.

Task 5: Validation Testing

MEA Development

The initial MEAs used in this program relied on the baseline MEA configuration, developed under a previous DOE program. These MEAs are based on an open cathode passive water recovery approach and the base configuration of the MEA is shown in Figure 64. The key features of the UNF passive water MEA are

a) A cathode liquid barrier layer (LBL) which is designed to both prevent water vapor loss form the MEA, thereby passively recovering the water within the fuel cell stack, and prevent liquid water penetration into the barrier layer by virtue of a high capillary pressure. In this approach the water loss is regulated by providing a low permeability to water vapor leaving the cell; however this also leads to a low permeability to oxygen and thus the LBL must be optimized to minimize water loss while providing sufficient oxygen access to maintain good electrochemical performance.

b) A microporous hydrocarbon based membrane which has a low methanol crossover and water electro-osmotic drag while allowing through engineered areas of porosity liquid water to be actively returned through the membrane due to the hydrostatic pressure developed in the cathode layer.
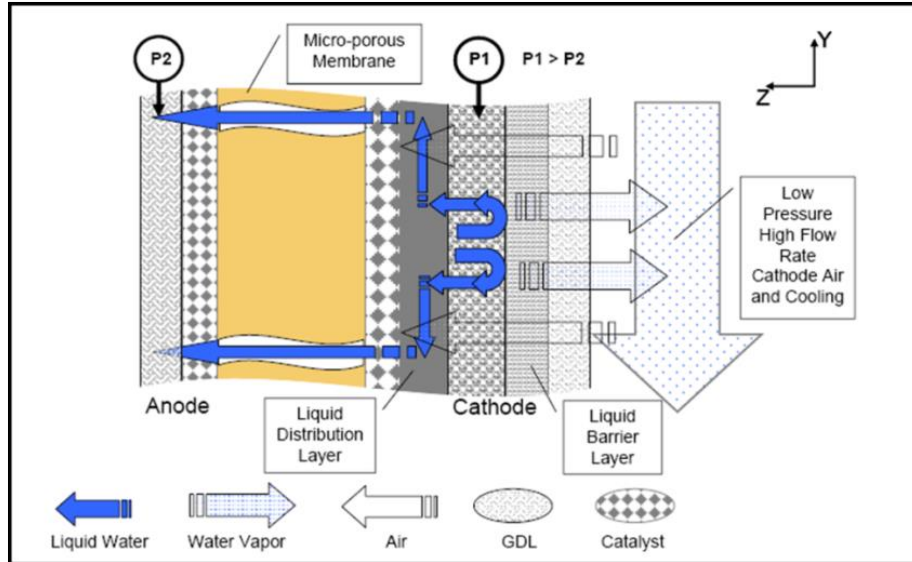
Figure 64 UNF Passive water recovery MEA

In a parallel DOE funded program at UNF we have continued the development of the MEA manufacturing uniformity, MEA durability, and performance characteristics. As these developments have been validated, in the separately funded MEA development program, we have incorporated several generations of improved MEAs as they have become available both to provide improved system performance and to validate the developed MEAs in a system environment. In this report we will discuss some of the key MEA developments and performance trends developed over this program.

Baseline MEA

The initial MEAs were produced using the baseline MEA configuration developed under the previous DOE program. The main advancement in these early MEAs was improved barrier layer and MEA reproducibility and control which was the result of improved manufacturing process and process control. The MEAs utilized a 20μm hydrocarbon membrane that had been engineered by drilling holes to provide areas of high water transport. In our development we developed a method for quantifying both the water vapor transport or permeability (K_{H_2O}) and the capillary pressure. The key parameter for the system design for water balance is the K_{H_2O} (mm/s) value which is a lumped constant as shown below

$$K_{H_2O} = \frac{[Diffusion\ Coefficient_{H_2O\ in\ Air}] * [Barrier\ Layer\ Porosity] * [Tortuosity]}{[Thickness\ of\ Liquid\ Barrier\ Layer]}$$

Figure 65 shows the performance of the baseline MEA in a short stack (8 cell test stack). With the improved manufacturing processes, very low standard deviations were obtained for stacks, which was further validated in the 40 cell system stacks. These initial MEAs utilized barrier layers with K_{H_2O} values between 1.4 and 1.6 mm/s. The system level performance of

these MEAs is presented in Table 9 These higher K_{H_2O} values were used to provide sufficient oxygen access to the MEA. MEA durability tests show excellent lifetime performance for continuous operation testing with lifetimes of the order of 10,000 hours for the baseline MEA configuration in short stack testing. However, these MEAs exhibited an unexpected and unusual off state degradation behavior which is typically not observed in DMFC systems. Moreover, similar rates of degradation were observed both at the system level and test station testing of short stacks under both recirculation and single pass testing. A considerable study of the MEA durability was undertaken at both the system and the stack level to address the degradation of the baseline MEAs including the MEA chemistry and manufacturing as well as the stack and system level operating parameters. From this testing the degradation was isolated to the MEA and not the system components or recirculation conditions.
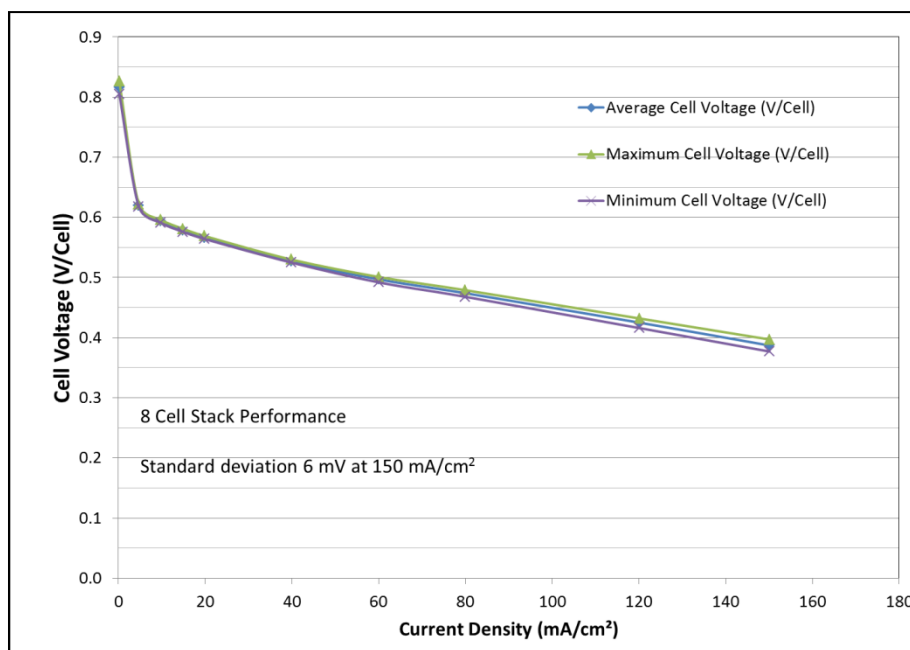
Figure 65 MEA performance with 0.8 M methanol, 50°C Stack temperature, anode flow rate 1.4 cm3/cell/min. Cathode flow rate controlled to maintain a stack temperature of 50°C (> 20X stoichiometric levels).

2ⁿᵈ Generation MEAs

The second generation MEAs developed under our parallel DOE funded MEA development program incorporated improvements in the MEA fabrication to increase the MEA durability to address the off state degradation issues highlighted above. In this generation of MEAs we optimized the anode electrode by incorporating a stabilized anode catalyst to minimize Ruthenium dissolution and crossover, and we improved cathode ink chemistries and wetting agents. Due the highly hydrophobic characteristics of our MEAs, an ink chemistry that adequately wets the LBL and allows the catalyst ink formulation be dispersed without providing a long term change to the LBLs wetting characteristics in the final MEA must be employed. By

optimizing the ink chemistries we were able to resolve the root cause of the off state degradation. Additionally, through optimization of both the LBL and MEA fabrication we were able to reduce the LBL K_{H_2O} values while maintaining good MEA performance when measured in short stacks. Lowering the K_{H_2O} value results in maintaining water balance in the MEA at higher temperatures and obtaining overall improved performance and allows operation of the system with pure methanol in the fuel cartridge. Figure 66 shows the performance of 2nd generation MEAs with a K_{H_2O} value of 1.27 mm/s. However, there are limits to the reduction in the K_{H_2O} value since sufficient oxygen access to maintain the oxygen reduction reaction on the cathode is required as can be seen from Figure 66, which includes the data for K values of 1.42 and 1.0 mm/s. The system level data shown in Table 9 validates that for a K_{H_2O} of 1.27 based MEA, a significant improvement in the specific energy and energy density can be attained.
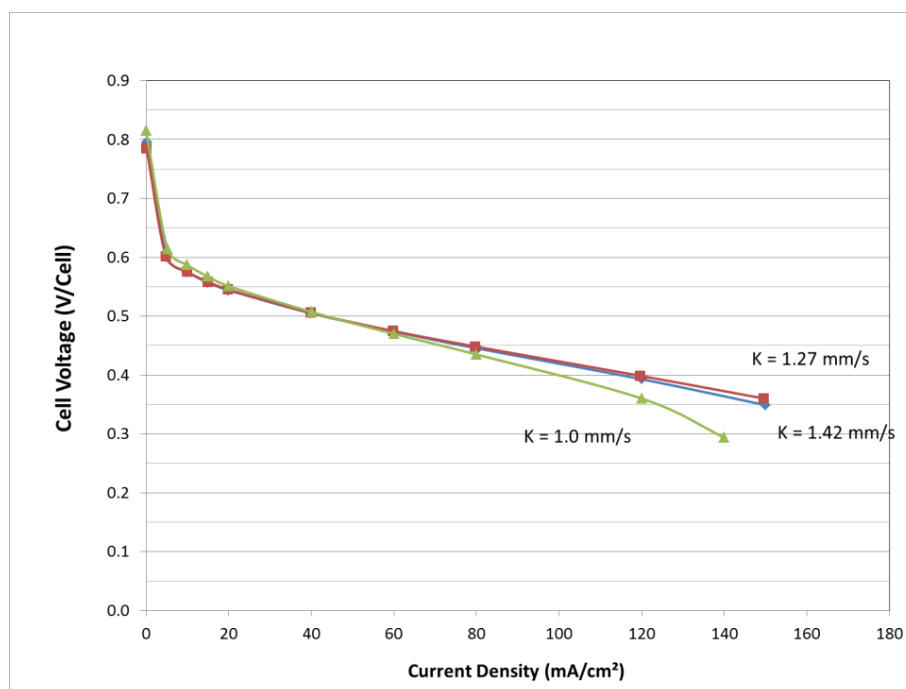
Figure 66 Average cell voltage of 2nd generation MEAs with various K_{H_2O} value liquid barrier layers. Performance measured at 0.8 M, 50°C, 1.4 cm^3/cell/min anode flow rate, cathode flow rate to maintain operating temperature.

3rd Generation MEAs

The 2nd generation MEAs allowed for energy density improvements at the system level by allowing operation at higher average temperatures and operation of the system with pure methanol fuel cartridges. However, while these MEAs utilize a low methanol crossover membrane, the methanol crossover is still too high under operating conditions due to the low thickness (20μm) used to obtain good performance in the baseline MEAs. This gives rise to

inefficiency at the system level due to the loss of methanol directly through the crossover. Moreover, it further reduces the MEA performance due to lowering the cathode potential due to the mixed potential formed by the methanol crossover. This is particularly a problem in the UNF passive water recovery MEA which has limited oxygen access as the LBL K_{H_2O} values are lowered to increase operating temperature further.

In the 3rd generation MEA the membrane thickness is increased to 45µm. This significantly reduces the methanol crossover to ½ or ⅓ of the crossover of the 20 micron membrane. Additionally through improvements in the MEA fabrication comparable electrochemical performance for the MEA has been attained. Figure 67 shows the performance of the 45µm membrane based MEA. Comparable performance is attained over the operating range. This allows us to reduce the Crossover is reduced and efficiency increased at the MEA level and at the system level. Additionally, since the crossover is lower a lower K_{H_2O} value can be used and thus the system performance increased further by allowing a higher operating temperature. Comparable performance has been obtained for 40 cell stacks and testing in the prototype system have shown improved performance, as discussed in Table 9.

Figure 67 MEA performance of 45 micron MEA.
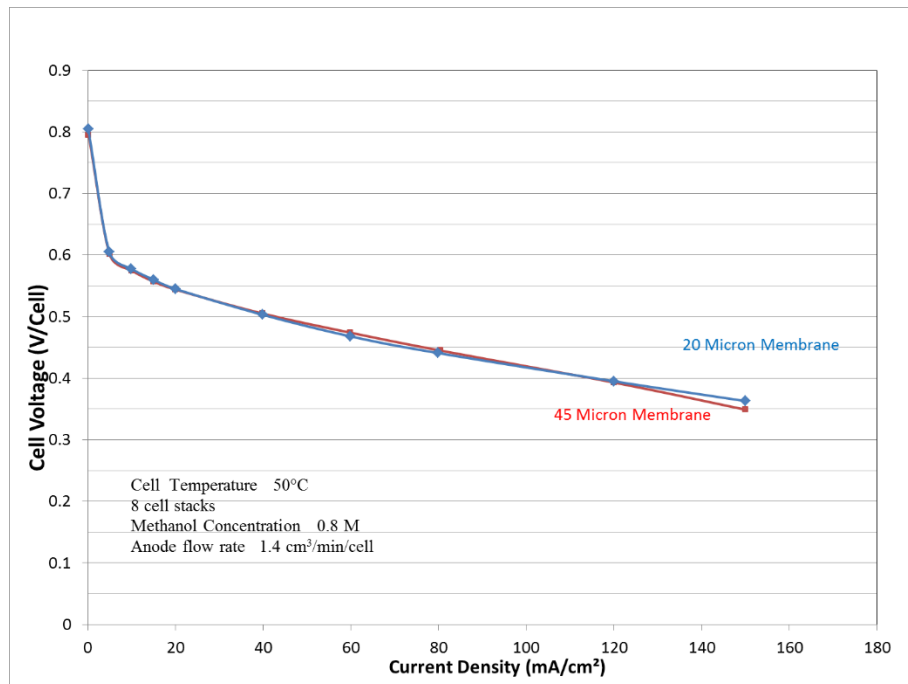
DP4 Testing & Optimization

Initial Testing

While the functioning unit was not able to be demonstrated at the Annual Merit Review, an assembled system was shown in its non-functioning configuration. However, it has been

demonstrated in the lab at UNF and shown internally to the UNF President, Provost, college Dean and department Director. While improvements are still forthcoming, the team is proud of its accomplishment. The unit is repeatedly able to start up, operate and shut down as desired. It can provide continuous power to a non-laptop load (i.e., a load which does not represent a battery to be charged) and also to a laptop which does not have a standard SMBus battery (e.g., Panasonic Toughbook CF-C1).

Testing of the integrated DP4 focused on improvement of its firmware robustness. The DP4 has been able to deal with permutations in operating conditions, both during startup and during normal operation, relatively well. It has been noted that the integrated system required a re-tuning on the control loops from the brassboard configuration, which was expected. One unexpected observation is a time delay in sensing a change in the methanol concentration. The root cause of this delay has been identified and this problem will be solved through a minor design iteration.

DP4 Noise Level Testing

The noise level testing was conducted on the DP4 using the dBA and dBC scales. The letters "A" or "C" following the abbreviation "dB" designate a frequency-response function that filters the sounds that are picked up by the microphone in the sound level meter. A frequency-response function, also called a weighting characteristic (meaning that some frequencies are given more weight or importance than others) can also be thought of as a tone control. It emphasizes or de-emphasizes sounds of certain pitches relative to others. The actual influence of the A- and C-weighting functions is illustrated in Figure 68. The vertical axis shows relative response in decibels and the horizontal axis shows frequency measured in Hz or cycles/sec. (which is a measure of pitch).

Notice that the A weighting filters out the low frequencies and slightly emphasizes the upper middle frequencies around 2-3 kHz. By comparison C weighting is almost unweighted, i.e., no filtering at all. A-weighting is used to measure hearing risk and for compliance with OSHA and MSHA regulations that specify permissible noise exposures in terms of a time-weighted average sound level or daily noise dose. C-weighting is used in conjunction with A-weighting (the dBA and dBC levels are compared) and for certain computations involving computation of hearing protector attenuation. C:\Users\n00009115\Documents\Neal\DMFC\Required Reports\DoE 5B\Final Report\Final Final Report\from-phil-6.18.2013.EE0000476 FTR edited rev3.docx
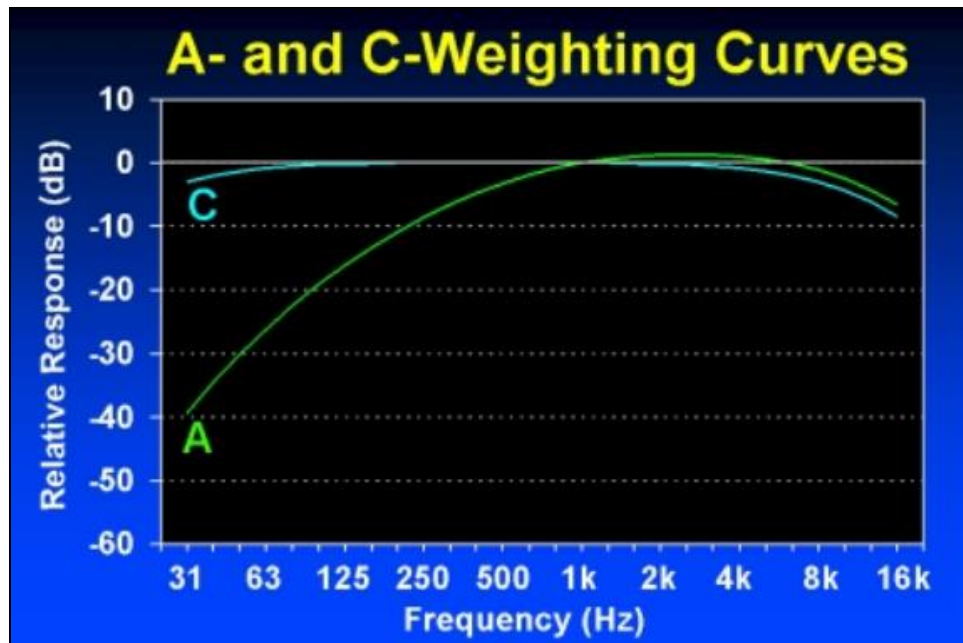
Figure 68 A and C weighted scales.

Using a hand-held sound meter, in a quiet area (all extraneous noise sources were turned off), the sound from the following positions were measured at a 1-meter distance from the DP4, as shown in Figure 69. The recorded data on both the dBA and dBC scales are in Table 8.
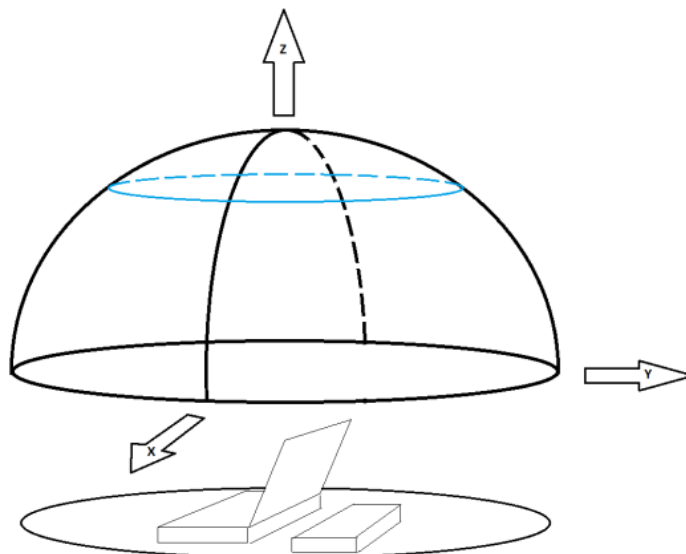
Figure 69 Orientation and axes

Nominal noise test was conducted with the fans at a nominal level, typically at 50% of maximum. At maximum power both the dBA and dBC tests showed very low noise production

(average of 52.7 dBA and 63.2 dBC, respectively) and showed no significant directional difference. Both dBA and dBC levels were higher than they were at nominal but not significantly.

Table 8 Results from orientation sensitivity of noise level testing.

X Axis (m)	Y Axis (m)	Z Axis (m)	Nominal Noise dBA (dB)	Nominal Noise dBC (dB)	Max Fan Speed Noise dBA (dB)	Max Fan Speed Noise dBC (dB)
0	0	0	43.7	57.9	55.1	68.2
-1	0	0	42.9	60.6	52.2	63.6
0	1	0	45.4	60.1	52.6	66.7
0	-1	0	41	59.2	51.4	63.4
1	0	0	41.8	57.5	51.3	60.3
-0.71	0.71	0	44.4	59.8	51.7	66.1
0.71	0.71	0	42.2	59	52.1	65.7
-0.71	-0.71	0	42	61	51.3	62
0.71	-0.71	0	42.3	59.5	51	60.1
0	0.71	0.71	43.3	58.4	54.2	64.8
0	-0.71	0.71	42	58.2	54.1	60.1
-0.71	0	0.71	43.4	59.2	54.4	60.6
0.71	0	0.71	42.5	59.1	54.2	59.6
		Average	42.8	59.2	52.7	63.2

K-Value Optimization

In order to achieve sufficient water and power generation, a mixture of 80% methanol and 20% water was used for fuel in the DP4. In collaboration with the other funded DOE program testing of membrane electrode assemblies (MEAs) with lower cathode barrier layer K-values revealed the ability to achieve nearly the same performance (Figure 70) with reduced water loss. A 40- cell stack with lower K-value MEAs was assembled for system testing and used with pure methanol. A 30% reduction in fuel consumption was measured due to the elimination of water in the fuel and a 3% increase in system efficiency was calculated due to optimized control strategy.

Operation Profile	Anode Electrode	Operating conditions	Cathode			
			Cathode Ink			Barrier Layer
			MEK	IPA	NPA	
8 On/16 Off	ELE 170	0.05 V Rest			X	As indicated
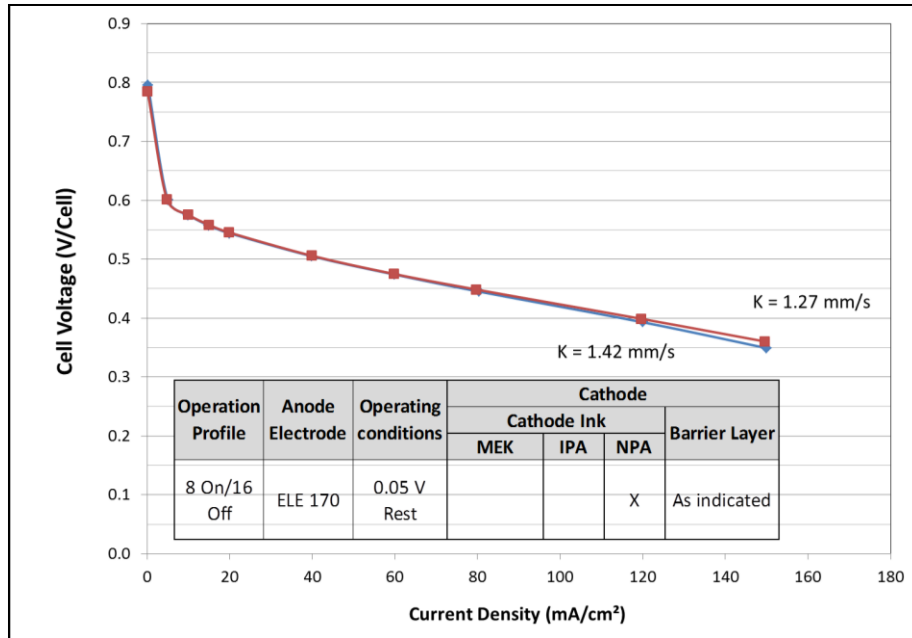
Figure 70 MEA testing with lower K-value produced nearly the same performance.

DP4 Validation Testing

In order analyze system performance and control strategy robustness with various MEA iterations, the open cathode DP4 design was tested for 72 hour durations. It was the goal to achieve a 20 W, 72 hour operation using the DOE DP4 system. During the first trial, the 1st generation MEAs were used, however the system was unable to meet the requirements of the 72 operation due to insufficient power generation by the stack. Unfortunately, during this trial, the MEAs that were used in the stack for the first trial were hand screen printed due to an untimely screen printer failure. However, the system was able to achieve successful operation for 54 hours. When the results are extrapolated to a seventy-two hour duration, the energy density that can be achieved approaches some of their highest performing systems in the 20-25 W power range.

A second trial was conducted with the 2nd generation MEAs, an improved control strategy and machine controlled screen printed MEAs. The results included in Table 9 show that the DOE DP4 was able to achieve a 23% increase in specific energy and a 26% increase in energy density. These results significantly exceed all other power system solutions (battery or fuel cell) in this power and duration range.

Finally, the DP4 system was tested with 3rd generation MEAs. These MEAs offered the advantage of operating at elevated stack temperatures resulting in improved reaction kinetics. As a result, the system was able to operate at an elevated output power level of 22 W. Relative to the 2nd generation MEAs an improvement of 27% and 30% was achieved in specific energy and energy density respectively.

Table 9 Results from independent evaluation of DOE DP4 system.

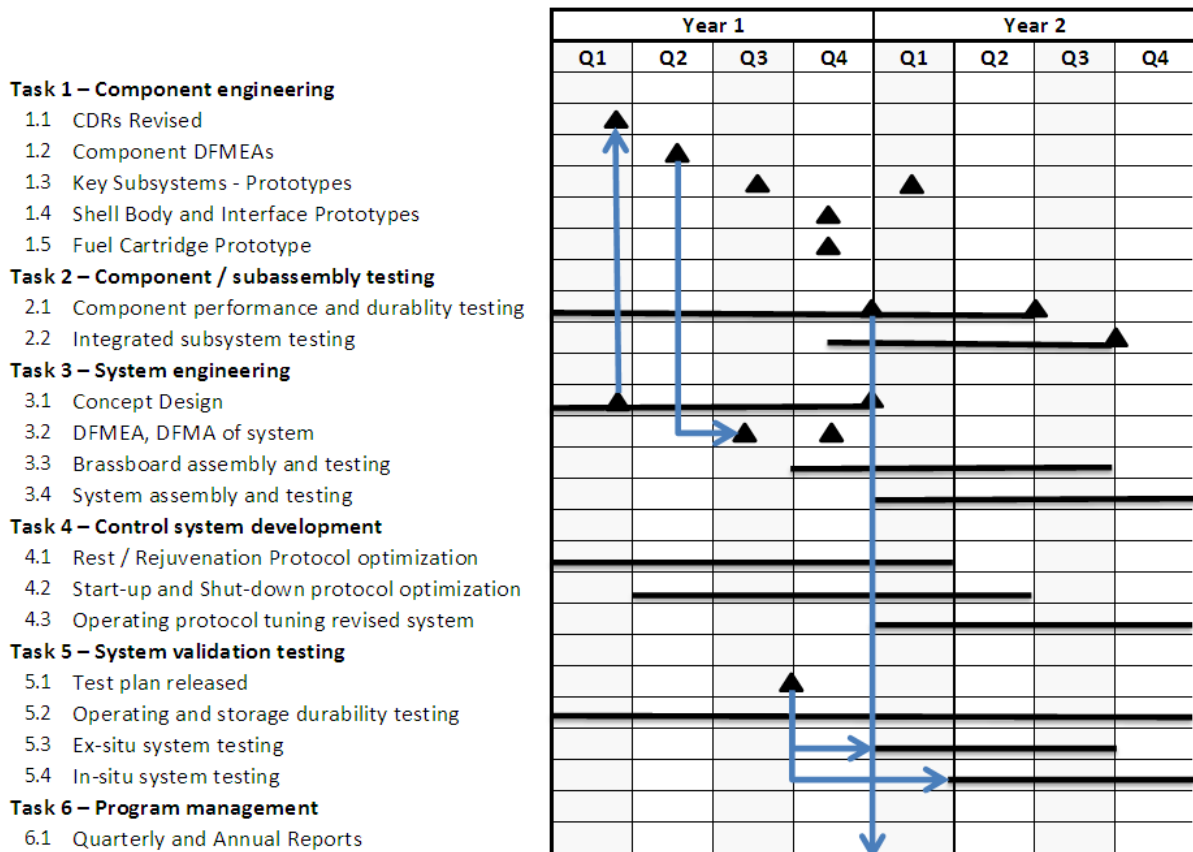|	1st Generation MEAs	2nd Generation MEAs	3rd Generation MEAs
System Run Time (hrs)	72*	72	72
Nominal Power Output (W)	20	20	22
Net Energy Produced by System (Wh)	1440	1440	1593
Total Energy Consumed (Wh)	8911	8264	6614
System Efficiency (%)	16.2%	17.4%	24.1%
System Weight (kg)	0.784	0.784	0.784
Weight of Mixed Fuel Consumed (kg)	2.015	1.495	1.197
Weight of System and Consumed Fuel (kg)	2.799	2.279	1.981
Specific Energy (Wh/kg)	514	632	805
System Volume (L)	0.673	0.673	0.673
Volume of Mixed Fuel Consumed (L)	2.548	1.890	1.513
Volume of System and Consumed Fuel (L)	3.221	2.563	2.186
Energy Density (Wh/L)	447	562	729

*Extrapolated from 54 hour duration.

Appendix

Tasks and Subtasks

Quarterly reports must address the tasks specified in the DoE award document.

The associated research will be conducted at several sites. They are defined as:
1. UNF – The University of North Florida, Jacksonville, FL.
2. UF – The University of Florida, Gainesville, FL
3. UNFNW – The University of North Florida Northwest (Vancouver, CA)
4. UNFSV – The University of North Florida, Silicon Valley (San Jose area, CA)

An overview of the project work plan is shown below:

	Year 1				Year 2			
	Q1	Q2	Q3	Q4	Q1	Q2	Q3	Q4
Task 1 – Component engineering								
1.1 CDRs Revised								
1.2 Component DFMEAs								
1.3 Key Subsystems - Prototypes								
1.4 Shell Body and Interface Prototypes								
1.5 Fuel Cartridge Prototype								
Task 2 – Component / subassembly testing								
2.1 Component performance and durablity testing								
2.2 Integrated subsystem testing								
Task 3 – System engineering								
3.1 Concept Design								
3.2 DFMEA, DFMA of system								
3.3 Brassboard assembly and testing								
3.4 System assembly and testing								
Task 4 – Control system development								
4.1 Rest / Rejuvenation Protocol optimization								
4.2 Start-up and Shut-down protocol optimization								
4.3 Operating protocol tuning revised system								
Task 5 – System validation testing								
5.1 Test plan released								
5.2 Operating and storage durability testing								
5.3 Ex-situ system testing								
5.4 In-situ system testing								
Task 6 – Program management								
6.1 Quarterly and Annual Reports								

The work plan consists of five engineering tasks plus a project management task.

Task 1

In Task 1, Component Engineering, a revised set of Component Design Requirements (CDRs) will be developed based on concept design (from Task 3) with revised component packaging and with integrated key sub-systems. The focus of this task is to both miniaturize the balance of plant components (i.e., the methanol sensor) and integrate them into subsystems (i.e., the fuel recirculation pump, the carbon dioxide separator, the retained liquid reservoir, and the methanol sensor integrated into a subsystem assembly). This proposed concept design utilizes UNF's existing core fuel cell stack design and system architecture. A Design Failure Mode Effects

Analysis (DFMEA) for each key sub-system will be developed and used to both guide the component design and define the test program in Task 2. Components (i.e., air supply, fuel recirculation pump, fuel feed pump/valve, etc.) and revised system packaging with fuel cartridge interface will be designed and prototyped in Tasks 1.3 and 1.4. A new fuel cartridge design will be developed in Task 1.5.

Task 1 Subtasks are:
      1.1 CDRs Revised – UF, UNF, UNFNW
      1.2 Component DFMEA – UF, UNF, UNFNW
      1.3 Key Subsystems – Prototypes – UF, UNF, UNFNW
      1.4 Shell Body and Interface Prototypes - UNFNW
      1.5 Fuel Cartridge Prototype - UNFNW

Task 2

Task 2 will focus on evaluating each of the components and subsystems against the defined CDRs. UNF's Fuel Cell Research Laboratory will conduct the required component, subsystem and integrated system testing to support this project. Initially, existing components will be evaluated for durability and failure modes and the results will be used to help define component requirements. Once available, the new design prototype components will then be evaluated for durability and robustness. Task 2.2 which consists of the evaluation of integrated subsystems will begin in 10 months.

Task 2 Subtasks are:
      2.1 Component Performance and Durability – UF, UNF, UNFNW
      2.22.2 Integrated Subsystem Testing – UF, UNF, UNFNW

Task 3

Task 3, System Engineering, will begin immediately. Task 3.1 consists of creating a detailed concept system from which the CDRs of task 1.1 will be defined. In parallel, the system DFMEA will be created and linked with the component / subsystem DFMEAs in task 3.2. As functional performance data from component and integrated subsystem testing becomes available, the system model will be refined. Design for Manufacturing and Assembly (DFMA) of the overall concept will be conducted to provide additional manufacturability and assembly requirements into the component and system CDRs. Subsystems will be integrated for testing as they become available, first on a brassboard (a table with components laid out) in task 3.3. This enables detailed instrumentation of the system and verification of subsystem design. Task 3.4 starts in month 12 and evaluates the integrated package, initially again with auxiliary instrumentation.

Task 3 Subtasks are:
      3.1 Concept Design - UNFNW
      3.2 DFMEA, DFMA of System – UNF, UNFNW, UNFSV
      3.3 Brassboard Assembly and Testing – UNF, UNFNW
      3.4 System Assembly and Testing – UNF, UNFNW

Task 4

Task 4, Control system development will optimize the key operational protocols for start-up, rest/rejuvenation, and shut-down, specifically to minimize both operational and storage degradation rates. Tasks 4.1 and 4.2 examine these protocols, initially in multiple single cells (8), then migrating to short stacks (10 cell), and then to full stacks starting at the program onset. Accelerated lifetime tests for micro-Direct Methanol Fuel Cell (micro-DMFC) systems are not readily available, nor have correlations been established. These two tasks are planned for the first 18 months. Starting in month 12, Task 4.3 will apply and examine these protocols in the system design, using system components, initially on a brassboard system (components laid out on a table), then on integrated packaged systems.

Task 4 Subtasks are:
  4.1 Rest/Rejuvenation Protocol Optimization – UNF, UNFNW
  4.2 Start-Up and Shut-Down Protocol – UNF, UNFNW
  4.3 Operating Protocol Tuning Revised System – UNF, UNFNW

Task 5

Task 5 is the System Validation testing. Task 5.1 develops a detailed test plan for the integrated system in month 9. This test plan will be driven by requirements of consumer electronics partners which will be solicited during this project. Task 5.2 will evaluate operational and storage degradation rates, starting with the core fuel cell stack technology at the beginning of the program and shifting in month 12 to integrated systems under nominal conditions. Tasks 5.3 and 5.4 will each evaluate both ex-situ and in-situ factors as per the test plan. As an example, materials compatibility will be tested using ex-situ tests (i.e., leaching tests in various methanol solutions) and control algorithm parameters will be tested in-situ (i.e., using the developed fuel cell system). UNF will partner with a leading research institution to conduct portions of this Task. A statistically significant sample of systems will be tested at nominal operating conditions and a further set of three each will be tested through the extreme test conditions. Operational and storage durability testing will be conducted over a twelve month period with a durability target of 2000 hours.

Task 5 Subtasks are:
  5.2 Test Plan Released – UNF, UNFNW
  5.3 Operating Storage and Durability Testing – UNF, UNFNW
  5.3 Ex-Situ System Testing – UNF, UNFNW
  5.4 In-Situ System Testing – UNF, UNFNW

Task 6

Task 6 is the Program Management and Reporting. The program shall provide Reports and other deliverables in accordance with the Federal Assistance Reporting Checklist following the instructions included therein and any additional reporting required under the American Reinvestment and Recovery Act. Also, UNF will participate in the DOE Fuel Cell Technologies Program Annual Merit Review and prepare and present detailed briefings of plans, progress, and results of the technical effort to DOE personnel, as requested by DOE. The project is planned as a 24 month program focused during the first 12 months on component requirements, design, prototyping and initial system integration. The key Go / No-Go decision gate shall be held immediately after Quarter 4, Month 12, based on the test results from an integrated prototype.

Task 6 Subtasks are:
  6.1 Quarterly and Annual Reports – UNF
  6.2 Go/No-Go Decision - UNF